O. OFLAZ

EXPERIMENTAL ANALYSIS OF FRICTION STIR WELDING

THE GRADUATE SCHOOL OF NATURAL AND APPLIED SCIENCES
OF
ATILIM UNIVERSITY

OZAN OFLAZ

A MASTER OF SCIENCE IN
THE DEPARTMENT OF MECHANICAL ENGINEERING

JANUARY 2025

ATILIM UNIVERSITY 2025

EXPERIMENTAL ANALYSIS OF FRICTION STIR WELDING

A THESIS SUBMITTED TO
THE GRADUATE SCHOOL OF NATURAL AND APPLIED SCIENCES
OF
ATILIM UNIVERSITY

BY

OZAN OFLAZ

IN PARTIAL FULFILLMENT OF THE REQUIREMENTS
FOR
THE DEGREE OF MASTER OF SCIENCE IN
THE DEPARTMENT OF MECHANICAL ENGINEERING

JANUARY 2025

Approval of the Graduate School of Natural and Applied Sciences, Atilim University.

_____

Prof. Dr. Ender KESKİNKILIÇ
Director

I certify that this thesis satisfies all the requirements as a thesis for the degree of **Master of Science in Mechanical Engineering, Atılım University**.

_____

Prof. Dr. Sadık Engin KILIÇ
Head of Department

This is to certify that we have read the thesis "EXPERIMENTAL ANALYSIS OF FRICTION STIR WELDING" submitted by **OZAN OFLAZ** and that in our opinion it is fully adequate, in scope and quality, as a thesis for the degree of Master of Science.

_____

Asst. Prof. Dr. Hakan KALKAN
Supervisor

Examining Committee Members:

Prof. Dr. Bilgin KAFTANOĞLU
Manufacturing Engineering Atılım University _____

Asst. Prof. Dr. Hakan KALKAN
Manufacturing Engineering Atılım University _____

Asst. Prof. Dr. Bahram LOTFI
Mechanical Engineering TOBB University _____

Date: *07.01.2025*

I hereby declare that all information in this document has been obtained and presented in accordance with academic rules and ethical conduct. I also declare that, as required by these rules and conduct, I have fully cited and referenced all material and results that are not original to this work.

Name, Last Name: Ozan OFLAZ

Signature:

ABSTRACT

EXPERIMENTAL ANALYSIS OF FRICTION STIR WELDING

Oflaz, Ozan

Master, Department of Mechanical Engineering

Supervisor : Asst. Prof. Dr. Hakan Kalkan

January 2025, 99 pages

In this thesis, 4 mm thick aluminium 5754 plates were butt welded. As a result of the applied FSW method, mechanical characterization and internal structure analysis were performed on the materials. Within the scope of mechanical characterization, tensile test and hardness test were applied, and the results were evaluated according to the test matrix. Additionally, the changes observed in the internal structure after welding were reported by SEM analysis.

One disadvantage of the FSW method is the excessive load exerted on the spindle. The aim of this study is to identify the parameters, specifically rotational and traverse speed, at which the spindle experiences the least load. All obtained results were examined by mathematical correlation. Friction stir welding parameters were determined for optimum hardness, tensile strength and force outputs from friction stir welding input parameters.

Keywords: Friction Stir Welding, microstructural analysis, solid-state welding, mechanical characterization, welding parameters.

ÖZ

SÜRTÜNME KARIŞTIRMA KAYNAĞININ DENEYSEL ANALİZİ

Oflaz, Ozan

Yüksek Lisans, Makine Mühendisliği Bölümü

Tez Yöneticisi : Dr. Öğr. Üyesi Hakan Kalkan

Ocak 2025, 99 sayfa

Bu tezde, 4 mm kalınlığında alüminyum 5754 plakalar uçtan kaynaklanmıştır. Uygulanan FSW yöntemi sonucunda malzemeler üzerinde mekanik karakterizasyon ve iç yapı analizi yapılmıştır. Mekanik karakterizasyon kapsamında çekme testi ve sertlik testi uygulanmış ve sonuçlar test matrisine göre değerlendirilmiştir. Ayrıca kaynak sonrası iç yapıda gözlenen değişimler SEM analizi ile raporlanmıştır.

FSW yönteminin bir dezavantajı, mil üzerine uygulanan aşırı yüktür. Bu çalışmanın amacı, milin en az yüke maruz kaldığı parametreleri, özellikle dönme ve ilerleme hızlarını belirlemektir. Tüm elde edilen sonuçlar matematiksel korelasyon ile incelendi. Sürtünme karıştırma kaynağı girdi parametrelerinden optimum sertlik, çekme dayanımı ve kuvvet çıktıları için sürtünme karıştırma kaynağı parametreleri belirlendi.

Anahtar Kelimeler: Sürtünme Karıştırma Kaynağı, mikroyapısal analiz, katı hal kaynağı, mekanik karakterizasyon, kaynak parametreleri.

To My Family

ACKNOWLEDGMENTS

I would like to express my gratitude to my thesis advisor, Asst. Prof. Dr. Hakan KALKAN, for his unique contributions and guidance throughout the thesis work. Additionally, I extend my thanks to the members of the thesis committee: Prof. Dr. Bilgin KAFTANOĞLU, Asst. Prof. Dr. Hakan KALKAN, and Asst. Prof. Dr. Bahram LOTFI.

I am also deeply grateful to the Research Engineers Çağlar Ceylan, Can Zümrüt, Korcan Küçüköztaş, and Ceren Atmaca from the Metal Forming Center of Excellence, as well as Asst. Prof. Dr. Ramazan Hakkı NAMLU from Atılım University's Mechanical Engineering Department, for their invaluable support.

Furthermore, I would like to thank my parents and my dear wife for their unwavering encouragement and support throughout this journey.

Lastly, I would like to express my sincere gratitude to TENMAK-BOREN for providing access to the Kistler dynamometer, which was essential for conducting the experiments in this study.

TABLE OF CONTENTS

ABSTRACT iii

ÖZ iv

ACKNOWLEDGMENTS vi

TABLE OF CONTENTS vii

LIST OF TABLES ix

LIST OF FIGURES x

LIST OF ABBREVIATIONS xiii

1. INTRODUCTION 1

2. FRICTION STIR WELDING 5

2.1. Friction Stir Welding Application 5

2.2 Weld Seam Form and Metallurgical Structure 6

2.3 Welding Parameters 7

2.4. Advantages of the Method 8

2.5. Limitations of the Method 9

3. LITERATURE REVIEW 10

3.1. Effects of machine parameters in friction stir welding 10

3.2. Effects of tool parameters on friction stir welding 12

3.3 Double Sided Friction Stir Welding Applications 15

3.4. Friction Stir Welding for AA 5754 Aluminium Alloy 19

4. OBJECT OF PRESENT INVESTIGATION 24

5. FSW EXPERIMENTS 26

5.1 Sample Preparations 27

5.2. Determination of Welding Parameters 29

5.2.1 Determination of Machine Parameters 29

5.3. Application of Friction Stir Welding 35

6. EXPERIMENTAL TEST AND ANALYSIS 37

6.1 Force Measurements 37

6.2. Mechanical Characterization Tests 47
6.2.1. Hardness Tests 48
6.2.2. Tensile Tests 54
6.2.3. One-Way Welded Tensile Tests 55
6.2.4. Bidirectional Welded Tensile Tests 64
6.3. Pearson Product Moment Correlation Coefficient 67
6.4. Surface Roughness 70
6.4.1. Stock Material Surface Roughness Measurements 72
6.4.2. Surface Roughness Measurements of Sample No. 74 76
6.4.3. Surface Roughness Measurements of Sample No. 134 78
6.4.4. Surface Roughness Measurements of Sample No. 254 80
6.5 Microstructural Analysis of Welding Zone 81
7. CONCLUSION 86
8. FUTURE WORK 89
REFERENCES 90
A. CODE OF PEARSON PRODUCT MOMENT CORRELATION COEFFICIENT 96
B.SEM IMAGES 97

LIST OF TABLES

Table 1 CNC Milling Machine Features 26
Table 2 The Influence of Materials, Tools, and Parameters on Performance 30
Table 3 Technical Parameter of Kistler Dynomemeter System [34] 40
Table 4 Forces measured in x, y, z axes according to different rotation speed and tool traverse speed 41
Table 5 Base Material Hardness Test Results 49
Table 6 Base Material Hardness Test Statisctic 50
Table 7 Hardness values and Welding Parameters 51
Table 8 Stock Material Tensile Test Results 57
Table 9 Parameter Table 57
Table 10 Tensile Test Results of Bidirectional Welded Specimens 66
Table 11 Correlation Heatmap of FSW Experiments 68
Table 12 Surface roughness results of stock material 72
Table 13 Surface Roughness Parameters and Profile Characteristics 73
Table 14 Profile Line Features 76
Table 15 Comparison of Surface Roughness Parameters Across Different Regions Sample No. 74 78
Table 16 Comparison of Surface Roughness Parameters Across Different Regions Sample No. 134 78
Table 17 Comparison of Surface Roughness Parameters Across Different Regions Sample No.254 80
Table 18 Feature Table [58] 82
Table 19 Table of Capabilities [22] 82

LIST OF FIGURES

Figure 1.1 Mazda Rx-8 Rear Door Outer Panel 3
Figure 1.2 The take-off moment of the Eclipse 500 manufactured using FSW 3
Figure 2.1 Friction stir welding in a butt joint configuration [5]. 6
Figure 2.2 Microstructure of friction stir welded aluminium alloy. A: Base material, B: Heat affected zone (HAZ), C: Thermomechanical affected zone (TMAZ), D: Dynamically recrystallized zone (DRZ) [5]. 7
Figure 5.1 CNC Milling Machine 26
Figure 5.3 75x75 AL 5754 sheet materials 27
Figure 5.2 Baykal Guillotine 27
Figure 5.4 Technical Drawing of the Fixture 28
Figure 5.5 Fixture CAD Model Isometric View 28
Figure 5.6 FSW Fixture 28
Figure 5.8 Sectional view of tool tip 34
Figure 5.9 a) Dynamometer and fixture assembly, b) Finished part, c) FSW process, d) Finished process 35
Figure 6.1 Kistler 9265B Dynamometer 38
Figure 6.2 Sensor placement of the Kistler dynamometer [34]. 39
Figure 6.3 Technical Drawing of the Kistler dynamometer [35] 39
Figure 6.5 Force and Time graph of Sample No. 154 45
Figure 6.4 Force and Time graph of Sample No. 77 45
Figure 6.6 Effect of Rotation Speed on Mean Forces 45
Figure 6.7 Effect of Tool Traverse Speed on Mean Forces 46
Figure 6.8 Mean Forces (F_y, F_x, F_z) Across Sample Codes 47
Figure 6.9 Indentation depth and standart forces 50
Figure 6.10 Effect of Rotation Speed on Hardness 52
Figure 6.11 Effect of Tool Traverse Speed on Hardness 53
Figure 6.12 Hardness Test 54
Figure 6.13 Measurement of the diameter of the cavity formed during the hardness test 54
Figure 6.14 Tensile samples cut by wire EDM 55

Figure 6.15 All Specimens 55
Figure 6.16 Wire Edm Machine 55
Figure 6.17 Technical Drawing of Tensile Test Specimen 56
Figure 6.18 Tensile Test Process 56
Figure 6.20 Engineering Stress- Strain graph of AL 5754 58
Figure 6.21 Engineering Stress-Strain graph of Sample No. 136-356-254 58
Figure 6.22 Engineering Stress-Strain graph of Sample No. 74-134-254 59
Figure 6.23 Combined Plot of Tensile Stress and Strain at Break (500 rpm Rotational Speed) 59
Figure 6.24 Combined Plot of Tensile Stress and Strain at Break (700 rpm Rotational Speed) 60
Figure 6.25 Combined Plot of Tensile Stress and Strain at Break (900 rpm Rotational Speed) 60
Figure 6.26 Combined Plot of Tensile Stress and Strain at Break (1100 rpm Rotational Speed) 61
Figure 6.27 Combined Plot of Tensile Stress and Strain at Break (1300 rpm Rotational Speed 61
Figure 6.28 Combined Plot of Tensile Stress and Strain at Break (1500 rpm Rotational Speed) 62
Figure 6.29 Combined Plot of Tensile Stress and Strain at Break (2000 rpm Rotational Speed) 62
Figure 6.30 Combined Plot of Tensile Stress and Strain at Break (2500 rpm Rotational Speed) 63
Figure 6.31 Combined Plot of Tensile Stress and Strain at Break (3500 rpm Rotational Speed) 63
Figure 6.32 Engineering Stress-Strain Curves of Aluminium Alloy AL 5754 Under Different Friction Stir Welding (FSW) Conditions 65
Figure 6.33 Alicona Infinite Focus 71
Figure 6.34 Samples no. 74 - 134 - 154 72
Figure 6.35 Stock material surface roughness histogram chart 74
Figure 6.36 Surface roughness measurement process of sample no. 74 76
Figure 6.37 Height Distribution of Sample No. 74 77
Figure 6.38 Sample 74, Region 1 Profile Graph 77

Figure 6.39 Sample 74, Region 2 Profile Graph 77
Figure 6.40 Sample 74, Region 3 Profile Graph 77
Figure 6.41 Sample 134, Region 1 Profile Graph 79
Figure 6.42 Sample 134, Region 2 Profile Graph 79
Figure 6.43 Sample 134 Region 3 Profile Graph 79
Figure 6.44 Sample 254, Region 1 Profile Graph 80
Figure 6.45 Sample 254, Region 2 Profile Graph 80
Figure 6.46 Sample 254 Region 3 Profile Graph 81
Figure 6.47 ZEISS MERLIN Scanning Electron Microscope used during the experiments [58] 81
Figure 6.48 Cross-sectional microstructures of aluminium welds processed with different parameters: a) Weld No. 136 showing defect-free structure, b) Weld No. 356 exhibiting internal defects and lack of fusion 83
Figure 6.49 Microstructural analysis of weld No. 136: a) Fine and oriented grains along the joining line, indicating proper grain refinement; b) Detailed view of grain orientation and deformation near the weld zone, highlighting the microstructural features. 83
Figure 6.50 SEM images of weld No. 136: a) Fine grains observed near the weld zone, indicating effective grain refinement; b) Higher magnification showing the detailed grain structure and orientation within the weld region. 84
Figure 6.51 SEM images comparing the microstructure of the base metal and weld center: a) Base metal showing uniform grain structure; b) Weld center displaying refined grains and grain alignment along the welding direction. 85

LIST OF ABBREVIATIONS

DRZ	Dynamically recrystallized zone
FSW	Friction Stir Welding
HAZ	Heat affected zone
TMAZ	Thermomechanical affected zone
MFCE	Metal Forming and Centre of Excellence
TRS	Tool Rotational Speed
TS	Traverse Speed
TTA	Tool Tilt Angle
Ra	Average roughness of profile
Rc	Mean height of profile irregularities of roughness profile
Rdq	Root-Mean-Square slope of roughness profile
Rq	Root-Mean-Square roughness of profile
Rp	Maximum peak height of roughness profile
Rp5	Mean peak height of roughness profile
Rsk	Skewness of roughness profile
Rsm	Mean spacing of profile irregularities of roughness profile
Rz	Mean peak to valley height of roughness profile
Rv	Maximum valley height of roughness profile
Rv5	Mean valley height of roughness profile
Rku	Kurtosis of roughness profile
Rmax	Maximum peak to valley height of roughness profile within a sampling length
Rt	Maximum peak to valley height of roughness profile

CHAPTER 1

1. INTRODUCTION

Joining is the process of joining two or more materials to form a permanent or temporary junction, as defined in an international standard ISO 857-1:2019 — Welding and associated processes — Terms and Definitions. The goal of this procedure is to ensure the materials' structural integrity and capacity to work together. International standards classify joining procedures such as welding, soldering, bonding, mechanical connections, and hybrid techniques. Soldering is a technique in which the filler metal is melted at a low temperature to form the junction, whereas welding uses heat and/or pressure to join materials. Adhesives are used in the bonding process to adhere surfaces, whereas mechanical connections make use of mechanical components such as rivets and screws [1].

Joining operations are widely used in manufacturing processes. These operations play an important role in the manufacturing process due to reasons such as the difficulty of producing parts with complex geometry, the necessity of materials in critical regions to have different components, and the fact that production is easier.

Among the joining operations, the welding method occupies a large place. Welding methods can be applied in a wide variety of ways, and each method has its own drawbacks and advantages. Therefore, it is essential to select appropriate welding parameters and welding methods according to the properties of the materials to be joined. “Some 50 different types of welding operations have been cataloged by the American Welding Society. Welding processes can be divided into two main groups: Fusion welding and solid-state welding. Fusion welding is done by melting the material and adding the filler material to the molten pool. The method in which filler metal is not used is called autogenous weld. Fusion welding involves a wide variety of processes” [2]. According to the American Welding Society, it is examined in 4 groups. These are arc welding, resistance welding, oxyfuel gas welding and other fusion welding processes. The second main group, solid state welding, is the method

in which materials are joined under combinations of heat and pressure. The heat used in this method is below the melting point and no filler metal is used. Welding methods belonging to this group are diffusion welding, friction welding and ultrasonic welding [2].

According to the American Welding Society, friction welding is a main welding process, and it was first developed in 1960, is applied by creating friction by touching a fixed part to an axially rotating part on a lathe. By contacting the parts, the first friction is created, then the rotation is terminated, and force is applied. In this method, since the material is upsetting and the resulting flashes are removed after the process, its dimensions change. Therefore, this needs to be considered at the design stage [3]. Friction welding is preferred commercially in the automotive, agricultural and aviation industries in the production of shafts and tubular parts.

Friction stir welding (FSW), one of the friction welding method, was developed by the Welding Institute of Great Britain in 1991. Although it is a new technique, it has shown rapid development compared to traditional methods [3]. Friction stir welding, which is applied to the top surface of two parts brought together with a rotating probe, has many advantages over traditional methods. Friction stir welding provides high strength, less crack formation. At the same time, since the materials are not melted, deformation is generally less. Therefore, it is easy to use on thin and delicate parts. Since the temperatures remain below the melting point, friction stir welding is suitable for materials with low melting points and even thermoplastic polymers can be easily applied. To demonstrate the capacity of the process, 135 meters of friction stir welding was used in the Eclipse 500 6-seater passenger aircraft produced by Eclipse Aviation of Albuquerque. The amount of rivet used was reduced by 60% and a variety of thermoplastics were used. It has been observed that the weld has a strength of 95% of the base material [3].

Friction stir welding (FSW) was first utilized in aircraft production in 2005, specifically on the loading ramp of the C-17 cargo aircraft. This process involved the joining of materials like AA7050 and T7451 for the components of the aircraft. Following this development, other companies also began adopting friction stir welding in their aircraft manufacturing processes. Eclipse Aviation Corporation replaced

traditional riveting with FSW in its aircraft production, eliminating the need for 7,000 rivets and fasteners in a single aircraft [4]. Today, friction stir welding continues to be used for assembling the frameworks, wings, and certain non-structural components of aircraft.

FSW is widely used worldwide in the production of fuel tanks, body parts, and suspension components of automobiles. The primary reasons for its preference are its speed and the lack of need for additional processing after welding [4]. Figure 2.8 shows an example of friction stir welding applied in the door construction of a Mazda vehicle.



Figure 1.1 Mazda Rx-8 Rear Door Outer Panel



Figure 1.2 The take-off moment of the Eclipse 500 manufactured using FSW

The FSW method, which has been applied in a wide variety of fields, has open areas for improvement. As a result of previous studies, determining the welding parameters

in experimental FSW studies on aluminium poses a problem. There is a lack of information regarding welding parameters, tool material and various parameters. At this point, it is important to determine tool rotational speed, tilt angle and other parameters correctly.

Friction Stir Welding (FSW) is a solid-state welding process that has revolutionized the joining of materials, particularly in applications where conventional fusion welding presents challenges. One of the primary advantages of FSW is its ability to minimize dimensional distortion during the welding process. Unlike fusion welding, where high heat input can cause significant thermal expansion and contraction, FSW operates below the melting temperature of the materials, reducing thermal stresses and preserving the dimensional accuracy of the work piece. FSW also offers solutions to the difficulties encountered when joining certain materials through fusion welding. For instance, aluminium alloys are prone to cracking, porosity, and loss of mechanical properties during fusion welding due to their high thermal conductivity and the formation of brittle intermetallic compounds. FSW eliminates these issues by avoiding the molten state entirely, resulting in stronger, defect-free welds with a fine-grained microstructure. Moreover, FSW enables the joining of dissimilar materials, which is often challenging in traditional welding methods due to differences in melting points and thermal properties. The solid-state nature of FSW allows for a seamless bond between materials with varying characteristics, expanding its applicability in industries such as aerospace, automotive, and shipbuilding [3].

In addition to its metallurgical benefits, FSW is also an environmentally friendly process. It does not require shielding gases, filler materials, or additional cleaning steps, making it a cleaner and more sustainable option compared to traditional methods. Overall, FSW addresses many of the limitations of fusion welding and provides a robust, efficient, and versatile solution for modern manufacturing challenges [3]

CHAPTER 2

2. FRICTION STIR WELDING

Friction Stir Welding (FSW) is a solid-state joining process introduced in 1991 by The Welding Institute (TWI) and has become a revolutionary technique in various industries such as aerospace, automotive, and shipbuilding. This process employs a non-consumable rotating tool that generates frictional heat, softening the material without reaching its melting point. As a result, FSW overcomes common issues found in conventional welding methods, such as porosity, cracking, and distortion. This makes FSW an excellent alternative for welding applications requiring high-quality joints with minimal defects [58].

In this chapter, the fundamentals of FSW will be discussed in detail, starting with its diverse applications across different sectors and its adaptability to various materials and thicknesses. The formation of the weld seam and the metallurgical structure changes during the process will be analysed to provide insights into the structural integrity of FSW joints. Additionally, the impact of critical welding parameters, such as tool geometry, rotational speed, and traverse speed, on the process's efficiency and weld quality will be explored. The advantages of FSW, including its ability to produce defect-free joints, reduced distortion, and environmentally friendly operation, will be highlighted. Finally, the limitations of the method, such as the challenges in welding certain materials and the initial setup costs, will also be addressed.

This chapter aims to provide a comprehensive overview of FSW, its applications, and its implications for industrial and research purposes, offering valuable insights into this innovative welding method.

2.1. Friction Stir Welding Application

During the FSW process, plastic deformation is created in the welded material and diffusion bonding occurs. In this process, which is mainly created through heat, the surfaces of the tool in contact with the part create friction heat. There are two main tages in FSW welding. These are plunge and dwell phase, traverse and welding phase

[5]. The parts to be welded are placed on the table with the necessary jigs and fixtures. While the tool is rotated at high speed, it slowly plunges into the work piece. The vertical force reaches its maximum when the tool pin contacts the work piece during the plunge movement. As the area heats up, the vertical force decreases due to the material softening [5]. The area called the tool shoulder ensures that vertical movement is stopped. It usually penetrates the work piece by 0.05-0.2 mm. The tool shoulder is the part that contributes the most to heat generation caused by friction [5].

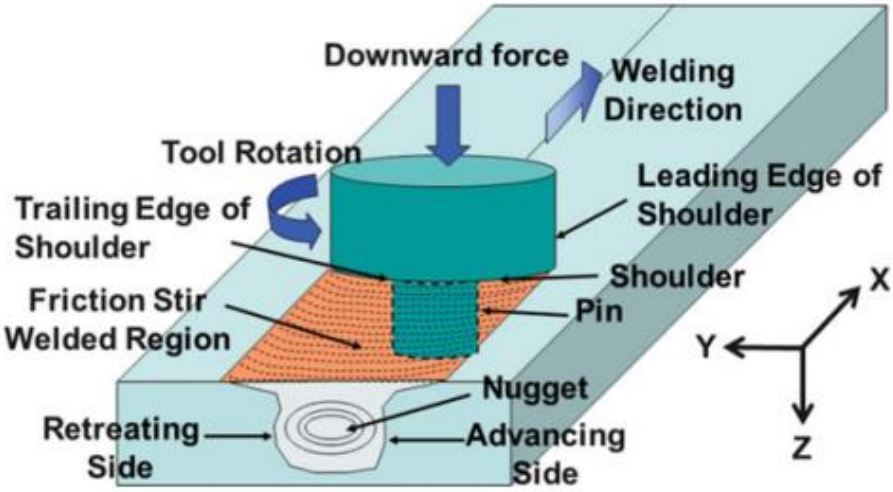

Figure 2.1 Friction stir welding in a butt joint configuration [5].

The area of the tool in contact with the work piece is called the tool shoulder. The shoulder may be concave or convex. The tool pin ensures the material flow inside the weld. The rotation rate of the tool has the largest contribution to heat input and material flow. The plunge movement parameters of the team are plunge rate, plunge depth, plunge force [5].

2.2 Weld Seam Form and Metallurgical Structure

In friction stir welding, there is no high heat input, and the heat affected zone is quite narrow. Different metallurgical structures emerge depending on the fusion welding method. From the weld center to the main material, there are the dynamically recrystallized region, the thermomechanical affected region, and the region under the influence of heat.

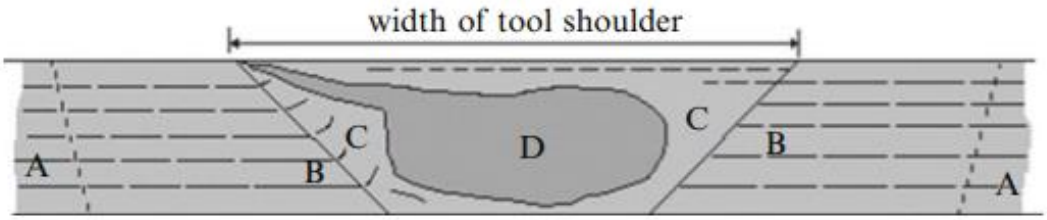

Figure 2.2 Microstructure of friction stir welded aluminium alloy. A: Base material, B: Heat affected zone (HAZ), C: Thermomechanical affected zone (TMAZ), D: Dynamically recrystallized zone (DRZ) [5].

HAZ: It is the area that is close to the primary content. Heat affects the material in this area, changing its composition and characteristics. There's no plastic deformation. In comparison to melting welds, this zone is often narrower in friction stir welding because of the lower heat input.

TMAZ: This region is adjacent to the HAZ region, where heat affects, and plastic deformation occurs. With the effect of mixing, a fine-grained structure is formed, and plastic deformation also occurs. The heat input generated during mixing changes the microstructure and mechanical properties of this region.

DRZ: The welding centre is where this area is situated. It is sometimes referred to as a welding ingot, despite seeming like a mound of metal. Its cross-section resembles a pattern of rings that alternate at regular intervals [5].

2.3 Welding Parameters

Although different welding parameters are selected for various materials, the tip size is generally chosen to be 0.2 mm smaller than the thickness of the material to be welded. Welding parameters directly affect weld quality. Therefore, it is of great importance for the action to be taken. The parameters that determine the performance of friction stir welding can be grouped into 3 main groups. These are;

1) Machine Parameters
    a) Tool Rotational Speed (TRS)
    b) Traverse Speed (TS)
    c) Tool Tilt Angle (TTA)
    d) Plunge Rate
    e) Axial Forces

2) Tool Parameters
    a) Shoulder Diameter and Profile
    b) Pin Diameter and Profile
    c) Pin Height
    d) Tool Material
3) Other Parameters
    a) Clamping and fixtures
    b) Dwell Time
    c) Work Piece Properties
    d) Welding Condition [12]

Although there are many parameters in friction stir welding, the most important ones are tool rotational speed and shoulder diameter. As the shoulder diameter increases, the heat input also increases due to the increase in the friction surface [6].

2.4. Advantages of the Method

Friction stir welding (FSW) has several significant advantages compared to traditional welding methods, making it a preferred choice for many applications. Metallurgically, FSW provides excellent weld quality and is applicable to a wide range of materials, including some that are considered “nonweldable” by traditional fusion methods. This process is particularly advantageous for materials like aluminium alloys, which may crack during fusion welding. FSW is a solid-state process, ensuring low distortion of the work piece, high joint strength, no loss of alloy elements, and a fine microstructure with no cracking. It also enables the welding of materials with different structures and alloys with high cracking sensitivity, which are frequently encountered in fusion welding methods. Most extruded or cast parts can be welded using this method.

In terms of cost and energy efficiency, FSW consumes far less energy than conventional welding methods, making it highly cost-effective. It is a relatively simple process that does not require filler wires, further reducing costs. Since it is generally applied on CNC machines, it is highly suitable for automation, adding to its efficiency. Unlike traditional methods, the oxide layer does not need to be removed immediately after welding in the FSW process, reducing maintenance requirements.

Environmentally, FSW is a sustainable option as no harmful gases are released during the process, and it does not require shielding gas, surface cleaning, or solvent degreasing. Additionally, it eliminates the production of fumes, gases, or smoke, enhancing safety and environmental friendliness. Postweld finishing is often unnecessary, and the absence of arc glare or reflected laser beams adds to its safety. Overall, FSW is a highly efficient process that combines metallurgical excellence, environmental benefits, and energy savings, making it a superior choice for modern manufacturing needs [3].

2.5. Limitations of the Method

It's crucial to prepare the surface before welding. As a result, prior application is needed. The front faces of the components are welded together first during the process. The components must be welded from the other side, though, if complete penetration is required. Designing the apparatus and fixtures is necessary since the work pieces must be fastened to the table. Certain alloy sheets still have modest welding speeds as compared to mechanical arc welding [6].

CHAPTER 3

3. LITERATURE REVIEW

The historical development of welding techniques dates to ancient times, with early methods such as forge welding being utilized to join metal parts. The advent of the Industrial Revolution in the 19th century marked significant advancements in welding, leading to the development of modern techniques like electric arc welding and gas welding in the early 20th century. These innovations have been extensively documented in welding literature.

In 1991, The Welding Institute (TWI) introduced Friction Stir Welding (FSW), a solid-state joining process that has since been widely adopted across various industries. FSW utilizes a non-consumable tool to join two facing workpieces without melting the material, resulting in high-quality welds with minimal distortion. Subsequent research has focused on the mechanical properties of FSW joints, exploring factors such as tensile strength, hardness, and microstructural characteristics. Recent studies have also examined the forces generated during the FSW process, aiming to optimize parameters and enhance process efficiency [19].

In this study, literature will be examined in terms of welding parameters. The studies conducted for each parameter are grouped into 4 main groups. First group machine variables, the second group is tool variables. Parameters such as clamping and fixtures and dwell time are excluded from the scope since they have low impact on welding performance. The third group is Double Sided Friction Stir Welding Applications, and the last group is Friction Stir Welding for AA 5754 Aluminium Alloy.

3.1. Effects of machine parameters in friction stir welding

Kafalı and Ay examined the mechanical properties and changes in the internal structure of the materials that applied FSW to 6013 aluminium alloys. Aluminium materials are widely preferred in the aviation industry due to their low density and high strength. This material, used in wings and fuselages, is usually joined with rivets. However, the riveting process causes the weight of the aircraft to increase, and the rivet holes create stress concentrations for fatigue cracks. In this case, it may be considered to resort to traditional welding methods, but in these methods, a

deterioration in mechanical behaviour is observed as the material is heated to the melting temperature. Considering the low weldability of high-strength materials, FSW is a method that is likely to give better results than traditional methods. In the study, hardness test, tensile test and fatigue test were applied, and the microstructure was examined using optical and electron microscopy. The ratio of the breaking stress of the welded material to the breaking stress of the welded main material gives the welding efficiency. In the study, 75% resource efficiency was achieved. Regions formed in the FSW method; main material, heat affected zone, thermo-mechanical heat affected zone and welding center. The lowest hardness and strength were observed in the weld center. Microstructural analysis showed that ductile fracture occurred [7].

Kurt, Boz and Ozdemir investigated suitable welding parameters for FSW in their study. They applied butt welding to Al materials at different traverse speeds which are 6.25, 10, 16, 20 mm/min and 20 mm/min and tool rotation speeds of 800 rpm. It was observed that the tensile strength increased as the traverse speed increased, and it was also concluded that the hardness values increased with the traverse speed [8].

In his study, Özbekmez examined the mechanical properties of CuZn30 sheets by combining them with electric arc welding and friction stir welding. In the study, a constant traverse speed of 12.5 mm/min and rotation speeds of 600, 630, 1000, 1600 rpm were used. After welding, tensile, bending and micro hardness tests were performed, and microstructure characterization was examined. While no welding errors occurred at 500, 600 rpm and 12.5 traverse speeds, the surface quality was poor at 1000 rpm. However, no situation affecting the strength occurred. Welding errors that reduce weld strength have been observed in joints made with electric arc welding. At the same time, edge chipping, starting and ending points, welding speed and slag residue errors occurred [9].

In his study, Cavaliere aimed to optimize the welding parameters using the multi-objective optimization software FRONTIER (ESTECO). According to the experimental results, he calculated the weights of the process parameters and developed correlations between different parameters. As a result, it was determined that the welding force generally depends on the hardness of the base material and shoulder/pin height. At the same time, it was determined that mechanical properties

generally improved at high speeds, while inhomogeneities in the microstructure were detected at low speeds [10].

AA 2050 is an aluminium alloy containing Li. It has been frequently preferred in the aviation industry recently. It is a material that is likely to be preferred over traditional materials due to its corrosion resistance, high strength and high damage tolerance. Kumar et al. welded 5mm thick AA2050-T84 plates with traverse speeds ranging from 1 mm/s to 4 mm/s. In the study, tool rotational speed was kept constant at 600 rpm and tool tilt angle was kept constant at 1.5°. The tool left-hand taper is threaded, made of H13 steel material. As a result of the work carried out, the nugget zone grain size in the weld center decreased from 17.9 μm to 10.5 μm. It has been observed that mechanical properties increase with increasing traverse speed. While the maximum tensile strength was 388.6 MPa, elongation was 9.19%, the bonding efficiency was observed to be 70.2% [11].

Venu et al. It is focused on optimizing the process parameters of the FSW method. Various experiments were carried out on AA2014-T651 plates using straight, tapered and threaded tapered cylindrical tool pin profiles. Mechanical properties such as tensile strength, yield strength, impact strength, elongation percentage and hardness tests were carried out. With the optimization tools performed using the multi-objective algorithm, the three most suitable combinations were found to be 940 rpm and 32mm/min, 1100 rpm and 40 mm/min, 1205 rpm and 45 mm/min. The results found are supported by experiments [12].

3.2. Effects of tool parameters on friction stir welding

In friction stir welding, tool parameters directly affect the quality of the welded material. Tool parameters are of great importance in terms of providing heat input to the process and controlling the flow of material during welding. For this reason, studies on tool parameters are included in this section of the report.

Banik et al. combined AA 6061-T6 material with friction stir welding technique using 3 different tool geometries. They researched which tool is best in terms of end-resource features. Three different geometries such as taper, taper-threaded and cylindrical threaded were used in the study, and they found that the geometry that gave the best welding properties was Taper-threaded. As a result of mechanical tests of the samples

taken from the weld made with TT tool, UTS-209.916 MPa, YS-128 MPa, percent elongation-13.26%, hardness-79.69 Hv were obtained [13].

Wu et al. investigated the effect of the tool tip on material flow and thermodynamic processes during friction stir welding of aluminium alloy plates. For this purpose, they developed a computational fluid dynamics model. Four tool designs with different tooth pitches were developed and then flow analysis of each was performed. As a result of the analysis, it was determined that as the number of teeth on the pin increases, the total heat production decreases. Thus, the maximum temperature reached during the process was reduced. In the scanning electron microscope analysis, it was observed that the boundaries of the thermos mechanically affected area matched each other [14].

Rajakumar and his colleagues performed friction stir welding experiments on aluminium parts that are generally joined by fusion welding. Comparing the tool parameters and welding quality in friction stir welding, the author analysed the effect of process and tool parameters to make connections faster and more reliably. As a result of the trials, tensile test, micro hardness and microstructure analysis were carried out. It has been determined that better mechanical properties are provided if 1400 rpm rotation speed, 60 mm/min welding speed, 8 kN axial force, 15 mm shoulder diameter, 5 mm pin diameter and 45 HRc tool are used [15].

Khan et al. conducted various experiments to realize materials that are difficult to join with traditional methods using friction stir welding with optimum tool parameters. As a result of the studies, it has been revealed that the most suitable friction stir welding materials are titanium, nickel and steel. As a result of the increasing shoulder diameter, the contact area between the base metal and the tool increases, thus increasing the heat input. The optimum shoulder diameter should be selected to prevent rapid wear of the tool and to ensure the best mechanical properties of the welded material [16].

Hepeng Jia, Kai Wu, Yu Sun, Fengfeng Hu, Yongyong Lin and Huade Zhang, studies were conducted on the determination and optimization of welding parameters for high-speed friction stir welding (FSW). In the article, a cost-effective experimental design was created by using the Taguchi method in the process of determining the welding parameters and maximum information was obtained with the minimum number of experiments. In the study, basic parameters such as tool rotational speed (4000, 5000,

6000 rpm), welding speed (3000, 4000, 5000 mm/min) and plunge depth (0.2, 0.25, 0.3 mm) were taken into consideration. The effects of these parameters on the weld quality were evaluated and the optimal parameter combination was determined as 5000 rpm rotational speed, 3000 mm/min welding speed and 0.25 mm plunge depth. The results show that this combination optimizes the mechanical properties and minimizes welding defects. This approach allowed the systematic optimization of welding parameters [17].

Cem Celal Tutum, a comprehensive study was conducted on the determination and optimization of welding parameters for the Friction Stir Welding (FSW) process. In this thesis, the welding parameters, tool rotation speed and welding speed, were optimized by both experimental and mathematical modelling. First, temperature distributions and material behaviours were analysed using thermal models, and residual stresses formed during welding were investigated. In the optimization process, algorithms such as Sequential Quadratic Programming (SQP) and Non-dominated Sorting Genetic Algorithm II (NSGA-II) were used to determine the ideal parameter combinations that maximize welding speed while minimizing residual stresses. In addition, in line with the experimental data and modelling results, the temperature and stress profiles formed during welding were evaluated in detail, and the effects of these parameters on weld quality were analysed. These approaches provided important guidance for increasing process stability and optimizing mechanical properties during the FSW process [18].

Many existing studies in literature have focused on the determination of mechanical properties of joints obtained by the FSW method. These studies have evaluated the effectiveness and performance of the method by examining the strength, hardness, and microstructural properties of the welded areas. However, in this study, a subject that was lacking in literature was addressed and a process analysis was performed by measuring the forces generated during the process. In this way, the effect of the basic parameters of the FSW method on the weld quality was examined in more detail and it was aimed at understanding the method better.

3.3 Double Sided Friction Stir Welding Applications

Bidirectional Friction Stir Welding (DS-FSW) is important due to its performance, especially in welding thick plates. In the traditional friction stir welding (FSW) method, the application of heat and deformation from a single surface can lead to incomplete bonding and porosity in the root area. In addition, in sectors such as aviation and automotive, where lightweight but high-strength materials are used, the homogeneity and strength advantages offered by this method are of great importance. Bidirectional processing provides improvements in the microstructure by ensuring that thermal and mechanical effects are distributed equally. For this reason, literature studies conducted with bidirectional friction stir welding are included in this section of the report.

Thakur et al. (2024) conducted a study to explore the influence of welding parameters on bidirectional friction stir welding (DS-FSW) for AA6061-T6 aluminium alloys. This research aimed to optimize the microstructural and mechanical properties of welded joints, addressing challenges like grain non-uniformity and inadequate precipitate distribution. The study was motivated by the need for improved joint strength and ductility in aerospace and automotive applications using thick aluminium plates. The researchers applied response surface methodology (RSM) to systematically vary process parameters, including rotational and transverse speeds during the two welding passes. They utilized advanced analytical techniques, such as EBSD, SEM, and TEM, to evaluate the microstructure and tensile tests for mechanical properties. The findings highlighted that optimized parameter significantly enhanced the welds' quality. The stir zone (SZ) exhibited refined grains, a high fraction of high-angle grain boundaries, and a uniform distribution of strengthening precipitates. This led to a maximum ultimate tensile strength of 223 MPa with 75% joint efficiency and 14% elongation. The fracture morphology confirmed a ductile failure pattern, while improper parameter settings resulted in defects and reduced strength. This study underscores the critical role of parameter optimization in achieving superior weld integrity and mechanical performance [19].

In the study published by Jiuxing Tang et al. in 2024, the effects of a new "splat cooling" assisted bidirectional friction stir welding (SDS-FSW) technology on the

weld quality of medium-thickness Al-Cu alloys were investigated. The researchers compared the conventional bidirectional friction stir welding (DS-FSW) and SDS-FSW methods and analysed the changes in the microstructure and mechanical properties in the weld area. The aim of the study is to obtain higher strength welds in Al-Cu joints with intensive industrial use. The SDS-FSW method reduced the peak temperature and high temperature during welding with the "splat cooling" used during the process, resulting in the formation of a thinner and more homogeneous intermetallic compound (IMC) layer. In the study, the microstructure and mechanical properties in the weld area were examined in detail using electron microscopes (SEM, EBSD, TEM) and mechanical testing devices. As a result, the maximum tensile strength of the joints obtained by the SDS-FSW method was measured as 159.26 MPa, which showed a 42% increase compared to the DS-FSW method. In addition, the welds obtained by the SDS-FSW method showed better deformation resistance by exhibiting mixed ductile-brittle fracture properties. These results reveal that SDS-FSW is an effective method to obtain stronger and more homogeneous welds in Al-Cu joints [20].

Tang et al. (2024) investigated the effects of synchronous bidirectional friction stir welding (SDS-FSW) on microstructure and mechanical properties of 6061 aluminium alloy. The aim of the study was to compare the SDS-FSW method with the conventional single-sided (SS-FSW) and sequential bidirectional friction stir welding (CDS-FSW) methods to improve the weld quality and obtain more homogeneous microstructure properties. The temperature distribution and material flow during welding were investigated by both experimental and numerical modelling. The results showed that SDS-FSW provided higher temperature input and more homogeneous temperature distribution. In particular, the SDS-FSW method provided a finer grain structure and balanced microhardness properties in the weld zone, increasing the mechanical strength. The maximum tensile strength was measured as 192.8 MPa in the SDS-FSW method, which was an improvement of over 30% compared to the SS-FSW method. In addition, rotating the upper and lower welding tools in opposite directions in the SDS-FSW method provided better material flow and microstructure homogeneity. This study reveals that SDS-FSW is an effective method for welding medium thickness aluminium alloys, especially in industries such as aerospace and automotive [21].

Tiwari et al. (2024) investigated the effects of SiC nanoparticles on the welding process of AA7075 and AA2024 aluminium alloys by bidirectional friction stir welding (DS-FSW). This study aimed to improve the quality of the weld and improve the mechanical properties in dissimilar aluminium alloys. In the study, microstructure and mechanical properties as well as crack growth rates were evaluated. By adding SiC nanoparticles to the weld zone, grain growth in the weld zone was suppressed and significant increases in weld quality were obtained. According to the research results, SiC nanoparticles formed smaller grain sizes in the weld stir zone, which led to a 62% increase in microhardness and significant improvements in tensile strength. Electron backscatter diffraction (EBSD) and scanning electron microscope (SEM) analyses revealed that high-angle grain boundaries were dominant in the weld zone and a homogeneous nanoparticle distribution was achieved. The addition of SiC increased the fatigue strength of the weld zone by reducing the crack growth rate. The Zener pin effect strengthened the grain boundaries, and the continuous dynamic recrystallization transformed the microstructure into a fine-grained structure. These results show that SiC nanoparticles significantly improved the mechanical properties of the DS-FSW welded metal matrix composites [22].

Hendrato et al. (2024) investigated the effects of one-step bidirectional friction stir welding (one-step DFSW) on weld mechanical properties and fatigue crack propagation rate in AA6061-T6 aluminium alloy. The research was carried out to reduce the long processing times of conventional bidirectional welding methods and to reduce costs. In the study, different rotational speeds (1500/900 rpm, 1500/1200 rpm, and 1500/1500 rpm) were used for the upper and lower tools, and the effects of these parameters on the microstructure, hardness distribution, tensile strength, and fatigue performance in the weld zone were investigated. The results showed that rotational speeds significantly affected the weld quality. The lowest fatigue crack propagation rate was obtained at a rotational speed of 1500/1500 rpm. At this speed, the material in the weld zone was mixed homogeneously, the microstructure turned into a fine-grained structure, and the hardness distribution was optimized. In fatigue tests, the Paris constants of the crack propagation rate were calculated as

$$C = 4.348 \times 10^{-8}, \quad n = 4.16 \tag{1}$$

However, the tensile strength of the welded joints showed 45% efficiency compared to the base metal. The study reveals that the welds obtained by this method are especially suitable for joining thick plates [23].

Ojo and Oboro (2024) evaluated the step bidirectional friction stir welding (SDFSW) method to reduce root defects of aluminium sheets. The study compared it with the conventional single-sided friction stir welding (SFSW) method to eliminate root defects and material flow deficiencies in thick aluminium sheets. The study investigated the microstructure, mechanical properties and fracture modes during welding of 6 mm thick aluminium sheets. The SDFSW method effectively eliminated root defects due to penetration by providing bilateral deformation and material flow consolidation. The results showed that SDFSW welds presented higher tensile strength (48.41 MPa vs. 34.24 MPa) and improved microstructure uniformity compared to single-sided welds. Fractography analyses revealed that SDFSW method exhibited a ductile behaviour in fracture mode and provided better load-carrying properties. This study emphasizes that SDFSW is an effective method to obtain high strength and flawless welds, especially for thick aluminium sheets [24].

Thakur et al. (2023) investigated the effects of different welding pass parameters on mechanical properties in welding processes performed on AZ31B magnesium alloy using bidirectional friction stir welding (DS-FSW) method. In the study, the process parameters of the first and second passes were optimized using the response surface method (RSM) and properties such as microstructure, microhardness and tensile strength in the weld zone were analysed. The results showed that the first and second pass parameters have a strong interaction on the microstructure in the weld zone. Finer grains were formed in the overlap zone compared to the first and second stir zones, and this provided a significant increase in microhardness. 84% joint efficiency and 12% elongation ratio were obtained under optimized welding conditions. Tensile test results revealed that the fracture behaviour of the welds performed with the DS-FSW method had a more complex and brittle-ductile structure compared to the base material. The heterogeneous structural features formed in the weld zone made the weak areas of the joints apparent. This study highlights that optimizing the bidirectional friction stir welding method is an effective way to obtain stronger and more homogeneous welds in light magnesium alloys [25].

3.4. Friction Stir Welding for AA 5754 Aluminium Alloy

M. Haghshenas et al. (2014) investigated the effects of diffusion bonding as a welding aid in a study conducted to join AA5754 aluminium alloy with high strength steels (DP600 and 22MnB5) by friction stir welding (FSW). The study evaluated the effects of two different types of steel coatings (Zn and Al-12Si) on the microstructure and mechanical properties in the weld zone. The parameters used during the FSW process (rotation speed, traverse speed, and pin penetration depth) were analysed in terms of the formation of intermetallic compounds in the weld zone and the effects on the welding performance. The results showed that low welding speeds improved the mechanical properties by affecting the formation of intermetallic compounds (e.g., FeAl and Al5Fe2). In particular, the FeAl compound provided higher toughness and strength, while the Al5Fe2 compound exhibited a more brittle structure. The thickness and type of intermetallic compounds in the weld zone played a decisive role on the strength of the welded joints. It was found that the joints made with DP600 steel exhibited higher strength and less brittleness than those made with 22MnB5 steel. In addition, steel coatings (Zn and Al-12Si) increased the efficiency of the weld and facilitated diffusion bonding. This study shows that high strength steels coated with AA5754 aluminium alloy can be successfully joined by FSW and that this has a wide application potential in industries requiring lightness and strength, such as automotive [26].

Costa et al. (2015) investigated in detail the effects of different material orientations and tool geometries on friction stir lap welding (FSLW) of AA 5754-H22 and AA 6082-T6 aluminium alloys. The study analysed the weld strength, microstructure and material flow using cylindrical and tapered pin geometries with different shoulder/pin diameter ratios. The findings showed that the weld strength is highly dependent on the material orientation, tool geometry and the size of the hooking defect formed during welding. In the material orientation, the placement of AA 6082-T6 as the top plate (D65 configuration) provided higher strength compared to the case where AA 5754-H22 was the top plate (D56 configuration). In the D65 configuration, the weld strength ranged from 90% to 100% of the maximum strength of the AA 5754-H22 material in terms of maximum load, while in the D56 configuration this ratio remained between 40% and 65%. The best results were obtained with the CN8 tapered tool, which has a

low shoulder/pin diameter ratio. Welds made with the CN8 tool resulted in less material flow in the weld zone and minimal hooking defects. The size and shape of the hooking defect have a significant effect on the weld strength. Larger hooking defects were detected in the D56 configuration, reducing the weld strength. In contrast, in the D65 configuration, less material flow and small hooking defects increased the weld strength [27].

Ghiasvand et al. (2023) analysed the effects of single-pass and double-pass welding methods on the microstructure and mechanical properties by joining AA 5754-H111 aluminium alloy and Mg AZ31-O alloy by friction stir welding (FSW). In the study, 500 rpm and 600 rpm rotational speeds and 30 mm/min and 45 mm/min traverse speeds were used, and the microhardness, tensile-shear strength and fracture behaviour of the welded joints were investigated in detail. According to the results obtained, the highest tensile-shear force was measured as 3121 N at 500 rpm rotational speed and 45 mm/min traverse speed in single-pass welding. The maximum tensile-shear force in double-pass welding was recorded as 2500 N on D600-45 sample. However, instead of increasing the weld strength, the double-pass welding process only improved the microstructure homogeneity. Microhardness analysis showed that Al12Mg17 and Al3Mg2 intermetallic compounds in the stir zone increased the hardness between 152 HV and 221 HV. In addition, the "hook" defect formed at 600 rpm rotational speed and low traverse speed reached the highest level of 2.23 mm. It was observed that the fracture in all samples started in the regions where the intermetallic compounds were present and progressed through the Mg alloy. This fracture occurred as a combination of ductile and brittle properties [28].

Datta and Bhargava (2024) investigated the joining of AA6061 and AA5754 aluminium alloys with 1.5 mm thickness by friction stir welding (FSW) method and evaluated the effects of different rotational speeds (950 rpm - 1400 rpm) and traverse speeds (50 mm/min - 100 mm/min) on the mechanical properties, microstructures and formation behaviours of welded samples. In the study, as a result of tensile tests, the highest tensile strength was measured as 197 MPa at 1400 rpm rotational speed and 75 mm/min traverse speed, and the ductility reached the maximum level with 12% at the same parameters. On the other hand, the lowest tensile strength and ductility were recorded as 131 MPa and 3% at 950 rpm rotational speed and 75 mm/min traverse speed, respectively. In the microhardness analysis, the hardness increase in the stir

zone (SZ) was observed especially at high rotational speeds and low traverse speeds. This situation shows that dynamic recrystallization is effective in this region. In the formation tests, it was determined that AA5754 has higher formation capacity compared to AA6061 and the formation behaviour of the welded samples is somewhere between the properties of both alloys [29].

Ferda Mindivan et al. (2024) investigated the joining of AA5754 aluminium alloy by friction stir welding (FSW) method and analysed the microstructure, mechanical properties and corrosion behaviour in the weld zone in detail. In the study, as a result of welding processes performed at 1600 rpm rotational speed and 125 mm/min traverse speed, the tensile strength of the welded samples was 84% of the strength of the base material and was measured as 196 MPa on average. The hardness values increased due to recrystallization in the nugget zone and varied between 100-120 HV. In corrosion analyses, the nugget zone and thermo-mechanically affected zone were found to have lower corrosion potential than the heat-affected zone but showed higher values in terms of corrosion current density. In particular, the highest corrosion current density was measured in the nugget zone with 128000 x 10^{-9} A/cm². In microstructure studies, it was observed that the risk of intergranular corrosion at grain boundaries increased due to the accumulation of Mg-rich phases in the nugget region. These findings reveal that AA5754 aluminium alloy can be successfully joined by FSW method, but additional surface treatment techniques may be required to increase the corrosion resistance of the nugget region [30].

Furkan Sarsılmaz et al. (2009) investigated the effects of different rotational speeds and advancement speeds on the mechanical properties of the weld zone by joining AA5754 and AA5083 aluminium alloys with friction stir welding (FSW). In the study, destructive (tensile, notch impact, fatigue) and non-destructive (fluoroscopic) tests were applied to the samples. In fluoroscopic examinations, it was observed that defects such as void and tunnel formation occurred in the weld seam at low rotational speed (900 rpm) and high advancement speed (250 mm/min). The best mechanical properties were obtained at 1400 rpm rotational speed and 250 mm/min advancement speed. In tensile tests, the B2 sample joined at 1400 rpm rotational speed and 250 mm/min advancement speed gave the best result with 178 MPa tensile strength and 16.5% elongation. With the same parameters, fatigue strength was measured as 64 MPa and showed a fatigue performance exceeding 10^6 cycles. On the other hand, due to weld

defects at low rotational speeds, tensile strength was recorded as 126 MPa and fatigue strength was only 23 MPa in specimen A2. In notch impact tests, the highest toughness was measured as 26 J in specimen B1 combined with 1400 rpm rotational speed and 160 mm/min traverse speed. The study shows that by selecting appropriate parameters, FSW method can produce welds with high mechanical performance [31].

Çakır and Çelik (2017) investigated the effects of welding parameters on mechanical and microstructural properties during the joining of AA5754 aluminium alloy and pure copper by friction stir welding (FSW). In the study, 780 rpm and 1330 rpm rotational speeds, 20 mm/min and 50 mm/min traverse speeds and 0 mm and 1 mm tool shift positions were used. Mechanical properties were evaluated by tensile test and microhardness measurements, and the microstructure was analysed by optical microscope. The highest tensile strength was obtained at 1330 rpm rotational speed, 20 mm/min traverse speed and 1 mm tool shift position and was measured as 165.5 MPa. This provided 80.18% welding performance compared to the strength of AA5754 base material. The lowest tensile strength was recorded as 50 MPa at 780 rpm rotational speed and 50 mm/min traverse speed. In microhardness analyses, hardness values varied between 54 HV (AA5754) and 88 HV (copper) at the weld centre. A more homogeneous microstructure was formed at 1330 rpm rotational speed, and it was determined that small copper particles were regularly distributed in the aluminium matrix. In contrast, large copper particles and a more irregular structure were observed at 780 rpm rotational speed. It was determined that tool positioning has a significant effect on weld quality. While voids and mechanical bonding deficiencies were observed in the microstructure in the "0" position joints, homogeneous mixing and higher tensile strength were obtained with 1 mm tool shift. The study shows that AA5754 and copper can be successfully joined by selecting appropriate welding parameters [32].

Tolun (2020) analysed the effects of different mixer tip geometries on weld strength, microstructure and mechanical properties by combining EN AW-5754 and EN AW-5083 aluminium alloys with friction stir welding (FSW). In the study, screw, conical and cylindrical mixer tip geometries were used, and welding operations were carried out with fixed parameters (450 rpm rotation speed, 50 mm/min traverse speed, 0-degree shoulder angle). The mechanical performance of the samples was evaluated with tensile tests and microhardness measurements. The results showed that the

highest weld strength was measured as 188.76 MPa in welds made with screw mixer tip. This value was determined as 172.34 MPa in welds made with conical mixer tip and 115.59 MPa with cylindrical tip. In optical microscope examinations, it was observed that screw and conical tips created smoother weld profiles, while gaps and roughness occurred in welds made with cylindrical tip. In microhardness analyses, it was determined that the hardness values in the weld zone in all samples were higher than the base material hardness. Especially in welds made with screw tips, the hardness in the weld zone reached up to 120 HV. This study shows that EN AW-5754 and EN AW-5083 aluminium alloys can be successfully joined with the FSW method and that the screw mixer tip geometry provides the highest weld strength and microstructure homogeneity [33].

CHAPTER 4

4. OBJECT OF PRESENT INVESTIGATION

The present study aims to explore and define the optimal process parameters for the friction stir welding (FSW) of 5754 aluminium alloy. This investigation builds on existing literature, which has extensively analysed the effects of traverse speed and rotational speed on weld quality. However, the scope of these prior studies remains fragmented, necessitating a comprehensive evaluation to achieve improved mechanical properties while minimizing tool wear and surface imperfections.

A key objective of this research is to identify process parameters that result in minimal forces exerted on the machine, thereby reducing tool damage and enhancing the operational efficiency of the welding system. Specifically, the study targets the following goals:

1. **Improvement of Mechanical Properties:** Achieve optimal values of hardness, tensile strength, and elongation.
2. **Enhancing Surface Finish:** Minimize surface roughness to produce a visually and functionally superior weld.
3. **Balancing Process Efficiency:** Optimize traverse speed and rotational speed to ensure high-quality welds without compromising the tool's integrity.

Context from Literature

Previous research has identified traverse speed and rotational speed as critical factors influencing the welding performance of aluminium alloys. Studies have demonstrated that excessively low rotational speeds (<500 RPM) fail to produce sufficient material mixing, resulting in poor weld quality. Conversely, excessively high rotational speeds (>3500 RPM) degrade the surface finish due to overheating and excessive plastic deformation.

Similarly, traverse speed plays a crucial role in controlling the heat input and mechanical properties of the weld. It has been observed that traverse speed below 10 mm/min lead to insufficient welding progress, whereas rates above 120 mm/min compromise the weld quality, resulting in suboptimal mechanical properties and structural defects. The sweet spot for achieving a balance between heat input and

mechanical properties lies within a narrower range, which this study aims to further refine.

Experimental Methodology and Observations

To achieve the stated objectives, this study systematically examines a wide range of rotational speeds (500–3500 RPM) and traverse speeds (10–250 mm/min). Preliminary trials revealed the following key findings:

- Rotational speed below 500 RPM resulted in inadequate material mixing, rendering the weld structurally deficient.
- Rotational speed exceeding 3500 RPM led to significant surface degradation due to excessive heat generation and turbulence.
- Traverse speed below 10 mm/min caused inefficient process times, while rates above 120 mm/min exhibited a sharp decline in weld quality.

This study identifies an optimized parameter range that ensures a balanced heat generation, effective material mixing, and minimal surface irregularities.

Expected Outcomes

By the conclusion of this research, it is expected that the following contributions will be made to the field of aluminium alloy welding:

1. **Refined Process Parameters:** Establishment of an ideal traverse speed and rotational speed range tailored for 5754 aluminium alloy.
2. **Enhanced Mechanical Insights:** Comprehensive understanding of the interplay between process parameters and mechanical properties.
3. **Improved Practical Guidelines:** Development of actionable recommendations for industrial applications, enabling cost-effective and efficient production practices.

In summary, this investigation addresses the gaps in existing literature by providing a systematic analysis of the critical process parameters for 5754 aluminium alloy. The results will not only advance the scientific understanding of FSW but also have significant practical implications for manufacturing industries aiming to optimize welding processes.

CHAPTER 5

5. FSW EXPERIMENTS

In friction stir welding applications, specially manufactured machines and CNC machines are used. In this study, the CNC Milling Machine located at Atılım University Metal Forming and Centre of Excellence was preferred due to its high precision processing, traverse speed and welding depth can be adjusted as desired. During the welding process, the parts were fixed to the table, and the force was measured with the help of a dynamometer. The calibration documents of all devices used during the experiment were checked and verification trials with previously known results were performed for test repeatability. The Dynonometer device belongs to the company Tenmak-Boren. The CNC milling, Electrical Discharge Machining, Zwick Tensile testing and hardness, Alicona InfiniteFocus non-contact 3D surface measurement devices belong to MFCE. The conformity documents of all devices used were checked. Tolerance ranges were taken into account.



Figure 5.1 CNC Milling Machine

Table 1 CNC Milling Machine Features

Features	4+1, total 5 axes
Table axis movements:	2400300 x 1000 mm

5.1 Sample Preparations

Sheet metal workpieces were prepared for the FSW process. The most basic workpiece is shown in Figure 5.3. These workpieces were prepared in the guillotine device in Figure 5.2 located in the Metal Forming and Excellence Center. A total of 166 sheet metal samples were cut. All sheets were prepared in the 0 direction by paying attention to the direction. The dimensions were preferred as 75x75 mm. The dimensions of the test and analysis samples to be made were considered in the measurement selection. It was calculated in such a way that 3 sub-size tensile samples and 1 Sem sample would be obtained in accordance with the standard. Then the samples will proceed to the FSW process and the necessary sample preparation process with EDM.



Figure 5.3 75x75 AL 5754 sheet materials



Figure 5.2 Baykal Guillotine

Fixture design is considered to have low impact on the result in FSW applications, but correct and gapless positioning of the work pieces is very important for the welding process. In addition, high forces occur when the tool tip touches the samples, so a fixture with appropriate thickness and strength is designed so that the work pieces remain fixed without moving during welding. A special design has been made in the fixture design to connect a Kistler dynamometer to take force measurements. Technical drawings can be seen from Figure 5.4 and 5.6. The completed fixture design can be seen from Figure 5.5.

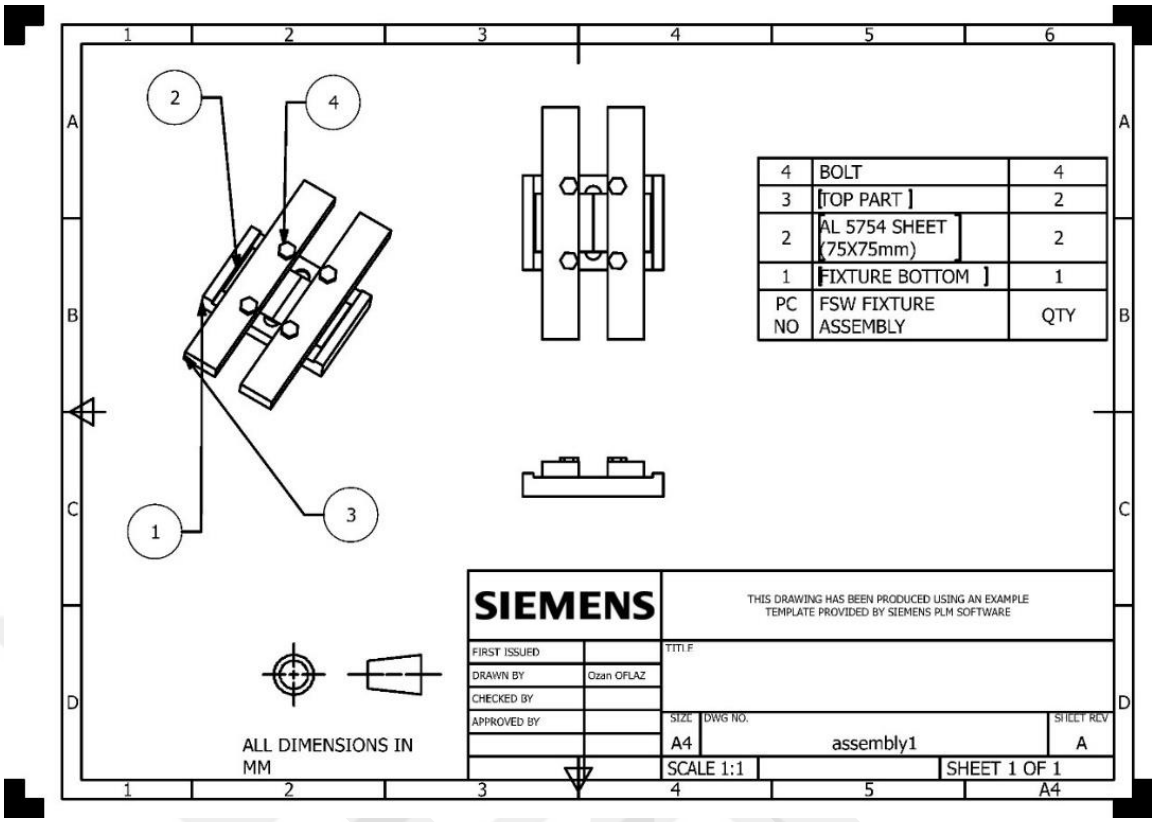

Figure 5.4 Technical Drawing of the Fixture

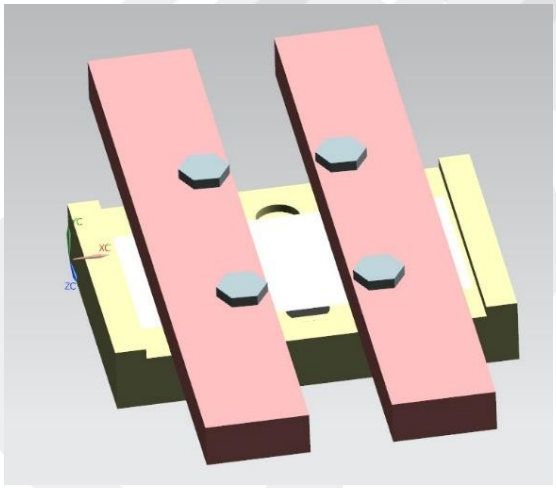

Figure 5.5 Fixture CAD Model Isometric View



Figure 5.6 FSW Fixture

Dynamometers provide invaluable data for tool manufacturing and production technology. They are used to analyse materials and tools, thanks to the measurement of mechanical forces across all components [34]. In this study, Kistler Brand 9265B model 3-axis cutting force dynamometer was used. The device has a piezoelectric force measurement system, which is quite different from other methods. The forces

acting on the quartz crystal element are converted into a proportional electric charge. The measurement range of such an element is very wide [35].

5.2. Determination of Welding Parameters

In determining welding parameters, an extensive review of the literature was conducted to analysed previous studies on Friction Stir Welding (FSW) processes. To achieve this, a systematic examination of review articles published in peer-reviewed journals was utilized as the primary source of information. These studies provided insights into commonly used experimental design plans, material selections, and welding conditions. Parameters such as tool rotational speed, welding speed, plunge depth, and tool pin profile were identified as critical variables influencing the mechanical properties and quality of weldments. Moreover, the review highlighted the optimal ranges of these parameters and their interdependencies, which serve as a guideline for future experimental setups. This comprehensive analysis forms the basis for selecting effective welding parameters tailored to specific materials and desired weld characteristics, ensuring high-quality and defect-free results in FSW processes.

5.2.1 Determination of Machine Parameters

Arkaprava Ray, Devendra Pendokhare and Shankar Chakraborty, in this study, comprehensively investigated four main multi-objective optimization techniques for the optimization of friction stir welding (FSW) processes. The researchers analysed many articles published between 2014 and 2023 and evaluated the applications of Desirability Function Approach (DFA), Metaheuristic Algorithms, Multi-Criteria Decision Making (MCDM) methods and Grey Relational Analysis (GRA) techniques in FSW processes. In the study, the experimental design plans, welding materials, pin materials, welding parameters and welding properties used were examined in detail and their effects on process optimization were analysed. In addition, the researchers revealed the advantages and limitations of the methods used for the optimization of these processes and suggested that the obtained findings could be used as a training dataset for machine learning based prediction models [36].

Table shows the applications of Design of Experiments (DOE) to optimize the design factors of Friction Stir Welding (FSW) processes. The aim is to establish relationships between different materials, design plans, tool materials, process parameters and results to effectively implement FSW. CCD (Central Composite Design) and BBD (Box-Behnken Design) are two popular methods used in experimental design and optimization processes. CCD is an approach developed especially for the creation of quadratic mathematical models. This method offers a design that includes central points, corner points and axial (star) points. In this way, it is possible to analyse the individual effects of different parameters and their interactions with each other more precisely. CCD is often preferred for optimizing results over a wide range of factors. On the other hand, BBD (Box-Behnken Design) is a method that focuses on the development of quadratic models but aims to reduce the number of experiments. This method avoids using corner points in each experimental combination, thus reducing experimental costs and increasing applicability in less complex systems. BBD is frequently used in cases where mechanical properties (such as tensile strength or elongation ratio) need to be optimized.

Table 2 The Influence of Materials, Tools, and Parameters on Performance

Author(s)	Material	Design plan	Pin material	FSW parameters	Response
Panneerselvam and Lenin [37]	Polypropylene	OA L16	Mild steel	PP (square, taper, triangular, threaded), WS (30-60 mm/min), TRS (1500-2250 rpm)	TS (23.172 MPa)
Vijayan and Rao [38]	AA2024 + AA6061	BBD	SKD-61 tool steel	TRS (1500-1900 rpm), WS (30-90 mm/min), AL (3-9 kN), PP (taper, square, straight cylinder)	UTS (143 MPa), EL (12%)
Venkateswarlu et al. [39]	AA2219 + AA7039	FFD	SS 310	TRS (500-1000 rpm), WS (20-40 mm/min), AL (5-8 kN)	UTS (262 MPa), EL (11%)
Ghaffarpour et al. [40]	AA5083-H12 + AA6061-T6	BBD	H13 tool steel	TRS (700-2500 rpm), WS (25-400 mm/min), SD (10-14 mm), TA (1-4°)	TS (221 MPa), EL (6.1%)

Table 2 The Influence of Materials, Tools, and Parameters on Performance (Cont.)

Rathinasuriyan and Kumar [41]	AA6061-T6	BBD	H13 tool steel	TRS (800-1200 rpm), WS (30-60 mm/min), WH (10-30 mm)	TS (198 MPa)
Lakshminarayanan [42]	Stainless steel	CCD	-	TRS (400-1200 rpm), WS (50-130 mm/min), SD (16-24 mm)	TS (587 MPa), NTS (660 MPa), IT (36 J), DOS (13%)
Amin et al. [43]	AA6061-T6	CCD	H13 tool steel	TRS (430-930 rpm), WS (80-200 mm/min)	EL (6.33%), UTS (204 MPa), MBF (6.216 kN)
Rao and Ramanaiah [44]	Al-Mg-Mn-Sc-Zr alloy plates	CCD	H13 tool steel	TRS (800-1600 rpm), WS (20-40 mm/min), AL (4-12 kN)	H (118.98 HV), UTS (238.54 MPa), EL (4.9%)
Periyasamy et al. [45]	AA7075-T651 + AA6061	CCD	High speed steel (HSS)	PD (4-8 mm), TO (0.3-1.5 mm), TA (-5°)	TS (267 MPa), MH (121 HV)
Verma et al. [46]	AA7039	CCD	H13 steel tool	TRS (1325-1812 rpm), WS (26-43 mm/min), TA (1.3-2°)	UTS (479.63 MPa), TE (19.12%)
Pandiyarajan et al. [47]	AA6061/ZrO2/C	BBD	HCHCr steel	TRS (600-1000 rpm), WS (45-55 mm/min), AL (4-6 kN)	TS (190 MPa), H (50 HRB)
Panaskar and Terkar [48]	AA6063-electrolytic tough pitch copper	CCD	H13 tool steel	TRS (1000-1400 rpm), WS (5-15 mm/min), zinc foil thickness (0-0.4 mm)	UTS (122.87 MPa)
Umar et al. [49]	AA6082/ZrO2/B4C	BBD	D2 tool steel	TRS (800-1200 rpm), WS (25-50 mm/min), AL (4-8 kN)	H-NZ (94.2 HV), UTS (239.98 MPa)
Senthil et al. [50]	AA6063-T6	CCD	HSS	TRS (1800-2200 rpm), WS (0.4-0.8 rpm)	UTS (167 MPa), YS (145 MPa), EL (8.3%)
Bindu et al. [51]	AA7068-T6	CCD	H13 tool steel	TRS (800-1400 rpm), WS (30-60 mm/min), AL (5-9 kN)	TS (516 MPa), EL (21.57%)
Kumar et al. [52]	AA2014 + AA7075	CCD	H13 die-steel	TRS (600-1400 rpm), WS (60-180 mm/rev)	UTS (516 MPa), EL (21.57%)

Table 2 The Influence of Materials, Tools, and Parameters on Performance (Cont.)

Sandeep and Natarajan [53]	AA7475 + polyphenylenesulfide polymer	BBD	H13 tool steel	TRS (900-1200 rpm), WS (5-15 mm/min), TA (1-3°)	TLSS (22.06 MPa)
Kumar and Balasubramanian [54]	AZ31B + AA6061	CCD	-	TRS (600-1000 rpm), WS (20-60 mm/min), TA (0-2°)	UTS (159.6 MPa), YS (145 MPa), EL (3.5%), H (96 HV)

To determine the optimal parameters such as rotational and traverse speed for the Friction Stir Welding (FSW) process, a detailed review of various studies in the literature was conducted. These studies provided insights into the commonly used machine settings for aluminium alloys, particularly for AL 5754, which served as a reference for parameter selection. The investigation focused on identifying feasible ranges of machine parameters to achieve successful welding while considering the limitations of the available equipment.

The welding experiments were conducted on a CNC milling machine, which had a maximum rotational speed limit of 3500 rpm. During the trials, it was observed that welding was unsuccessful at rotational speeds below 500 rpm, as the material failed to bond effectively. Consequently, 500 rpm was set as the minimum speed for further experimentation. A range of machine settings, including traverse and rotational speeds, were tested based on the most frequently used parameters reported in the literature.

The initial experiments revealed critical insights into the interaction between the rotational speed, traverse speed, and welding quality. Based on these findings, a design of experiments (DOE) approach was employed to systematically explore the parameter space and optimize the welding process. This systematic approach allowed for the identification of parameter combinations that produced defect-free welds with improved mechanical properties.

The selected machine parameters and the optimized experimental design demonstrated compatibility with the AL 5754 material, yielding high-quality welds. This process established a reliable foundation for subsequent FSW experiments, ensuring consistent results under the constraints of the available CNC milling machine.

5.2.2. Tool Tip Design

Tool tip design is critical for the Friction Stir Welding (FSW) process and directly affects the weld quality. While designing the tool tip, the most appropriate design was applied after using the studies in literature and various trials.

In the study conducted by Aman Kumar et al., the Friction Stir Welding (FSW) process for 7075 aluminium alloy was comprehensively investigated in terms of tool geometry selection, environmental parameters and mathematical modelling. It was emphasized that FSW is a superior alternative to conventional welding methods with the advantages of low process temperature and minimal deformation. In the study, the effect of tool geometry on weld quality was discussed in detail and it was determined that conical and triflat pin geometries produced different results in terms of heat density and mechanical performance. In addition, the effects of environmental factors (e.g. humidity, temperature) on the weld microstructure and mechanical properties were investigated. In the study, the effects of process parameters on weld quality were analysed with mathematical modelling and optimization strategies were developed [55].

A threaded tool was initially designed for the Friction Stir Welding (FSW) process to enhance material mixing and heat generation. However, during trial welding experiments, it was observed that the aluminium material tended to clog the spaces between the tool's threads. This clogging not only disrupted the material flow but also hindered the heat distribution, resulting in suboptimal weld quality. The accumulation of material between the threads caused irregularities in the weld zone, leading to incomplete bonding and a reduction in mechanical strength.

To address this issue, a modified tool design with a notched pin profile was developed. The notched tool was specifically engineered to improve material flow and eliminate the clogging observed with the threaded tool. The notches facilitated better mixing of the aluminium material by creating additional flow paths and reducing the accumulation of material around the tool. This design adjustment significantly improved the welding process by ensuring uniform material mixing and consistent heat distribution.

Preliminary tests with the notched tool demonstrated superior weld quality, characterized by enhanced mechanical properties and a defect-free weld zone. The results indicated that the notched pin design effectively addressed the limitations of the threaded tool, making it a more suitable choice for welding aluminium components in the FSW process.

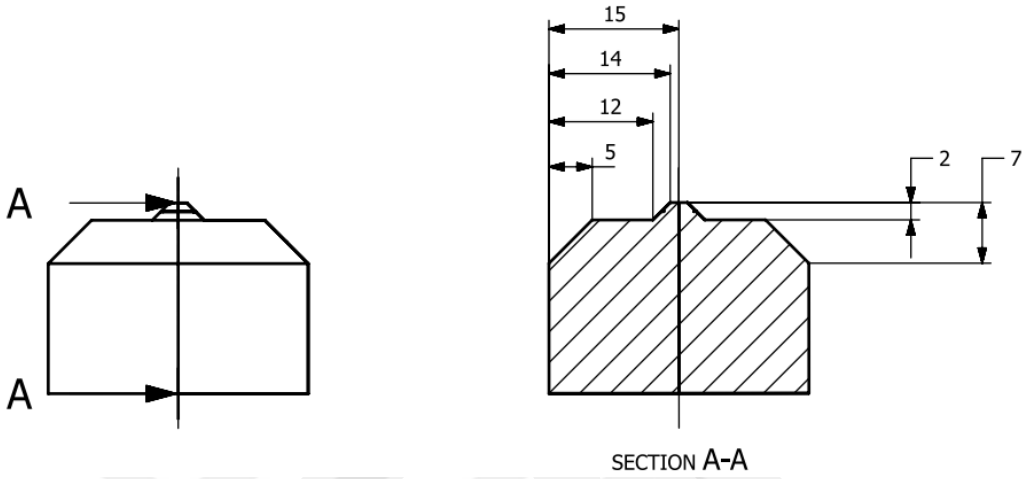

Figure 5.7 Sectional view of tool tip

The image illustrates the geometric design of a tool pin used in the Friction Stir Welding (FSW) process. The design is presented in two views: the external profile and a cross-sectional view along the A-A axis. The external view highlights the overall shape of the tool pin, which includes a tapered top section with sharp edges designed to interact with the material during welding. This tapering ensures efficient heat generation and material flow. The cross-sectional view provides detailed dimensions of the tool. The total height of the tool is 15 mm, with a 5 mm upper section designed for precise engagement with the material. The tapered shoulder section, measuring 7 mm in thickness, allows for better control of heat distribution and material mixing. The additional 2 mm layer above the shoulder further contributes to stabilizing the welding process. These design elements ensure effective material deformation and bonding, critical for producing high-quality welds in the FSW process. This specific tool geometry is optimized for welding parameters and material type, ensuring improved mechanical properties and defect-free joints.

5.3. Application of Friction Stir Welding

166 sheets were subjected to friction stir welding process with the specified traverse and rotational speed parameters with CNC Milling machine in Metal Forming and Excellence Center. As a result, 83 welded sheets were obtained.

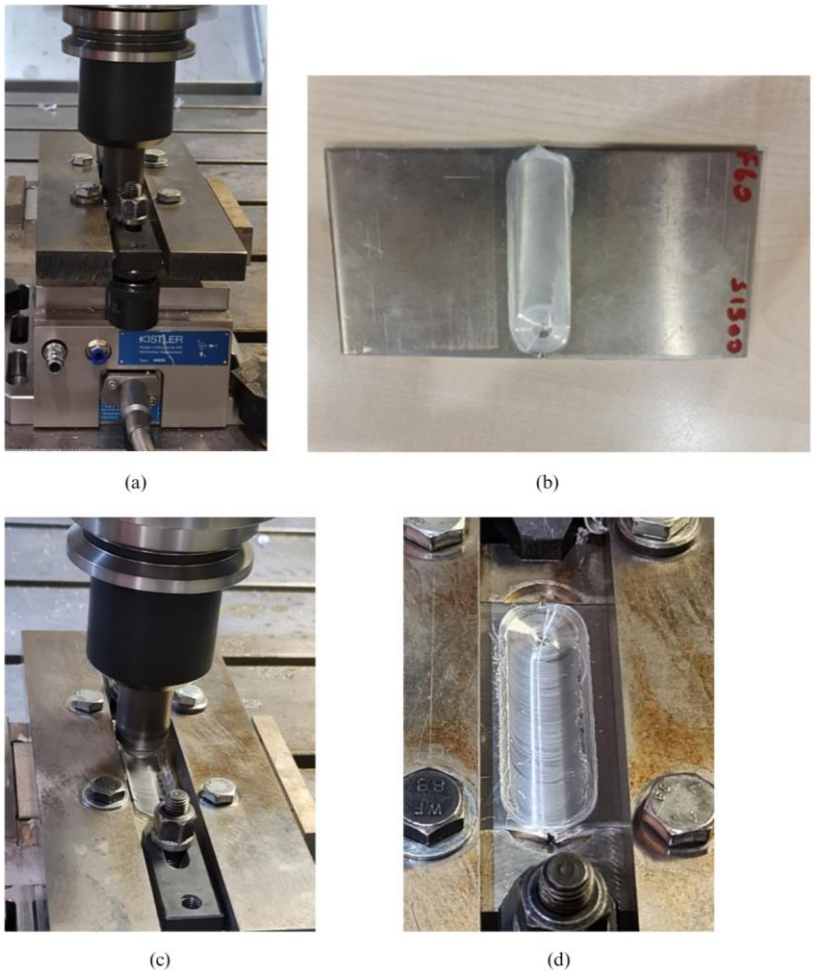

Figure 5.8 a) Dynamometer and fixture assembly, b) Finished part, c) FSW process, d) Finished process

In Figure 5.8 images (a) and (c), aluminium samples processed on the CNC milling machine used during the Friction Stir Welding (FSW) process are seen. The samples are fixed to the machine and secured with clamping elements to ensure stability during the welding process. The tool used in the FSW process and the process in which the sample moves along the welding axis are visualized. Image (b) shows an aluminium

sample with the FSW process completed. The weld mark shows that the process was performed properly and that there are no surface defects on the part. This is an indicator of high quality and appropriate welding parameters. In image (d), the weld seam obtained after the welding process is shown in detail. Details that emphasize the precision and smoothness of the process are clearly observed. In your thesis study, these images can be used to discuss the effects of processing parameters and tool geometry on the welding quality.

CHAPTER 6

6. EXPERIMENTAL TEST AND ANALYSIS

After the Friction Stir Welding (FSW) process was completed using predetermined parameters, mechanical characterization was performed on the welded samples to evaluate the properties of the weld zone. This characterization involved surface roughness measurements, hardness measurements, and tensile testing, along with microstructural analysis using a scanning electron microscope (SEM). Additionally, force measurements were conducted during the welding process to assess the relationship between the applied forces and the resulting mechanical and microstructural properties of the weld area. These combined evaluations provided a comprehensive understanding of the welding parameters and their effects on the material.

6.1 Force Measurements

The forces acting on the tool during Friction Stir Welding (FSW) process are of great importance in terms of the quality of the weld, the joint properties of the material and the optimization of the welding parameters. FSW basically provides the joining of materials with a solid-state welding process by applying high temperature and pressure with a rotating tool. During this time, various forces such as axial (vertical) force, advance force and lateral force occur on the tool. These forces directly affect the depth of the weld, joint strength and surface quality.

The axial force formed on the tool determines the pressure applied to the surface of the material and helps to form deformation with thermal effects. If the axial force is not sufficient, complete joining cannot be achieved in the weld area, thus defects may occur in the weld line. On the contrary, a very high axial force can cause excessive deformation of the material and even wear on the tool surface. Therefore, having an optimal level of axial force is critical to guarantee the welding quality.

The advance force allows the tool to effectively fuse the material as it moves along the weld line. Insufficient feed force may cause the tool to not fully penetrate the material

and the weld area to not gain a homogeneous structure. At the same time, lateral force also ensures the stability of the tool during FSW and contributes to obtaining a flat weld line by preventing the tool from deviating from the weld line.

Correct control of the forces on the tool minimizes the defects that may occur in the microstructure of the material, improves the grain structure and weld performance. To obtain durable and homogeneous welds, especially in industrial applications, correct adjustment and monitoring of the forces generated on the tool during FSW is vital to the success of the welding process.

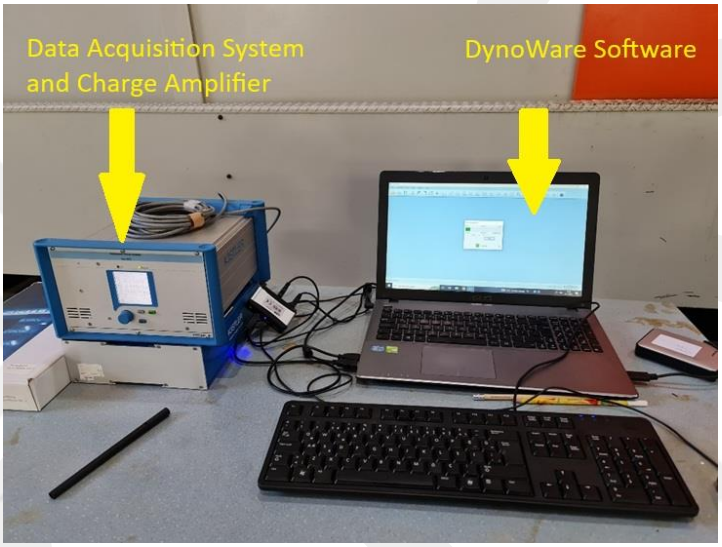

Figure 6.1 Kistler 9265B Dynamometer

Kistler 9265B dynamometer at Atılım University was used for force measurements. Table-1 shows rotation speed, tool traverse speed and forces in x, y, z directions. The table contains the values of the forces on the tool during Friction Stir Welding (FSW) for different rotational speeds (rpm) and traverse speeds (Tool Traverse Speed). This data is valuable in understanding how the forces generated during the FSW process affect the weld quality.

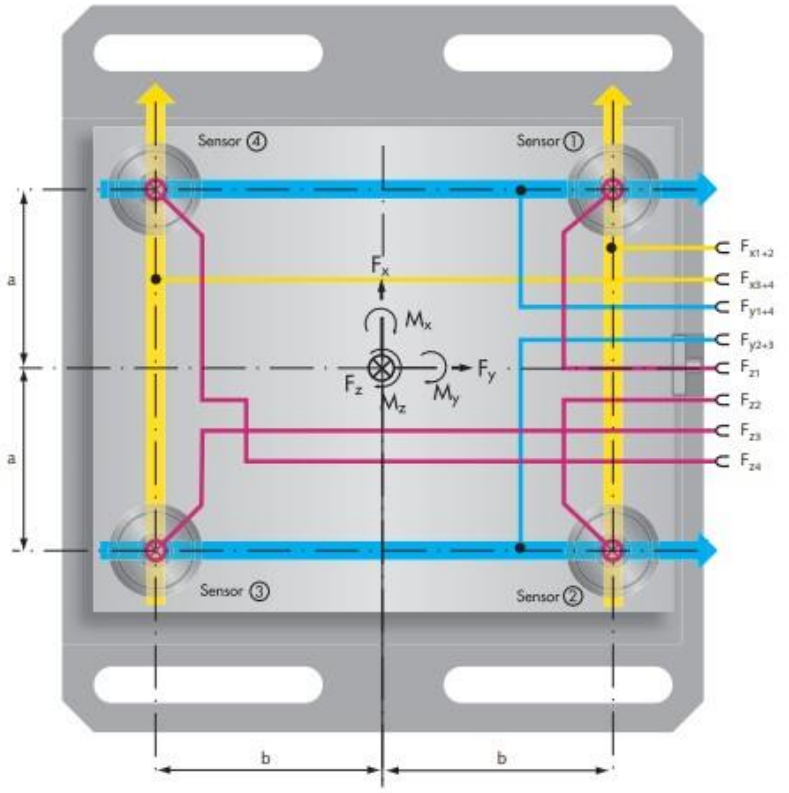

Figure 6.2 Sensor placement of the Kistler dynamometer [34].

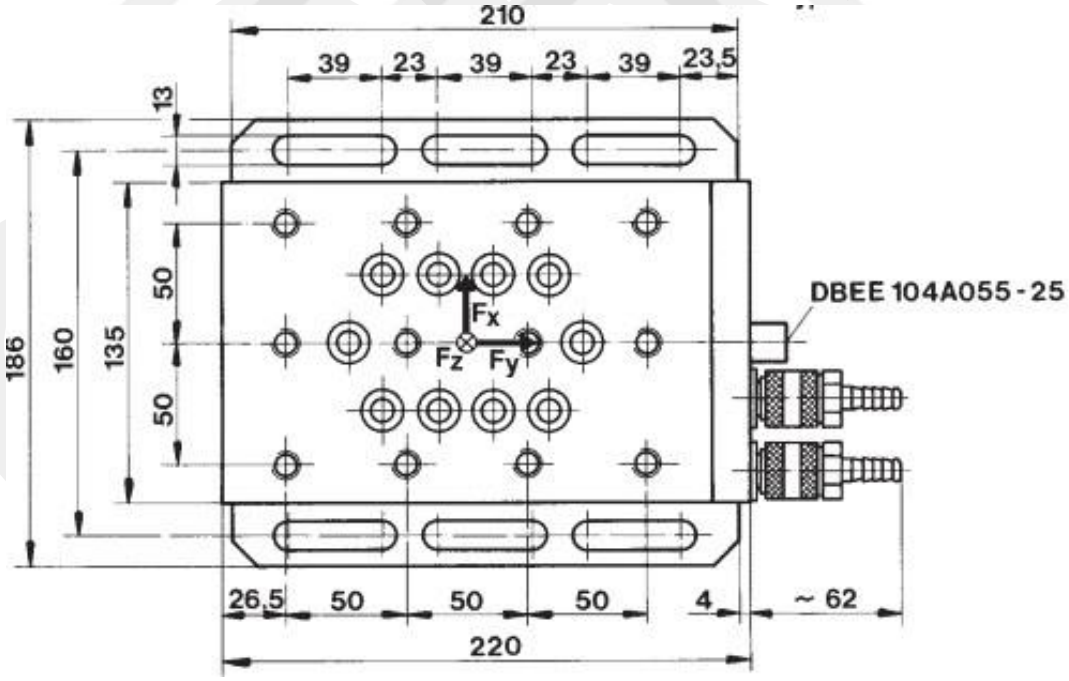

Figure 6.3 Technical Drawing of the Kistler dynamometer [35]

Calculation of the three forces and three moments.

$$F_x = F_{x1+2} + F_{x3+4}$$
$$F_y = F_{y1+4} + F_{y2+3}$$
$$F_z = F_{z1} + F_{z2} + F_{z3} + F_{z4}$$
$$M_x = b(F_{z1} + F_{z2} - F_{z3} - F_{z4})$$
$$M_x = b(F_{z1} + F_{z2} - F_{z3} - F_{z4})$$
$$M_y = a(-F_{z1} + F_{z2} + F_{z3} - F_{z4})$$
$$M_z = b(-F_{x1} + 2 + F_{x3} + 4) + a\left(F_{y1} + 4 - F_{y2} + 3\right) \text{ [35]}$$

Table 3 Technical Parameter of Kistler Dynomemeter System [34]

Measuring Range	-15…15 KN
Overload	-20/20 KN
Threshold	<0,01
Sensitivity	8 Pc/N
Natural Frequency (Mounted)	1,5 kHz
Operating Temperature Range	0…70 °C
Temperature Coefficient of Sensitivity	-0,02 %/°C
Weight	20 Kg

- **Effect of Rotation Speed and Traverse Speed:** Significant changes are observed in the forces measured at different rotational and traverse speeds. Increasing rotational speed (rpm) and traverse speed (Tool Traverse Speed) generally increases the forces generated on the tool. It is observed that the forces increase significantly, especially at high rpm values, which may increase the risk of wear on the tool.

- **Force Change in X, Y and Z Axes:** F_x, F_y and F_z forces represent the force components on the tool during FSW. It is observed that the Fz force is generally higher than the other components, emphasizing the dominant role of axial

forces in the process. F_x and F_y forces are the forces that occur in the lateral and forward directions and can affect the stability of the process.

- **Maximum Values of Forces:** The maximum values of the F_x, F_y and F_z forces measured for each speed parameter are also added to the table. These maximum values provide critical information to understand how the tool performs under the highest load. Careful monitoring of these forces during the FSW process helps prevent overload situations and possible failure situations.

- **Weld Quality and Force Relationship:** This data emphasizes the importance of controlling the forces on the tool in terms of weld quality. High forces can create higher temperatures and deformations in the weld area, but excessive loads can lead to wear or cracks on the tool and material surfaces.

Table 4 Forces measured in x, y, z axes according to different rotation speed and tool traverse speed

Sample Code	**Rotation Speed (N)**	**Tool Traverse Speed (v)**	**F_x Mean**	**F_y Mean**	**F_x Mean**	**$F_{x\,MAX}$**	**$F_{y\,MAX}$**	**$F_{z\,MAX}$**
	(rpm)	**mm/min**	**(N)**	**(N)**	**(N)**	**(N)**	**(N)**	**(N)**
Stock	-	-						
51	500	10	956,6	765,9	4250	3685	3736	10150
52	500	20	466,2	45,01	4757	3270	2780	13050
53	500	30	677,3	384,2	4619	3975	3412	12010
54	500	40	362,2	64,74	7583	4323	2815	13620
55	500	60	377,6	217	8070	3229	3185	11880
56	500	80	486,9	245,9	7551	3215	2628	12280
57	500	100	528,6	110,1	9140	2799	3338	12320
58	500	120	301,5	134,5	8944	3098	2653	13010

Table 4 Forces measured in x, y, z axes according to different rotation speed and tool traverse speed (Cont.)

59	500	150	988,3	83,4	4914	5202	4047	9910
71	700	10	361,1	43,22	4418	2264	2050	13730
72	700	20	372,05	39,05	5140	2437	2267	15450
73	700	30	487,7	153,3	4677	2433	2575	15690
74	700	40	737,5	195,7	4850	2379	2316	16050
75	700	60	868,7	309,9	5241	2543	2639	15110
76	700	80	762	172,9	8521	2580	2174	16560
77	700	100	826,1	187,1	10230	2732	2503	17560
78	700	120	959,1	406,2	7880	2712	2539	15520
79	700	150	1125	410	4044	3246	3685	8556
91	900	10	350,6	74,15	3767	1965	1923	15120
92	900	20	356,4	171,6	3714	2352	2508	10190
93	900	30	499,5	148,1	3760	2636,7	2693	12340
94	900	40	479,1	114,5	5502	2530	2526	14150
95	900	60	807,9	254,9	4440	2488	2755	13010
96	900	80	880,3	278	4769	2077	2154	12570
97	900	100	903,6	289,1	5722	2010	2415	13410
98	900	120	981,2	312	6164	2248	2342	14030
99	900	150	1101	400,7	7152	1945	1717	9970
111	1100	10	365,3	127,7	3350	1673	1832	13810
112	1100	20	397,1	60,85	4318	1862	1814	13170
113	1100	30	485,3	32,11	4703	1746	1629	13000
114	1100	40	801,8	37,87	3397	1705	1695	13490
115	1100	60	994,4	58,78	3914	1802	1862	13020
116	1100	80	1030	32,94	4776	1733	1734	12390
117	1100	100	791,1	222,6	5557	2375	2505	13210
118	1100	120	824,1	181,3	6343	2313	2198	12790
119	1100	150	1099	300,9	8857	1635	1354	11230
131	1300	10	356,3	30,12	2960	1783	1751	11660

Table 4 Forces measured in x, y, z axes according to different rotation speed and tool traverse speed (Cont.)

132	1300	20	552,5	29,71	2364	1417	1366	11210
133	1300	30	778,8	67,1	2476	1354	1364	12440
134	1300	40	789,4	84,15	3261	1559	1480	12650
135	1300	60	895	88,36	3637	1490	1379	11840
136	1300	80	865,5	124,2	4753	1583	1580	12130
137	1300	100	1028	137,6	4674	1575	1513	11630
138	1300	120	1051	122,8	5262	1615	1690	12220
139	1300	150	1016	173	8019	1461	1187	11720
139-1	1300	250	1047	413	7609	1594	1367	8946
151	1500	10	316	90,7	2351	1619	1577	9610
152	1500	20	546,1	58,99	2043	1156	777	8511
153	1500	30	709,7	29,6	2084	1227	712	8241
154	1500	40	809	77,24	2180	1284	976	7915
155	1500	60	876,8	72,28	2621	1309	1181	8101
156	1500	80	936,8	92,12	3721	1359	1160	8880
157	1500	100	887,9	87,44	4717	1365	1119	8496
158	1500	120	1069	155,9	3660	1413	1104	8213
159	1500	150	1072	277,9	7497	1401	1052	9919
159-1	1500	250	1512	460,9	10590	1964	817	16130
201	2000	10	391,3	56,1	1921	1091	937	10420
202	2000	20	461	123,3	2304	1555	729	11100
203	2000	30	477,3	157,2	3105	1057	531	12110
204	2000	40	564,2	206,6	2579	1047	593	9978
205	2000	60	568,6	291,8	3408	1001	661	11530
206	2000	80	607,5	267,8	3884	1065	569	12040
207	2000	100	678,6	303,2	3946	1082	709	11470
208	2000	120	733,4	315,2	3195	1065	637	9134
251	2500	10	258,8	115	2092	923	590	10540
252	2500	20	260	38,73	2893	832	611	11160

Table 4 Forces measured in x, y, z axes according to different rotation speed and tool traverse speed (Cont.)

253	2500	30	307,8	115,4	3327	936	559	11710
254	2500	40	337,9	154,9	3265	948	490	12110
255	2500	60	389,7	168,5	4343	907	512	12420
256	2500	80	468,8	185,7	4893	883	485	11850
257	2500	100	538,6	213,3	5489	1018	451	11420
258	2500	120	613,9	210,8	5130	1022	488	10230
2591	2500	250	1183	505,8	7540	1428	593	10500
2592	2500	500	1571	1303	15570	1853	719	13700
351	3500	10	239,4	90,6	1255	1067	600	8670
352	3500	20	309,5	125	1401	910	472	11120
353	3500	30	353,7	282	2754	818	390	10840
354	3500	40	410,5	344,1	2915	733	437	11120
355	3500	60	597,9	518	5587	998	362	12210
356	3500	80	642,1	637,7	6560	1025	446	11940
357	3500	100	669,4	741,6	7060	980	497	10790
358	3500	120	862,9	693,4	8027	1017	401	10690
3591	3500	250	920,9	488	6312	1145	524	8345

Table 4 shows the measurement results of all samples connected to the Dynamometer and welded. F_y is the direction of progress, F_x is the lateral direction and Fz is the vertical, i.e. the direction of axial force. As expected in the test results, the highest force is in the Fz direction. The F_x, F_y and F_z Mean values in the table are the average of the forces measured during the welding process. The maximum forces are the highest force value measured in the friction stir welding process depending on time. In all processes, the highest force occurred on the F_z axis, i.e. the direction of axial force. The moment when this force is at its highest is when the tool touches the work pieces.

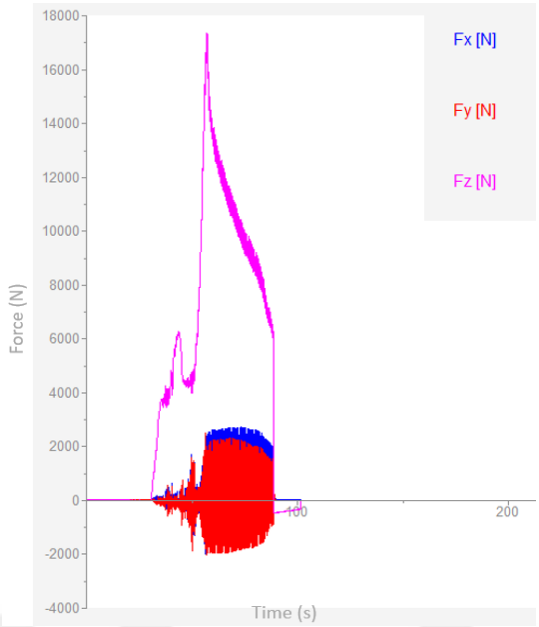

Figure 6.4 Force and Time graph of Sample No. 77

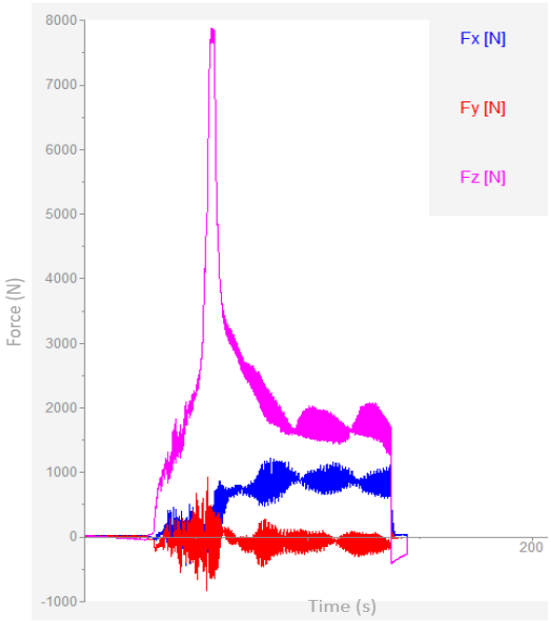

Figure 6.5 Force and Time graph of Sample No. 154

Figure 6.4 is the force and time graphs of Sample No. 77 (700 rpm Rotational Speed and 100 mm/min traverse speed), figure 6.5 is the force and time graphs of Sample No. 154 (1500 rpm Rotational Speed and 40 mm/min traverse speed) measured in Dynoware software. The lowest F_z Max force was obtained in weld sample No. 154, and the highest F_z Max force was obtained in weld sample No. 77.

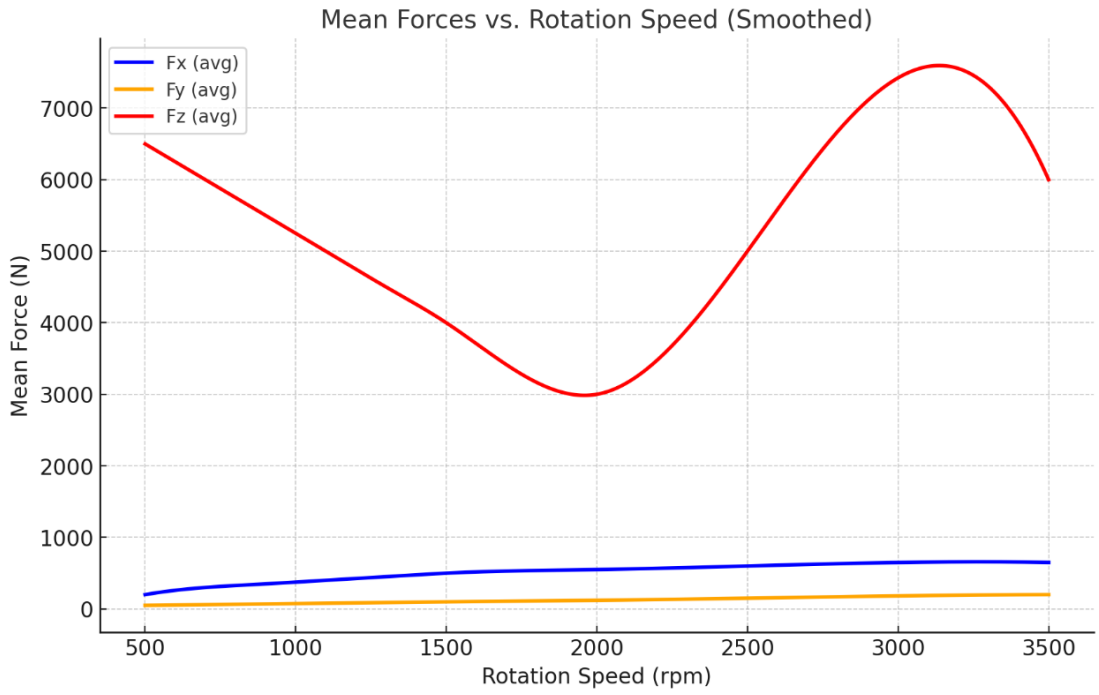

Figure 6.6 Effect of Rotation Speed on Mean Forces

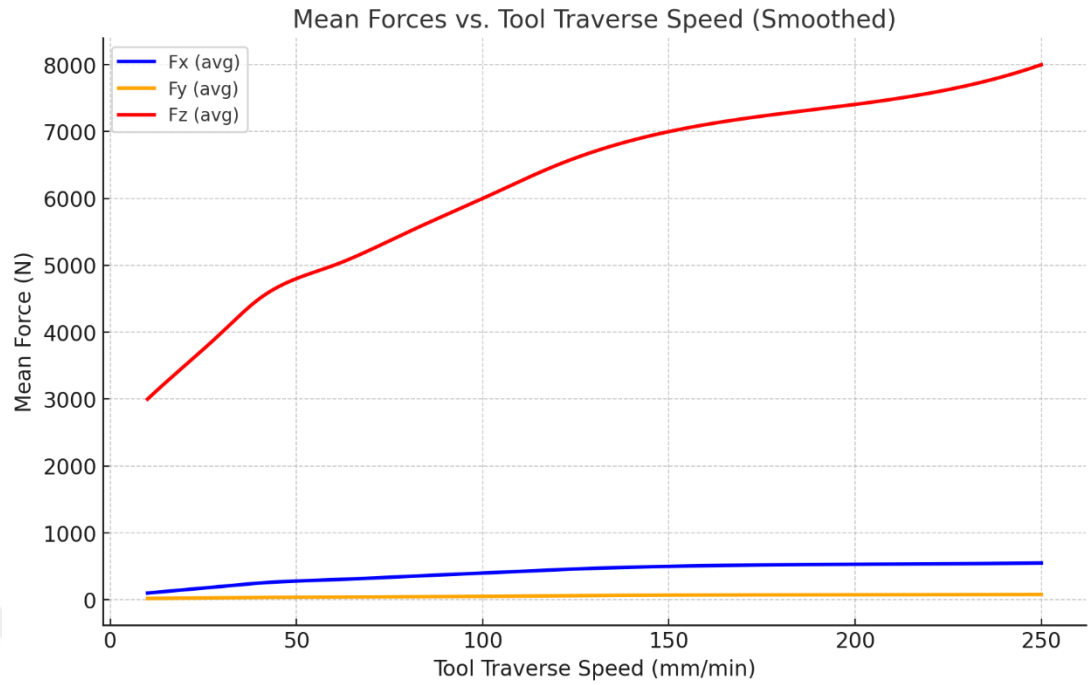

Figure 6.7 Effect of Tool Traverse Speed on Mean Forces

Figure 6.6 shows the effect of rotation speed on forces. The F_x force shows very small changes as the rotation speed increases and generally remains at low levels. This situation shows that F_x is not much affected by rotation speed. Similarly, the F_y force also follows a constant course and shows that the effect of rotation speed on F_y is minimal. In contrast, the F_z force shows a more pronounced change with rotation speed. The Fz force, which is initially high, decreases as the rotation speed increases and reaches its minimum level around 2000 rpm. Then, F_z increases again as the rotation speed increases. This shows that rotation speed has a significant effect on the F_z force and that the forces respond differently in certain speed ranges.

Figure 6.7 examines the effect of tool traverse speed on forces. The F_x force shows a slight increase as the traverse speed increases, but this increase is quite regular and not obvious. This situation shows that F_x is less sensitive to traverse speed. The F_y force, on the other hand, remains constant at low levels and is almost unaffected by traverse speed. In contrast, the F_z force shows a continuous increase trend as the traverse speed increases. It shows an almost linear increase starting from 10 mm/min to 250 mm/min. This situation shows that the traverse speed has a strong effect on the F_z force and that the F_z force increases significantly at higher traverse speeds.

The F_z force is significantly affected by both parameters (rotation speed and traverse speed), while the F_x and F_y forces are less sensitive to these parameters. Changes in the F_z force can play a decisive role in tool load, energy consumption and material deformation during machining. Therefore, it is of great importance to correctly optimize the rotation speed and traverse speed parameters by considering the F_z force to increase machining efficiency and optimize tool strength.

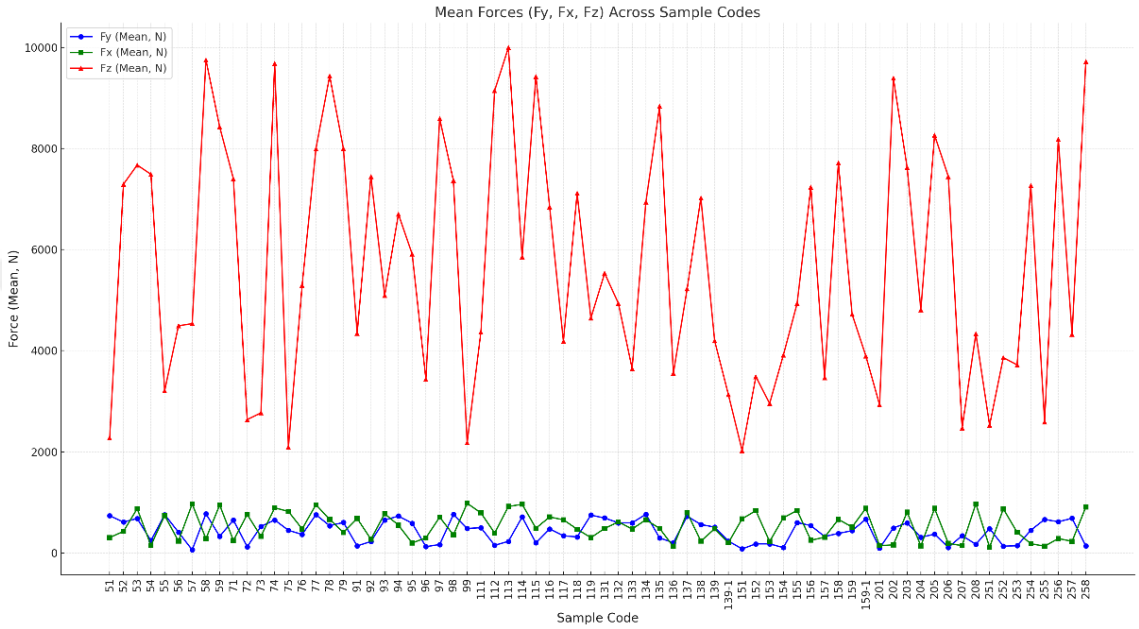

Figure 6.8 Mean Forces (F_y, F_x, F_z) Across Sample Codes

When the average forces are examined, the highest forces are observed as F_z, F_x and F_y, respectively. It is expected that the vertical force (F_z) is the highest. The reason why the lateral force (F_x) is measured higher than the force in the direction of advance (F_y) is thought to be due to Anisotropy on the sheet metal. In addition, although the sheet metals are subjected to clamping force in the direction of advance, minimal gaps can occur between the sheets. However, the fixtures fully support the sample in the horizontal axis.

6.2. Mechanical Characterization Tests

Friction stir welding (FSW) causes heat and mechanical deformations in the material during the process. To evaluate the welding parameters (advance speed, rotation speed, etc.), mechanical characterization of the welded area must be performed. In this way, the mechanical properties of the welded area can be better understood.

Mechanical characterization tests generally include methods such as hardness, tensile, bending, impact strength and fatigue tests. Each test helps to determine different mechanical properties of the material. For example, the bending test helps to understand the properties of the material such as flexibility, ductility and fracture strength, while this information provides important details about the elastic and plastic deformation capacities of the material. In this thesis study, hardness measurements were taken from the welded area, and then tensile tests were performed. With these tests, it was aimed to determine the general strength characteristics of the welded area and the hardness distributions of the most critical parameters. Other tests were excluded from the scope as they were thought to contribute less directly to understanding the properties of the material formed after the welding process.

6.2.1. Hardness Tests

FSW creates a new joint by affecting the microstructure of the processed material under high temperature and pressure. Determining the mechanical properties of the weld zone formed in this process is important for evaluating the success and durability of the welding process. Hardness measurement helps us understand the structural changes in different zones (weld seam, thermomechanical affected zone and thermally affected zone) formed during the weld.

- **Assessment of Weld Quality:** The FSW process aims to obtain a homogeneous and durable joint in the weld area. Hardness measurements are used to determine whether the hardness obtained in the weld area is equal and at the desired level. High hardness differences can create weakness in the weld area, which can shorten the life of the weld joint.
- **Thermomechanical and Thermal Effect Analysis:** Since the weld area and its surroundings are exposed to high temperatures in the FSW process, different structures known as thermomechanical affected zone (TMAZ) and thermally affected zone (HAZ) are formed. These regions may exhibit properties different from the original hardness of the material.
- **Fatigue and Wear Resistance:** Hardness is generally associated with the wear resistance and fatigue life of the material. Hardness measurement in FSW welds is an important indicator for estimating the durability and wear resistance

of the weld area under mechanical loads. Hardness can be used as an indicator of fatigue strength, especially in welds that will be subjected to cyclic loading.

- **Evaluation of Process Parameters:** Parameters such as tool rotation speed, traverse speed and pressure applied in the FSW process affect the hardness of the weld zone. These parameters affect the thermal distribution and material flow during welding, creating different hardness profiles. Hardness measurements provide a tool to understand whether process parameters are optimized.
- **Examination of Microstructural Properties:** During the FSW process, the internal structure of the material changes under the influence of the rotating tool. Measurements of hardness help us analyse the phase transformations and grain structure that occur because of these microstructural changes. Structural changes, especially grain refinement or recrystallization, affect the hardness values and determine the strength of the weld joint.

There are many methods for measuring hardness. The most used methods are Vickers, Rockwell and Brinell. Each has its own advantages. We used the brinell measurement method in our tests. The reason for our choice is that Brinell hardness measurement allows the evaluation of materials with large grain sizes or the measurement of very high hardness levels. The diameter of the ball usually varies between 1 and 10 mm. The ball is pressed against the surface of the material with a certain force and the penetration diameter is measured to obtain the hardness value. The hardness unit is expressed as Brinell (HB).

Table 5 Base Material Hardness Test Results

Nr	Fmax (N)	hmax (µm)	hmin (µm)	DeltaF (N)	Delta Fend (N)	d (µm)	HB 2.5 / 10
5	612.9	141.9	129.7	0.02047	0.09547	1146.9	57.13
6	613.0	137.8	125.8	0.02051	0.09551	1140.8	57.78
7	612.9	139.1	126.5	0.01955	0.09455	1146.4	57.18

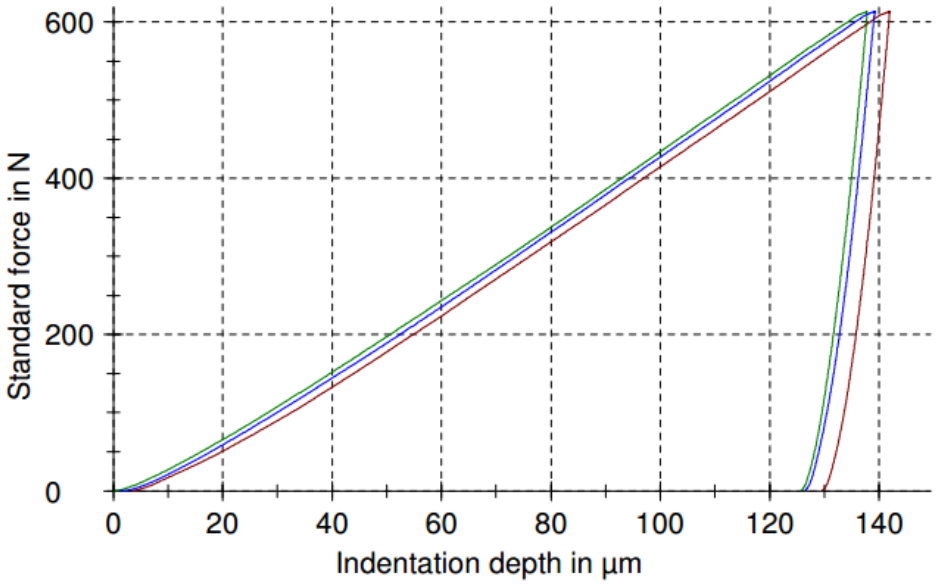

Figure 6.9 Indentation depth and standart forces

Table 6 Base Material Hardness Test Statisctic

Series	n = 3	Fmax (N)	hmax (µm)	hmin (µm)	DeltaF (N)	Delta Fend (N)	d (µm)	HB 2.5 / 10
x		613.0	139.6	127.4	0.02018	0.09518	1144.7	57.36
s		0.0	2.1	2.1	0.0005437	0.0005437	3.4	0.36
v		0.01	1.50	1.62	2.69	0.57	0.30	0.63

In samples from 51 to 59, the surface roughness was high because the traverse speed was low. Therefore, hardness data could not be obtained. Table 5 shows the Brinell hardness measurement results of all samples obtained because of single-sided Friction Stir Welding. The average results from 3 regions are shared in the table.

Table 7 Hardness values and Welding Parameters

Sample Code	**Rotation Speed (N)**	**Tool Traverse Speed (v)**	**Hardness**		**Sample Code**	**Rotation Speed (N)**	**Tool Traverse Speed (v)**	**Hardness**
-	rpm	mm/min	(HBW)		-	rpm	mm/min	(HBW)
Stock	-	-	57.36		138	1300	120	71.48
71	700	10	77.76		139	1300	150	67.51
72	700	20	74.80		151	1500	10	72.48
73	700	30	74.43		152	1500	20	72.00
74	700	40	74.80		153	1500	30	73.18
75	700	60	75.48		154	1500	40	71.55
76	700	80	72.13		155	1500	60	70.67
77	700	100	71.25		156	1500	80	71.09
78	700	120	71.65		157	1500	100	70.33
79	700	150	70.56		158	1500	120	70.83
91	900	10	71.06		159	1500	150	65.15
92	900	20	70.61		201	2000	10	68.51
93	900	30	70.76		202	2000	20	69.29
94	900	40	70.90		203	2000	30	66.56
95	900	60	71.73		204	2000	40	68.92
96	900	80	73.18		205	2000	60	67.79
97	900	100	74.20		206	2000	80	68.50
98	900	120	75.37		207	2000	100	67.56
99	900	150	71.69		208	2000	120	67.31
111	1100	10	-		251	2500	10	66.12
112	1100	20	64.00		252	2500	20	66.95
113	1100	30	67.13		253	2500	30	67.43
114	1100	40	67.26		254	2500	40	68.17
115	1100	60	70.62		255	2500	60	67.50
116	1100	80	71.48		256	2500	80	66.69
117	1100	100	73.06		257	2500	100	67.09
118	1100	120	73.07		258	2500	120	68.03
119	1100	150	67.68		351	3500	10	68.34
131	1300	10	72.45		352	3500	20	68.16
132	1300	20	72.70		353	3500	30	66.74
133	1300	30	72.12		354	3500	40	65.15
134	1300	40	73.45		355	3500	60	68.95
135	1300	60	71.51		356	3500	80	61.78
136	1300	80	71.18		357	3500	100	60.74
137	1300	100	72.10		358	3500	120	63.07

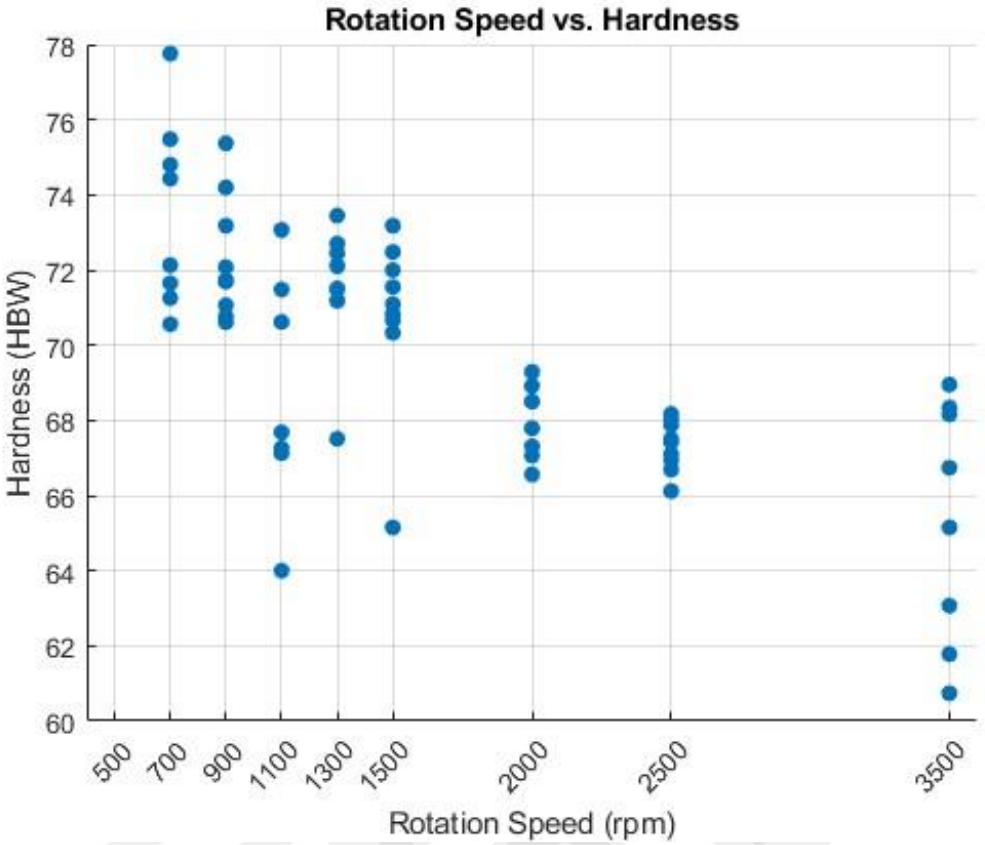

Figure 6.10 Effect of Rotation Speed on Hardness

The figure 6.10 shows the relationship between Traverse Speed (rpm) and Brinell Hardness (HB). Low rotation speed (700–1300 rpm) and low-medium rotational speeds (10 60 mm/min) are more ideal parameters for hardness. High speeds (both rotation and traverse) reduce the hardness values of the metal. This can be associated with situations where the heat and mechanical effects generated during welding become uncontrollable. Both speed factors should be considered together to determine the optimum process parameters. Because the change of a single parameter may not be sufficient to explain the hardness alone.

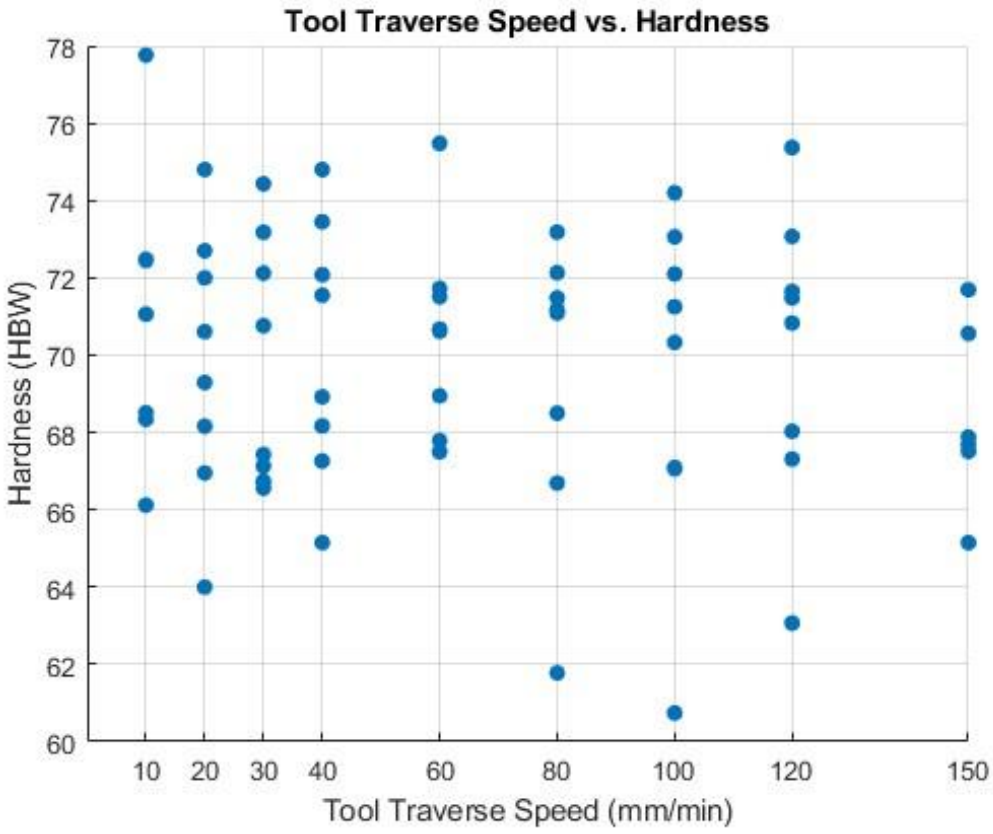

Figure 6.11 Effect of Tool Traverse Speed on Hardness

Figure 6.11 shows the relationship between Tool Rotational Speed (mm/min) and Hardness (HB). There is no significant trend between the hardness values with the increase in tool traverse speed. At low traverse speeds (10-40 mm/min), the hardness values are distributed in a wide range and vary between 64 HBW and 78 HBW. It is seen that the hardness values are mostly concentrated around 68-72 HBW in this region. At medium traverse speeds (60-100 mm/min), the hardness values exhibit a similarly wide distribution and are concentrated in the range of 62-76 HBW. It is noteworthy that at high traverse speeds (120-150 mm/min), the hardness values show a slight decrease and are generally concentrated in the range of 64-72 HBW. In general, it can be said that the effect of tool traverse speed on hardness exhibits an inconsistent and complex distribution.



Figure 6.12 Hardness Test

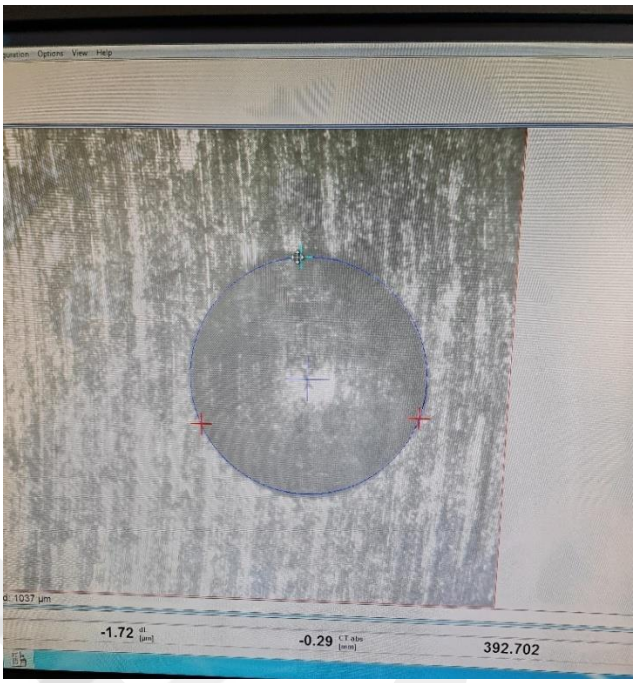

Figure 6.13 Measurement of the diameter of the cavity formed during the hardness test

6.2.2. Tensile Tests

As in every welding process, in friction stir welding (FSW) process, there are some changes in the microstructure of the material in the weld area. These may be encountered as texture changes, hardness differences. Since it is known that the microstructure determines the mechanical properties, the strength properties of the weld area can be determined with tensile tests. In addition, since weld strength is an important data for the automotive or shipbuilding sectors, the tensile test can also be used for quality control purposes after the welding process is performed with FSW.

The main purpose of performing tensile tests in this thesis is to find out which parameter produces the best mechanical properties. For example, the tests performed can verify how the weld area strength is affected by higher forces formed at high speeds or in the Z-axis. In this way, it is an important test for the optimization of welding parameters and is also important in terms of verifying the results.

6.2.3. One-Way Welded Tensile Tests

A total of 83 tensile samples, 3 each, were prepared with wire edm machine in MFCE with parameters at different traverse and rotation speeds.



Figure 6.14 Tensile samples cut by wire EDM



Figure 6.15 All Specimens



Figure 6.16 Wire Edm Machine

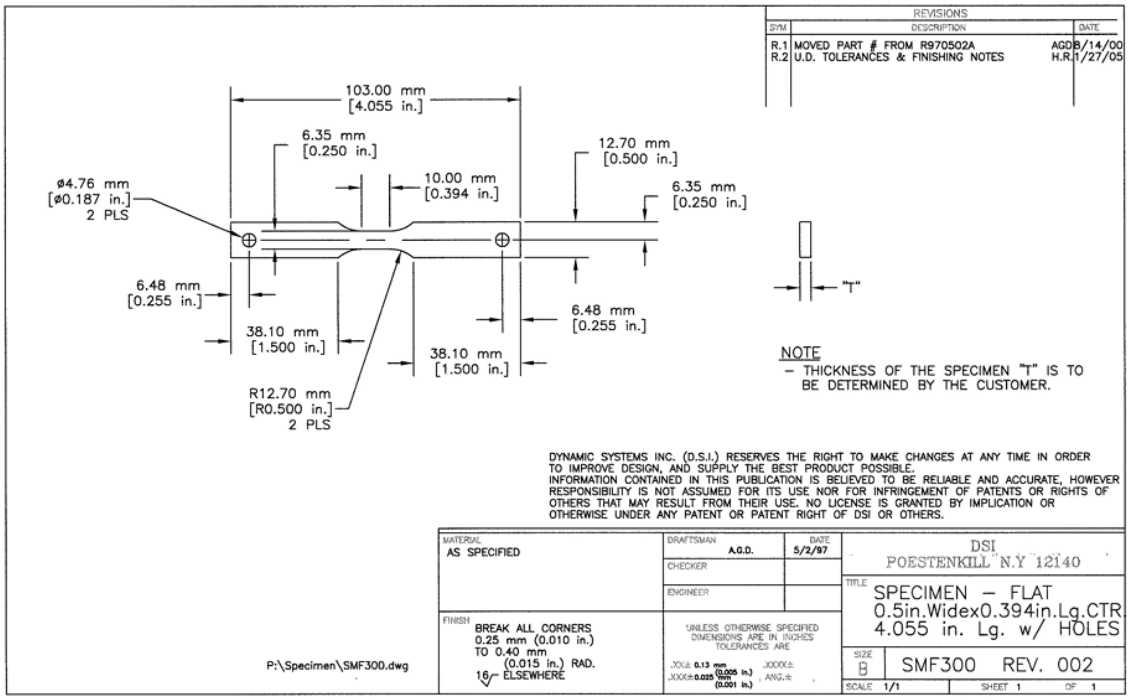

Figure 6.17 Technical Drawing of Tensile Test Specimen

Tensile tests were performed using the Zwick Z300 Tensile testing machine according to the "ISO 6892-1 Tensile Test on Metals at Ambient Temperature" standard.



Figure 6.18 Tensile Test Process

Tensile testing was performed on the untreated material for initial and comparison purposes. The results are given in Table 8 and Graph 8.

Table 8 AL 5754 Stock Material Tensile Test Results

Specimen thickness	**4**	**mm**
Strain at break	29,6521	%
Uniform elongation	15,1458	%
Total strain at maximum tensile strength (corr.)	23,2058	%
Total strain at break (corr.)	35,4162	%
Specimen width	6,35	mm
Maximum yield strain	5	%
Maximum extension	50	mm
Tensile strength	228,901	MPa
Proof stress at non-proportional elongation 0.2%	117,79	MPa
Travel after break	5	mm

Table 9 FSW Test Parameters

Heading	ATILIM UNIVERSITESI
Test Location	Metal Forming Center of Excellence
Date	
Tester	Res. Eng. Ozan OFLAZ
Test standard	DIN EN 10002-1,04/1991, ISO 10113,05/1991 and ISO 10275,02/1993 Tensile tests on metals with determination of the vertical anisotropy and the hardening exponents
Test Machine	Zwick//Roell Z300E
Specimen type	Flat
Speed, E-Modulus	6 mm/min
Speed in the yield range	6 mm/min
Speed, yield point	6 mm/min
Test speed	6 mm/min

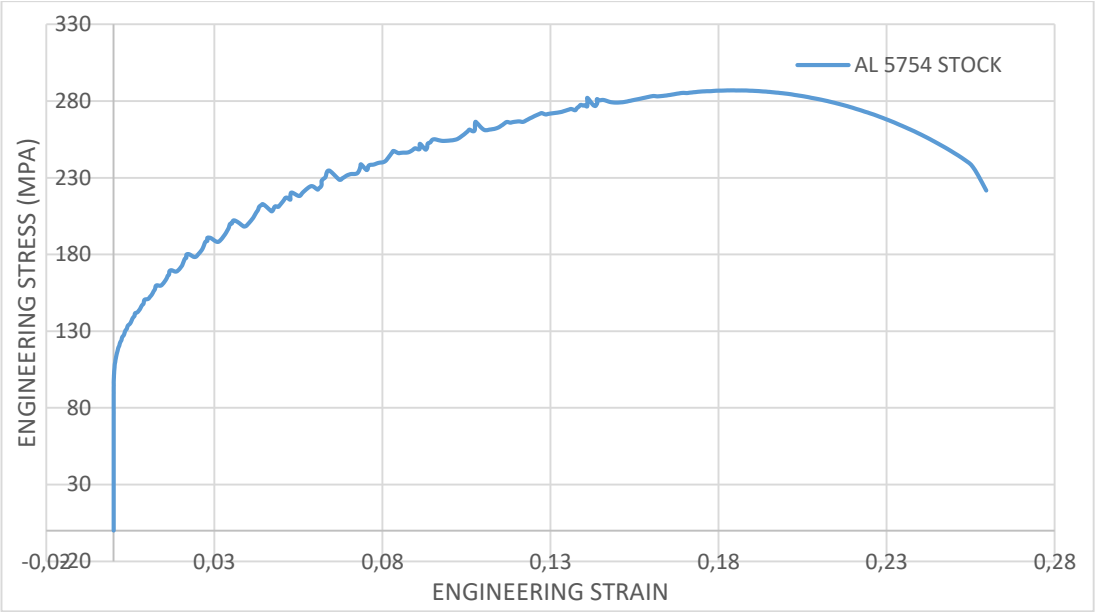

Figure 6.19 Engineering Stress- Strain graph of AL 5754

Figures 6.20 and 6.21 show the results of the tensile tests of the stock aluminium 5754 material at room temperature in MFCE. The tests were obtained repeatedly from samples prepared in the 0 direction at room temperature. Graph 11 shows the Engineering Stress and Engineering Strain tensile test curves of the stock material at room temperature. Welded Specimen Comparative graphs are given in Graph 12. The resulting materials have one-way welding. The samples with the best, average and worst yield strength are samples numbered 136, 254 and 356, respectively.

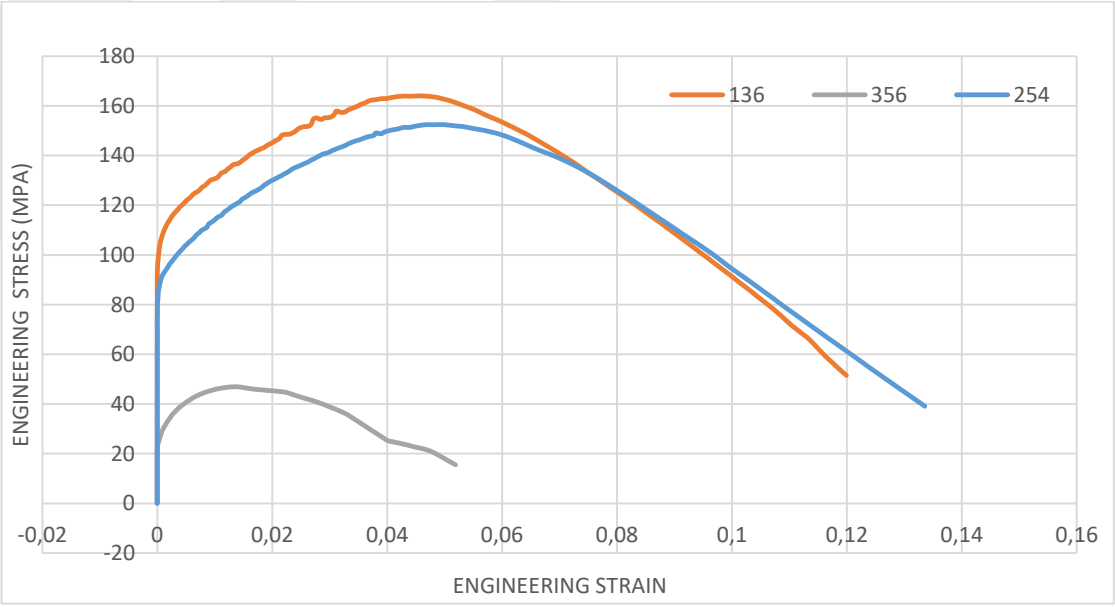

Figure 6.20 Engineering Stress-Strain graph of Sample No. 136-356-254

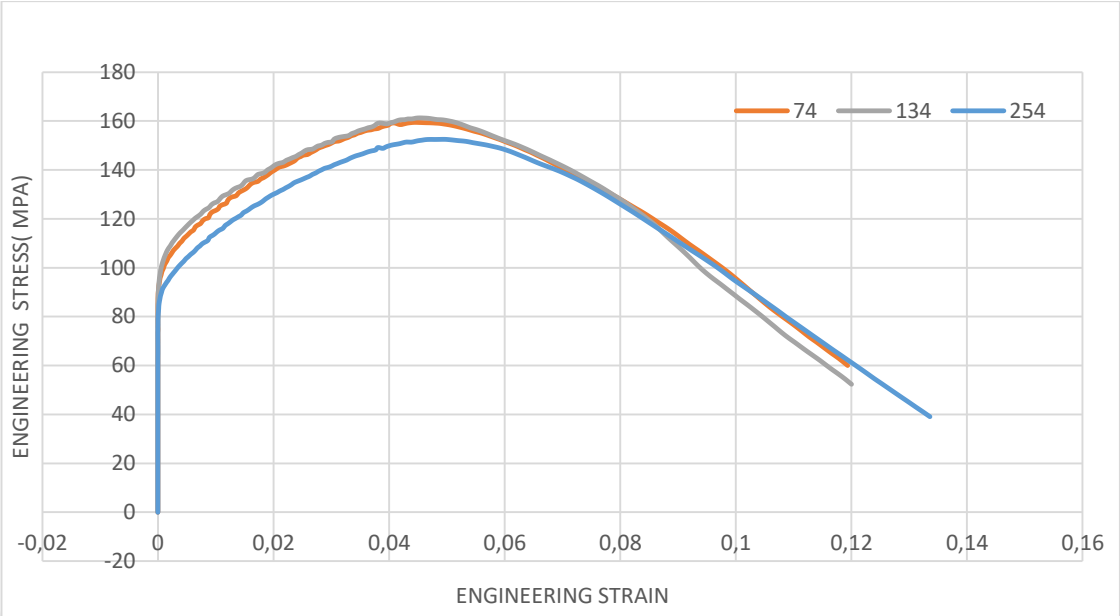

Figure 6.21 Engineering Stress-Strain graph of Sample No. 74-134-254

The flow curve of the samples with average and above success is shown on figure 6.22. Surface roughness was taken in these samples.

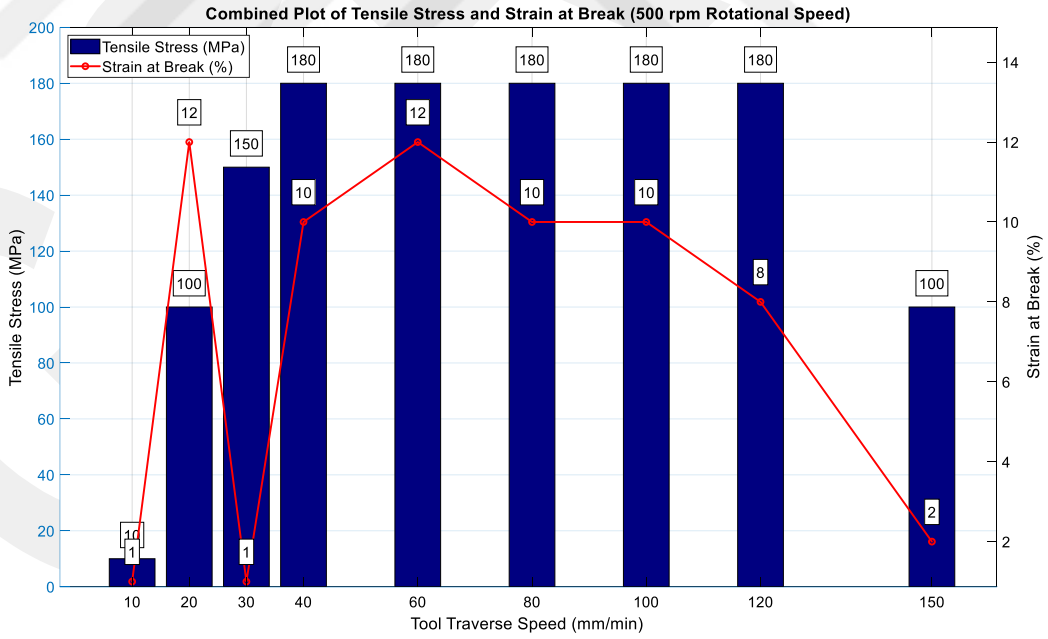

Figure 6.22 Combined Plot of Tensile Stress and Strain at Break (500 rpm Rotational Speed)

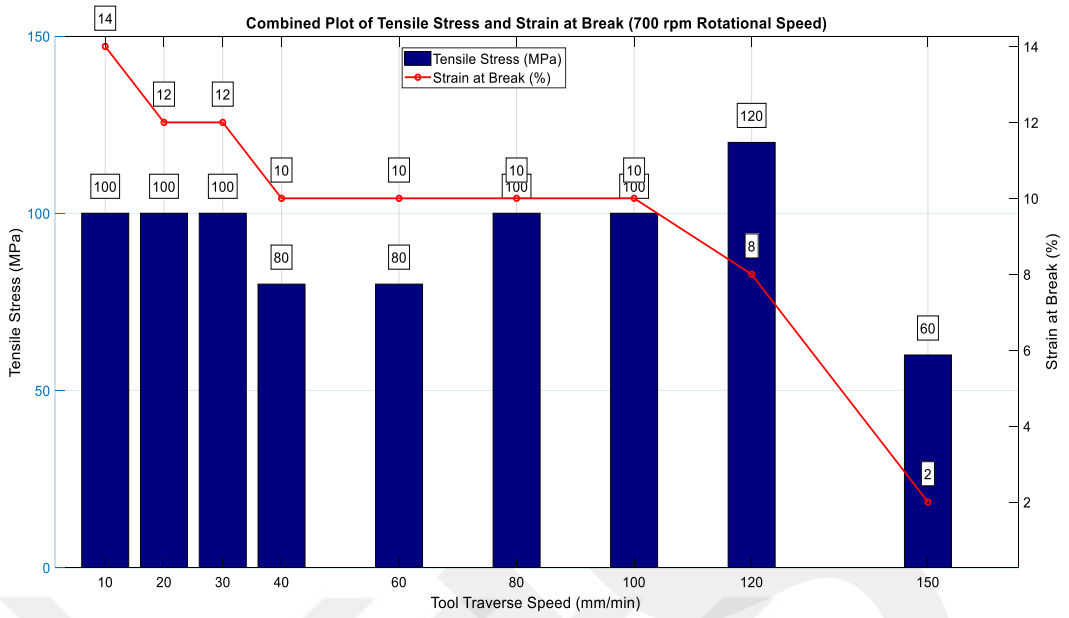

Figure 6.23 Combined Plot of Tensile Stress and Strain at Break (700 rpm Rotational Speed)

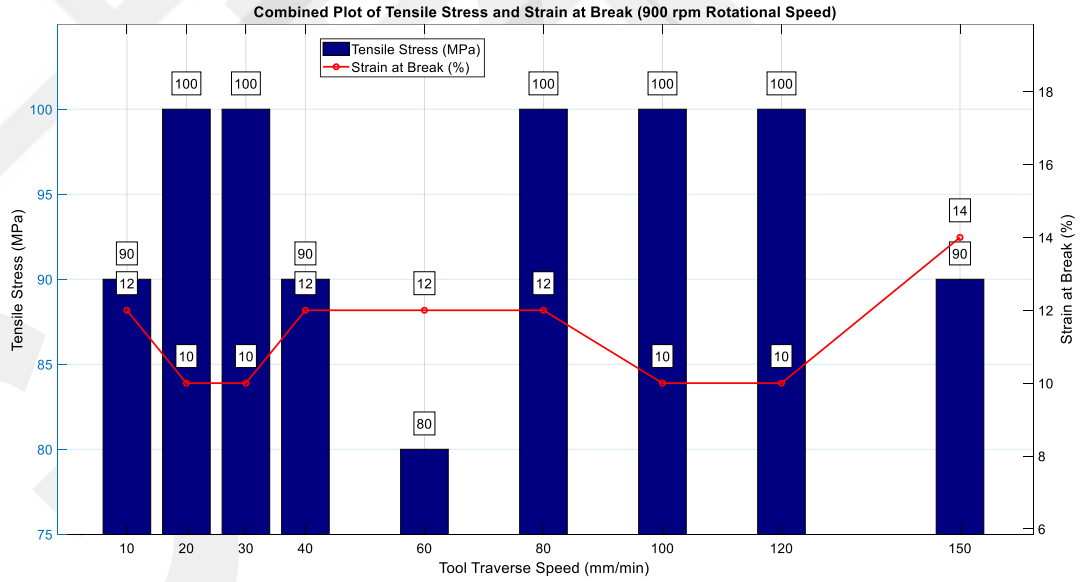

Figure 6.24 Combined Plot of Tensile Stress and Strain at Break (900 rpm Rotational Speed)

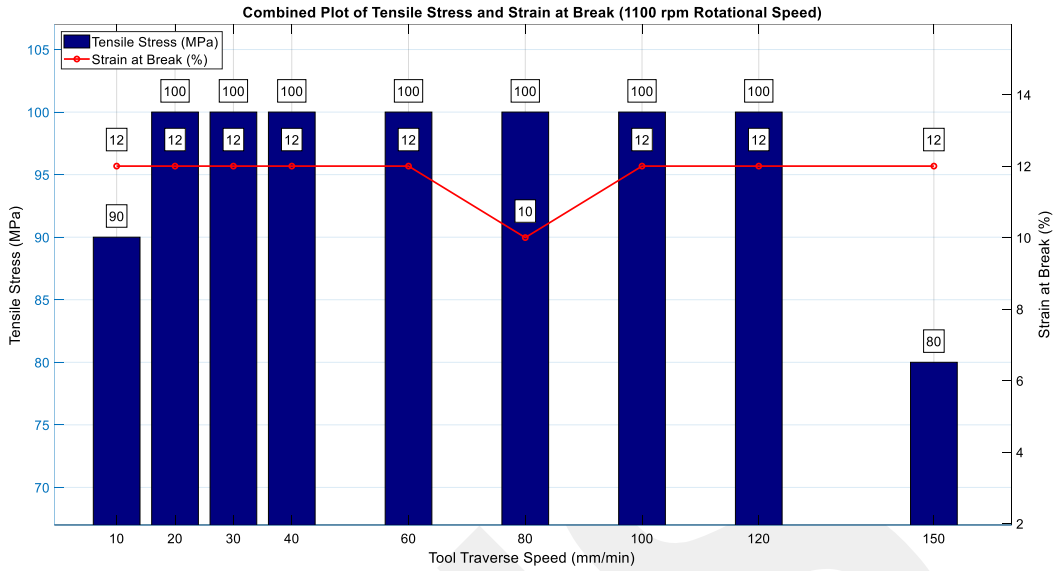

Figure 6.25 Combined Plot of Tensile Stress and Strain at Break (1100 rpm Rotational Speed)

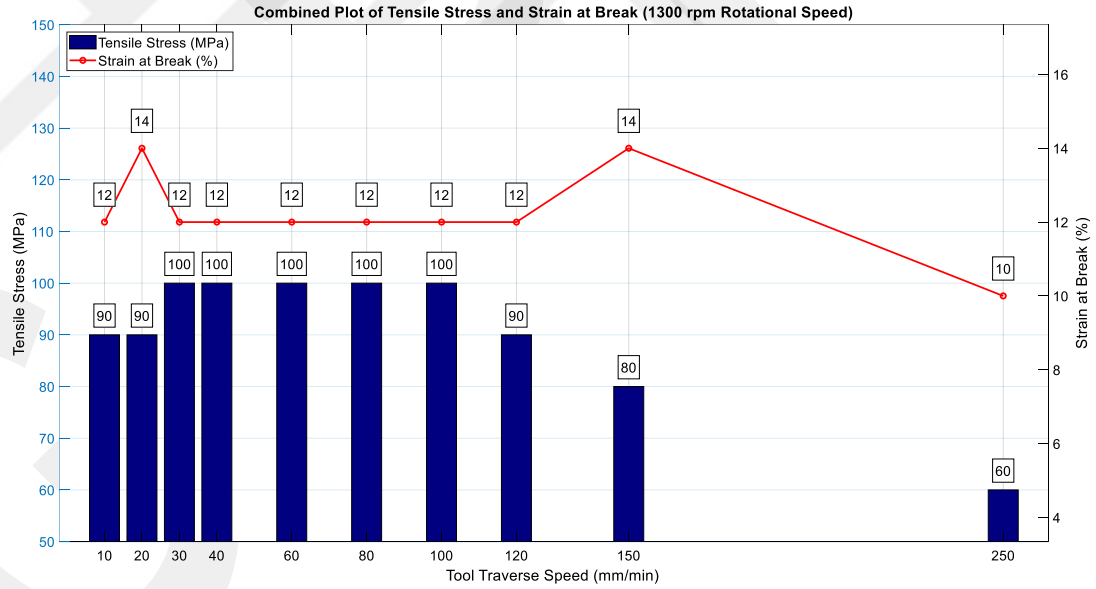

Figure 6.26 Combined Plot of Tensile Stress and Strain at Break (1300 rpm Rotational Speed

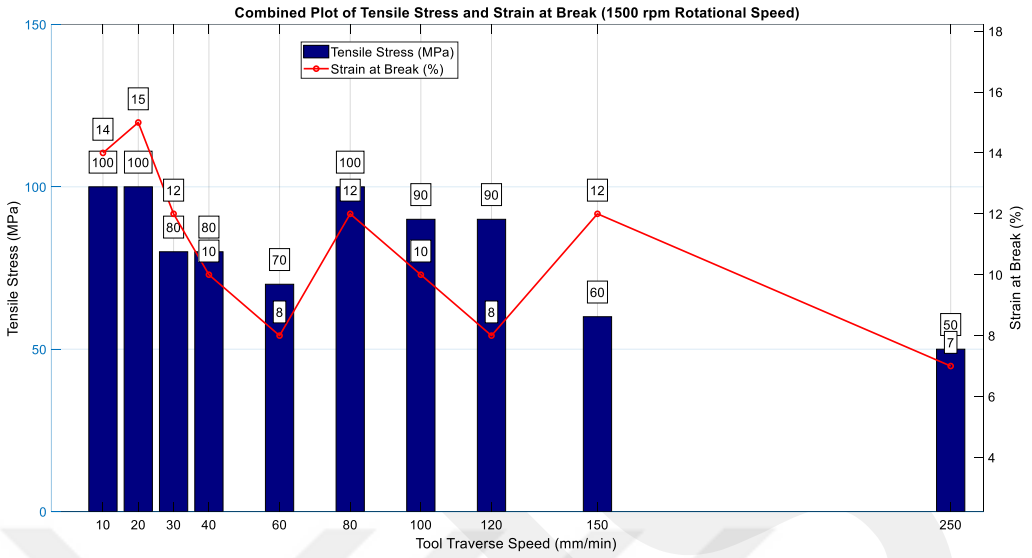

Figure 6.27 Combined Plot of Tensile Stress and Strain at Break (1500 rpm Rotational Speed)

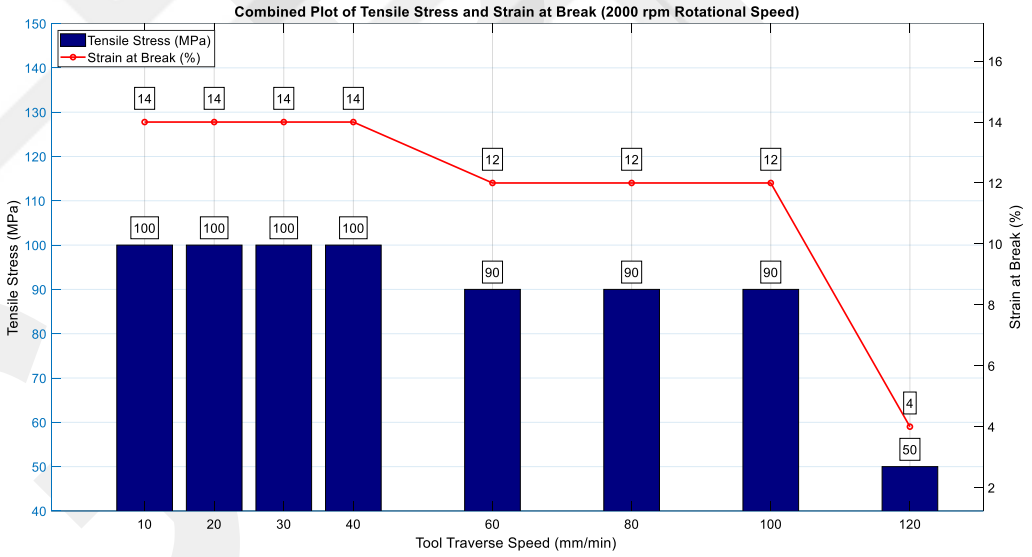

Figure 6.28 Combined Plot of Tensile Stress and Strain at Break (2000 rpm Rotational Speed)

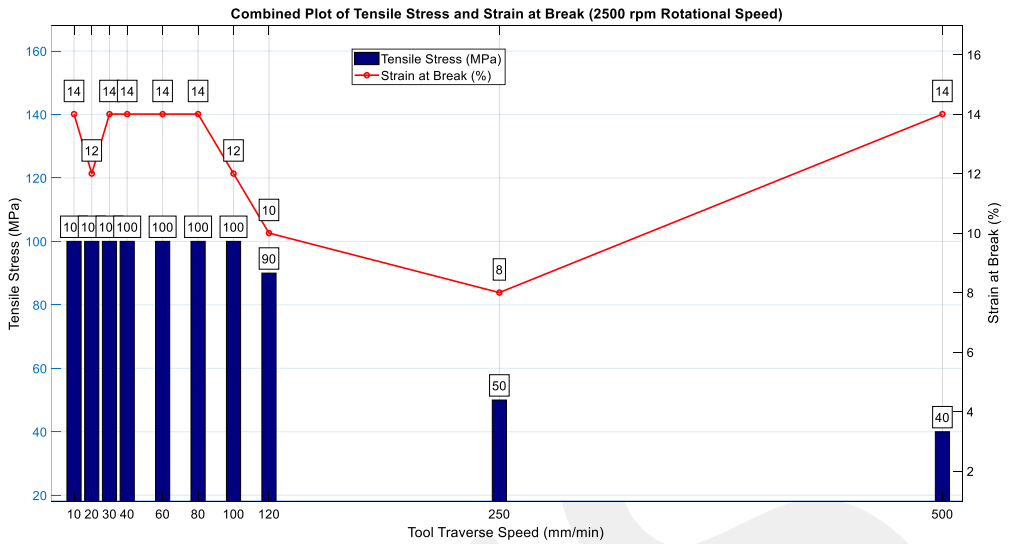

Figure 6.29 Combined Plot of Tensile Stress and Strain at Break (2500 rpm Rotational Speed)

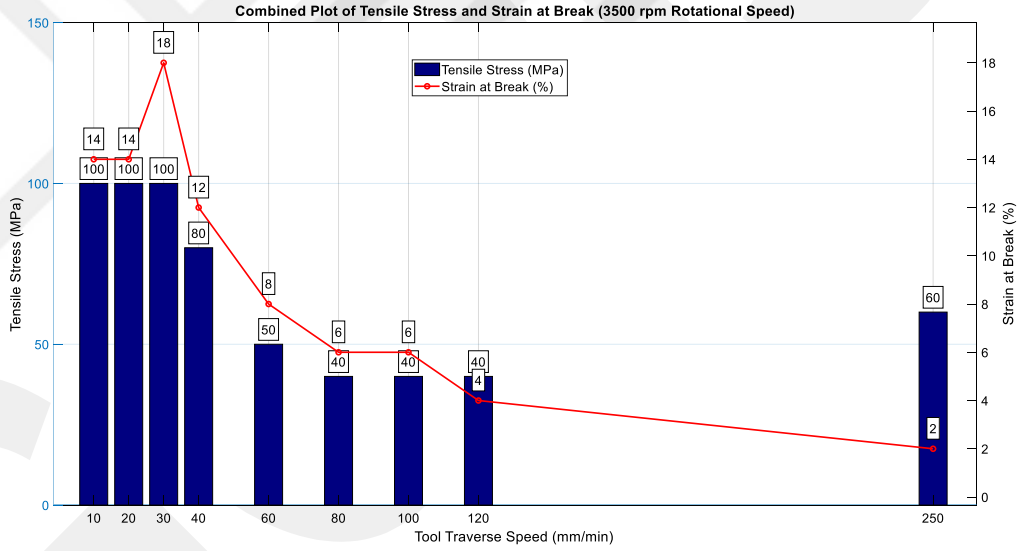

Figure 6.30 Combined Plot of Tensile Stress and Strain at Break (3500 rpm Rotational Speed)

The test results of the tensile test samples produced after the unidirectional friction stir welding process are given in the graphs. In each graph, Tensile stress (MPa) and Strain at break (%) for different rotational speeds are shown side by side. In this way, the comparison of elongation and mechanical strength against rotational speeds is clearly seen. The graphs in option b are shown in the axis Tensile stress (MPa) in the y-axis Tool traverse speed (mm/min) in the x-axis. Graphs The graphs in option a are shown

in the axis Strain at break (%) in the y-axis Tool traverse speed (mm/min) in the x-axis.

6.2.4. Bidirectional Welded Tensile Tests

In the article titled "Double Side Friction Stir Welding Effect on Mechanical Properties and Corrosion Rate of Aluminium Alloy AA6061", Danang Priyasudana, Simonne Andrean Crisdion, Poppy Puspitasari, Triyono, Jamasri and Andoko authors investigated the effects of bidirectional friction stir welding (DS-FSW) on mechanical properties and corrosion rate of AA6061 aluminium alloy. In the study, welding was performed by changing the upper and lower tool rotation speeds (1500 RPM and 900 RPM) and tool axis positions and the obtained results were evaluated. In radiographic tests, some samples were observed to have joint defects called "Incomplete Fusion" (IF); it was stated that these defects occurred due to low thermal input and rapid cooling. In microstructure analyses, fine-grained recrystallization was detected in the weld zone, but it was determined that there was no phase transformation. In hardness tests, sample B showed the highest hardness value in the weld zone. In bending tests, sample D showed 41.86 MPa in position 1G. While sample A provided the highest strength with tensile value and 13.23% elongation in 4G position, sample A obtained a tensile value of 38.18 MPa. Impact test results revealed that sample D had the highest impact toughness value with 9.35 J/mm². In corrosion tests, sample B in 1G position had the highest corrosion rate (0.63856 mm/year), and sample A welded at 900 RPM had the lowest corrosion rate (0.058567 mm/year). This study shows that bidirectional FSW parameters have significant effects on microstructure, mechanical properties and corrosion behaviour [27].

As a result of literature research, although it is not used much, it was predicted that even higher mechanical properties than the stock material could be obtained when friction stir welding is applied to both sides of the plate. For this reason, sample preparation processes were re-applied with 3 different speeds and 8 different traverse speeds for bidirectional welding, and force measurements were not taken during these welding. After welding, 3 bidirectional welded tensile test plates were prepared from each plate.

In cases where the traverse speed exceeded 120 mm/min, a serious decrease was observed in the tensile test results and hardness data at each rotational speed. For this reason, traverse speed parameters up to 120 m/min were used in the tests where welding would be done in two directions. For the bidirectional welding test, 24 tests were performed.

When the mechanical properties obtained in the bidirectional FSW (Friction Stir Welding) applications were evaluated, it was observed that different parameters had significant effects on the strength of the material. While 29% higher tensile strength was obtained in the bidirectional FSW sample with 700-120 parameters compared to the stock material, this value was recorded as 24% in the 700-100 parameter sample. On the other hand, 11% increase was observed in the 2500-120 parameter sample, 5% in the 1300-10 sample and 2% in the 2500-10 sample. In addition, the 700-100 parameter bidirectional FSW sample had the longest elongation data among the stock material and other bidirectional welded samples. These results show that the bidirectional welding processes, especially in the 700 series parameters, improve both the strength and ductility of the material.

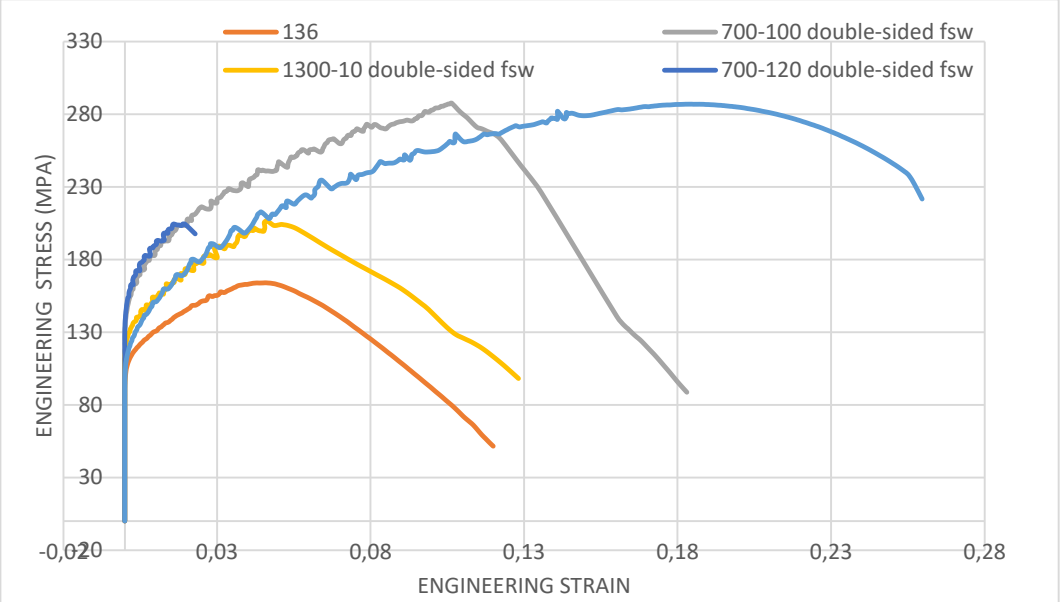

Figure 6.31 Engineering Stress-Strain Curves of Aluminium Alloy AL 5754 Under Different Friction Stir Welding (FSW) Conditions

As a result of the mechanical tests, sample number 136 had the best tensile strength data among the single-sided welding applications. In addition, the Engineering stress-strain graph for the stock material was included in the analysis. In bidirectional FSW

applications, it was determined that the samples with parameters 700-120 offered high tensile strength, but the amount of elongation remained limited. On the other hand, the bidirectional welding sample with parameters 700-100 had the most successful test result in terms of elongation and also showed the second highest tensile strength value. These findings reveal that the 700 series parameters exhibit different performances, especially in terms of elongation and strength.

Table 10 Tensile Test Results of Bidirectional Welded Specimens

Rotation Speed	**Tool Traverse Speed**	**RP 0.2**	**Rm**	**A**
(rpm)	**mm/min**	**Mpa**	**Mpa**	**% Elongation at Break**
AL 5754 Stock		117,79	228,90	29,65
2500	10	121,09	160,42	11,51
2500	20	63,25	96,01	7,32
2500	30	112,18	112,43	10,00
2500	40	86,11	107,67	9,98
2500	60	77,32	113,00	8,97
2500	80	79,44	111,78	12,38
2500	100	131,05	234,48	33,90
2500	120	131,46	219,35	25,03
1300	10	124,45	180,94	13,68
1300	20	65,37	100,94	12,14
1300	30	95,57	108,23	7,45
1300	40	77,78	88,92	8,10
1300	60	78,27	105,56	10,49
1300	80	103,81	105,45	5,52
1300	100	49,69	50,23	4,28
1300	120	100,66	100,9	10,62
700	20	106,18	112,04	10,02
700	30	64,54	66,00	5,87
700	40	76,47	76,73	1,24
700	60	83,24	83,42	6,35
700	80	70,66	71,69	3,98
700	100	146,52	238,23	20,08
700	120	152,35	186,62	2,32

6.3. Pearson Product Moment Correlation Coefficient

The Pearson Product Moment Correlation Coefficient (PPMCC) is a statistical coefficient that determines the direction and size of a linear relationship between two continuous variables. It is typically represented by the letter "r" and has a value between -1 and 1.

- r = 1 indicates a perfect positive linear relationship between two variables. As one variable increases, the other increases at the same rate.
- r = -1 indicates a complete negative linear relationship between two variables. As one variable grows, the other lowers at the same rate.
- r = 0 indicates that there is no linear relationship between the two variables.

$$r = \frac{\sum(x_i - \bar{x})(y_i - \bar{y})}{\sqrt{\sum(x_i - \bar{x})^2 \cdot \sum(y_i - \bar{y})^2}} \quad (2)$$

The variables are continuous, and the level of measurement is at least interval. There must be a linear relationship between the variables. The dataset must be regularly distributed. Positive r value indicates a positive association between two variables. Negative r value indicates a negative association between two variables. The magnitude of r indicates the strength of the relationship. Pearson Correlation is a strong tool, particularly for evaluating linear relationships; nevertheless, it cannot capture nonlinear relationships, thus use with caution.

One of the important advantages of PPMCC is that it is simple to calculate and gives a direct result. This is an effective method to quickly assess whether data has a linear relationship. It is also a very successful tool for analyzing linear relationships. However, PPMCC also has some limitations. The first of these is that it only considers linear relationships; therefore, incorrect results may occur if the relationship between the variables is not linear. It is also based on the assumption that the variables are normally distributed, and reliable results may not be obtained if this assumption is not met. Another important limitation is that outliers can significantly affect the correlation coefficient. Therefore, it is important to consider the effect of outliers when performing the analysis. Although PPMCC is a powerful tool for understanding linear relationships in statistics, it is necessary to consider the context and the limitations of the method when interpreting the results [60]. The code written in Python for the analysis is included in Appendix A. The table shows the result of the correlation analysis. The following code was written to perform correlation analysis.

Table 11 Correlation Heatmap of FSW Experiments

Correlation Heatmap of FSW Expreiments																		
-0,31	-0,5	0,05	-0,8	-0,3	0,34	-0,3	-0	0,04	0	0,04	-0,3	-0,5	0,1	-0,8	-0,7	0	1	Rotation
0,68	0,05	0,14	0	0,62	0,36	0,61	-0,3	-0,3	-0,2	-0,2	-0,2	-0,1	-0,3	0,15	-0	1	0	Tool
0,04	0,28	-0,1	0,65	0,03	-0,4	0,32	0,27	0,21	0,17	0,18	0,38	0,55	0,11	0,67	1	-0,02	-0,73	Hardness
0,5	0,31	-0,1	0,86	0,52	-0	0,08	-0,2	-0,2	-0,2	-0,2	0,06	0,29	-0	1	0,67	0,15	-0,75	SO mm2
-0,26	-0,4	-0	-0	-0,3	-0,1	-0,1	0,06	0,13	-0	-0,2	-0,1	-0,1	1	-0	0,11	-0,25	0,1	LO
-0,1	0,32	0,03	0,22	-0	-0,8	-0,1	0,77	0,57	0,76	0,57	0,93	1	-0,1	0,29	0,55	-0,13	-0,5	RP 0.2
-0,26	0,25	0,03	-0	-0,2	-0,8	-0,3	0,87	0,72	0,88	0,73	1	0,93	-0,1	0,06	0,38	-0,23	-0,27	Rm
-0,31	0,19	0,01	-0,3	-0,3	-0,5	-0,3	0,72	0,83	0,72	1	0,73	0,57	-0,2	-0,2	0,18	-0,19	0,04	Ag
-0,31	0,19	0,03	-0,3	-0,3	-0,6	-0,3	0,93	0,7	1	0,72	0,88	0,76	-0	-0,2	0,17	-0,24	0	A
-0,48	-0	-0	-0,3	-0,4	-0,7	-0,3	0,86	1	0,7	0,83	0,72	0,57	0,13	-0,2	0,21	-0,27	0,04	Agt
-0,45	0,08	0	-0,3	-0,4	-0,8	-0,3	1	0,86	0,93	0,72	0,87	0,77	0,06	-0,2	0,27	-0,29	-0,04	At
0,34	0,01	0,03	0,09	0,22	0,25	1	-0,3	-0,3	-0,3	-0,3	-0,3	-0,1	-0,1	0,08	0,32	0,61	-0,26	F_x
0,44	-0	0,08	0,03	0,36	1	0,25	-0,8	-0,7	-0,6	-0,5	-0,8	-0,8	-0,1	-0	-0,4	0,36	0,34	F_y
0,99	0,55	-0	0,55	1	0,36	0,22	-0,4	-0,4	-0,3	-0,3	-0,2	-0	-0,3	0,52	0,03	0,62	-0,33	F_z
0,53	0,49	-0,1	1	0,55	0,03	0,09	-0,3	-0,3	-0,3	-0,3	-0	0,22	-0	0,86	0,65	0	-0,8	F_x MAX
-0,02	-0	1	-0,1	-0	0,08	0,03	0	-0	0,03	0,01	0,03	0,03	-0	-0,1	-0,1	0,14	0,05	F_y MAX
0,51	1	-0	0,49	0,55	-0	0,01	0,08	-0	0,19	0,19	0,25	0,32	-0,4	0,31	0,28	0,05	-0,45	F_z MAX
1	0,51	-0	0,53	0,99	0,44	0,34	-0,5	-0,5	-0,3	-0,3	-0,3	-0,1	-0,3	0,5	0,04	0,68	-0,31	F Mean
F	F_z	F_y	F_x	F_z	F_y	F_x	At	Agt	A	Ag	Rm	PR0.	LO	SO	Hardness	Tool	Rotation	

+1: Strong positive relationship (as one increases, the other increases).

-1: Strong negative relationship (as one increases, the other decreases).

0: No linear relationship at all.

Rotation Speed (N) and Tool Traverse Speed (v): Nearly zero correlation (r=0.00r), As can be seen in the Correlation Heat Map of FSW Experiments, there is zero correlation, that is, it shows that the rotation speed and the movement speed are independent of each other. Since both data are input for the source, it is expected that no correlation can be established.

Rotation Speed (N):

- **Hardness:** Strong negative correlation (r=−0.73r), suggesting that higher rotation speeds reduce material hardness. It is clearly observed that low tool traverse speed is more suitable for material hardness, while material hardness decreases at high speeds.
- **RP 0.2 (Yield Strength):** Negative correlation (r=−0.5r), It was observed that there was an inverse relationship between Rotational Speed and Yield strength (RP 0.2). High Rotational speed adversely affected strength after welding.
- **Elongation:** Nearly zero correlation (r=0.00r), As can be seen in the Correlation Heat Map of FSW Experiments, there is zero correlation, that is, it shows that the rotation speed and the elongation of tensile specimen are independent of each other.
- **F_x MAX:** Very strong negative correlation (r=−0.80r), meaning rotation speed has a significant impact on reducing maximum force values.

Tool Traverse Speed (v):

- **Hardness:** Moderate positive correlation (r=0.67r), indicating that higher traverse speeds may positively affect hardness.
- **RP 0.2 (Yield Strength):** A very low negative correlation was observed. (r=−0.13r), There is almost no relationship between yield strength and tool traverse speed.

- **Elongation:** A correlation of almost 0 was observed. (r=-0.24r), A very low negative correlation was observed. Therefore, it is difficult to tell the relationship between the two by looking at the heat map.
- **F_x_mean, F_y_mean, F_z_mean:** Positive correlations with all force components, showing that traverse speed increases the forces acting during welding.

6.4. Surface Roughness

Surface roughness refers to the microscopic irregularities of the surface. It is usually characterized by high-frequency surface fluctuations and small-scale surface profile features. In industrial manufacturing processes and engineering applications, surface roughness is a critical parameter in determining product quality, functionality and performance. In the Friction Stir Welding method, surface roughness is a critical factor that directly affects the weld quality. Low surface roughness ensures that the material flow is more regular, heat generation is kept under control and the strength of the weld area is increased. Keeping the surface roughness at the appropriate level for the FSW process is necessary to obtain more robust, durable and high-performance weld joints.

Surface roughness is usually measured by various parameters such as Ra, Rz and Rt. These parameters are used to evaluate the overall profile of the surface and its microscopic peaks and valleys:

- **R_a (Average Roughness):** Represents the average amount of deviation from the surface profile. The Ra value is the most common roughness parameter that expresses the overall irregularity of the surface.
- **R_z (Peak-Valley Height):** Indicates the difference between the highest and lowest points on the surface.
- **R_t (Total Height):** Indicates the distance between the highest point on the surface and the deepest valley.

Alicona Infinite Focus device was used in surface roughness measurements. Alicona Infinite Focus, which is located within the Metal Forming Centre of Excellence, is a highly sensitive and fast optical measurement system. The surfaces of the components

are measured with multifunctional microprocessors [56]. Among the competencies of Alicona Infinite Focus are surface roughness measurements, surface texture measurements, creation of 3D forms of micro-manufactured parts and cutting tool measurements in many areas. Thanks to its vibration isolation, it also enables the form and roughness measurement of large and heavy components [56]. With its forward-backward moving table and rotation table, measurements of parts with many different geometries can be performed using 6 different optical lenses. Operating with a fully automatic measurement principle, Alicona Infinite Focus minimizes the error rate [56].



Figure 6.32 Alicona Infinite Focus

The stock material represents material on which no welding process has been performed. To compare the surface roughness, measurements were first made on the stock material that had not been processed at all. A comparison was made between the stock materials and the materials with the smoothest surface visually. For this purpose, samples no. 74, 134, 254 were selected. In the tensile test, samples numbered 74, 134 and 254, which can be considered as the average tensile strength of the general tests and above, were selected. The aim was to observe the surface quality on an average weld. In samples such as 356, which have lower tensile strength, the surface quality was too bad to be examined.

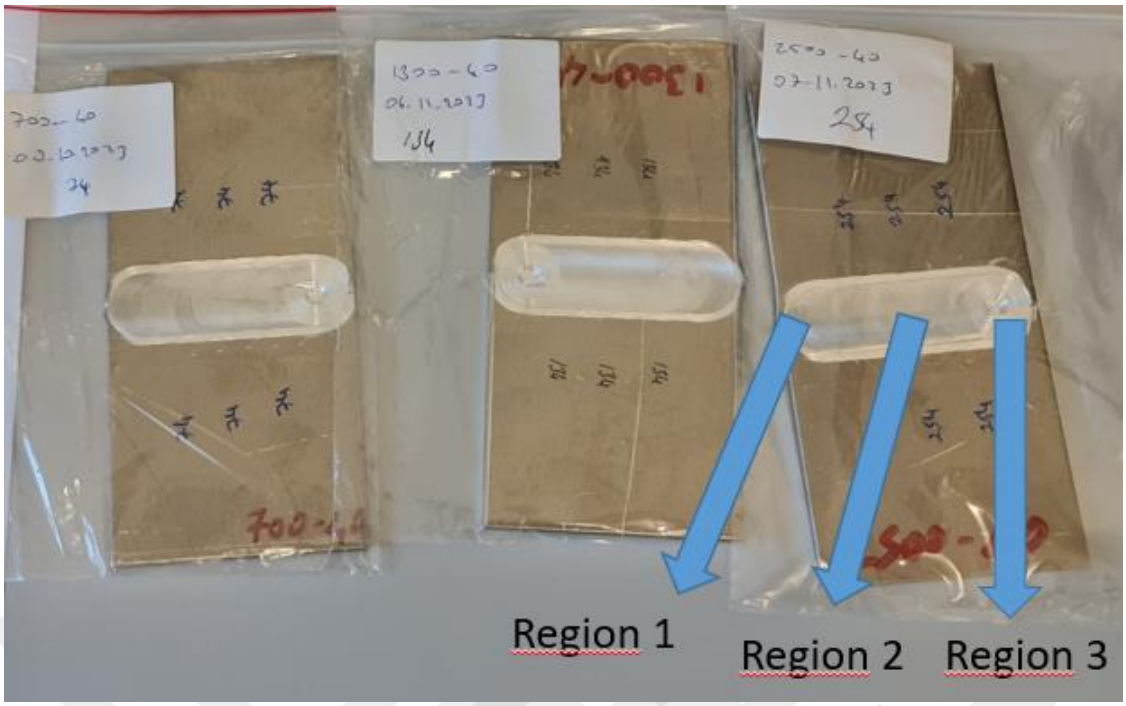

Figure 6.33 Samples no. 74 - 134 - 154

6.4.1. Stock Material Surface Roughness Measurements

Measuring the surface of stock material is a critical step in assessing the surface condition and quality of the material prior to machining. These measurements determine the natural roughness level of the material, allowing you to anticipate potential difficulties in the manufacturing process and select appropriate machining parameters.

Table 12 Surface roughness results of stock material

Name	Value	Unit	Description
Elements	1640	-	Number of data values
Classes	193	-	Number of histogram classes
Mean Value	0.01	µm	Mean value of data values
Standard Deviation	0.61	µm	Mean value of standard deviation

Table 13 Surface Roughness Parameters and Profile Characteristics

Name	Value	Unit	Description
$\mathbf{R_a}$	0.48	µm	Average roughness of profile
$\mathbf{R_q}$	0.61	µm	Root-Mean-Square roughness of profile
$\mathbf{R_t}$	3.84	µm	Maximum peak to valley height of roughness profile
$\mathbf{R_z}$	3.03	µm	Mean peak to valley height of roughness profile
$\mathbf{R_{max}}$	3.74	µm	Maximum peak to valley height of roughness profile within a sampling length
$\mathbf{R_p}$	1.62	µm	Maximum peak height of roughness profile
$\mathbf{R_v}$	2.22	µm	Maximum valley height of roughness profile
$\mathbf{R_p5}$	1.41	µm	Mean peak height of roughness profile
$\mathbf{R_v5}$	1.62	µm	Mean valley height of roughness profile
$\mathbf{R_c}$	1.86	µm	Mean height of profile irregularities of roughness profile
$\mathbf{R_{sm}}$	89.81	µm	Mean spacing of profile irregularities of roughness profile
$\mathbf{R_{sk}}$	0.0043312	-	Skewness of roughness profile
$\mathbf{R_{ku}}$	3.4908	-	Kurtosis of roughness profile
$\mathbf{R_{dq}}$	0.065983	-	Root-Mean-Square slope of roughness profile
$\mathbf{R_t/R_z}$	1.2696	-	Extreme Scratch/Peak value of roughness profile (>=1), higher values represent larger scratches/peaks
l	2.52773	mm	Profile Length
$\mathbf{L_c}$	250.00	µm	ΛC: cut off wavelength

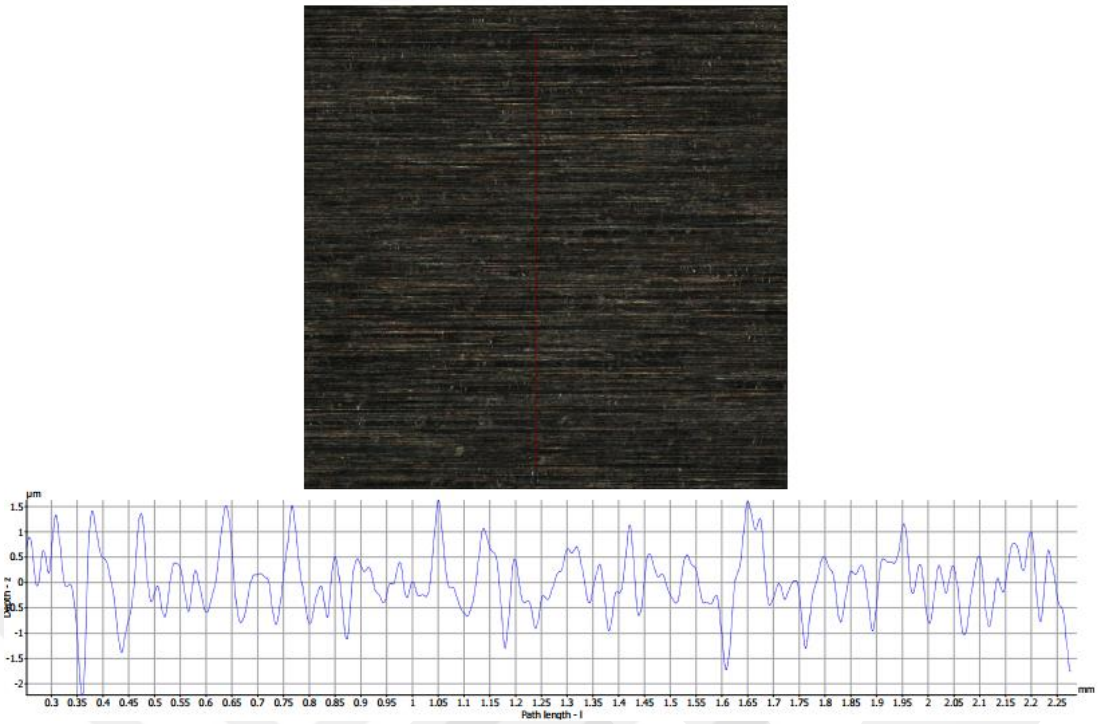

Figure 6.34 Stock material surface roughness histogram chart

R_a and R_q Values:

R_a (Average Roughness): The value of 0.48 µm indicates that the surface has a generally homogeneous and acceptable roughness. This is a favorable starting point for stock material.

R_q (Root-Mean-Square Roughness): The value of 0.61 µm, in line with Ra, confirms that the surface roughness is low and provides a suitable baseline for further processing.

R_t and R_z Values:

R_t (Maximum Peak-to-Valley Height): With a value of 3.84 µm, this parameter reflects the maximum difference between the highest peak and the lowest valley on the surface. It suggests the presence of localized roughness.

R_z (Mean Peak-to-Valley Height): At 3.03 µm, it demonstrates that the surface profile fluctuations are within a reasonable range.

R_{max} and Related Parameters:

R_{max}: The value of 3.74 µm represents the highest surface irregularity detected, indicating the absence of major defects on the surface.

R_c and R_{sm}: The mean height of surface irregularities (1.86 µm) and their spacing (89.81 µm) suggest that the surface irregularities are evenly distributed, and the stock material exhibits a homogeneous microstructure.

R_{sk} and R_{ku} Values:

R_{sk} (Skewness): The value of 0.0043312 suggests that the surface profile is symmetrical, with balanced distribution between peaks and valleys.

R_{ku} (Kurtosis): At 3.4908, this indicates sharper peaks and valleys in the surface profile, which is a characteristic of the material's natural state.

R_{dq} and ΛC Values:

R_{dq}: A low value of 0.065983 reflects a surface with minimal slope, indicating overall smoothness.

λ_C (Cut-off Wavelength): The value of 250.00 µm denotes the wavelength range used for roughness analysis, which is sufficient for understanding the surface profile.

The surface roughness values of this stock material show that the material has a smooth and homogeneous structure in its unprocessed state. Especially low Ra and Rq values indicate that the surface is suitable for processes such as polishing or surface coating after processing. Reasonable levels of values such as Rt and Rz indicate that there are no major roughness or irregularities on the surface of the stock material and therefore will provide significant advantages in the processing process.

These measurements reveal that the material provides a suitable basis even for applications requiring high surface quality. This data can be used as a reference to compare the surface properties before and after processing.

6.4.2. Surface Roughness Measurements of Sample No. 74

When measuring surface roughness, the welded area was divided into three horizontal zones. The characteristics of the lines are shown in Table 14.

Table 14 Profile Line Features

Name	length (µm)	angle (°)	x_1 (µm)	y_1 (µm)	x_2 (µm)	y_2 (µm)
L1	27777.78	0	84641.64	20264.93	87419.42	20264.93
L2	22261.29	0	84661.57	20261.32	106922.86	20261.32
L3	24600.57	0	84659.80	20271.74	109260.37	20271.74
Mean	16.54655	0	84.65433	20.26599	101.20088	20.26599
Std. Dev.	11.98133	0	0.01103	0.00529	11.99219	0.00529
Min	2.77778	0	84.64164	20.26132	87.41942	20.26132
Max	24.60057	0	84.66157	20.27174	109.26037	20.27174
Sum	49.63964	0	253.96300	60.79798	303.60265	60.79798
Median	22.26129	0	84.65980	20.26493	106.92286	20.26493
Robust	23.43093	0	84.66068	20.26132	108.09162	20.26132
Count	3	-	-	-	-	

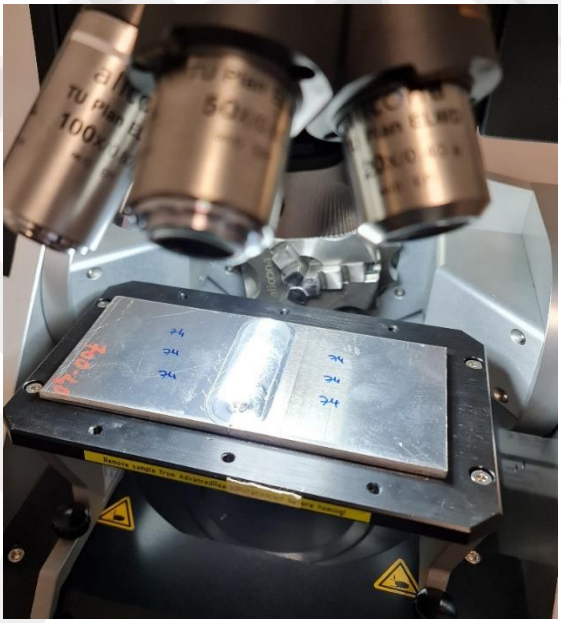

Figure 6.35 Surface roughness measurement process of sample no. 74

In figure 6.16 the colour scale shows the height distribution of the surface (in mm) and visualizes the height differences on the surface.

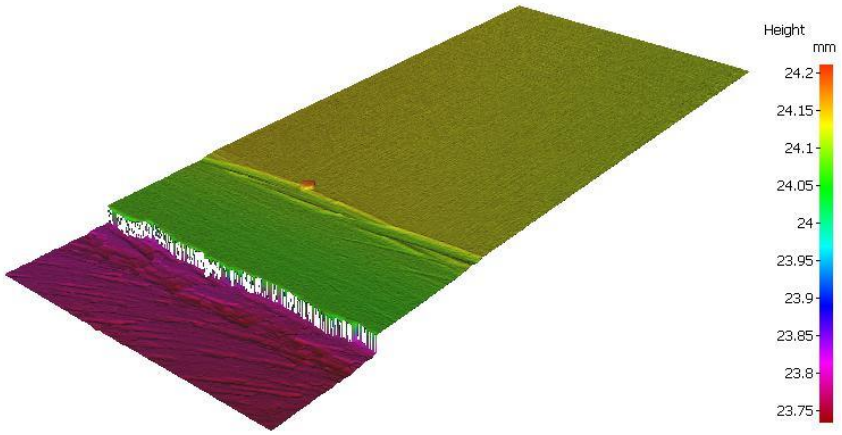

Figure 6.36 Height Distribution of Sample No. 74

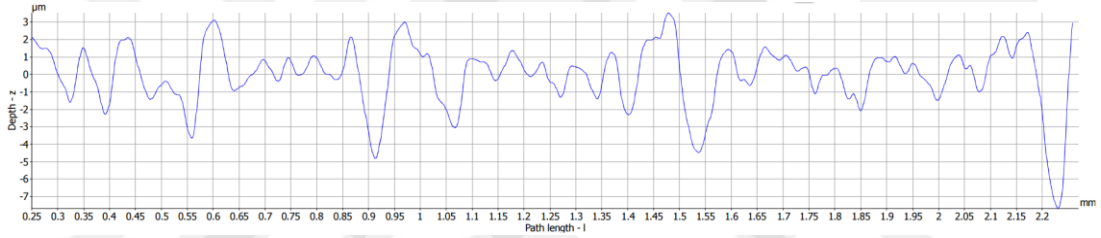

Figure 6.37 Sample 74, Region 1 Profile Graph

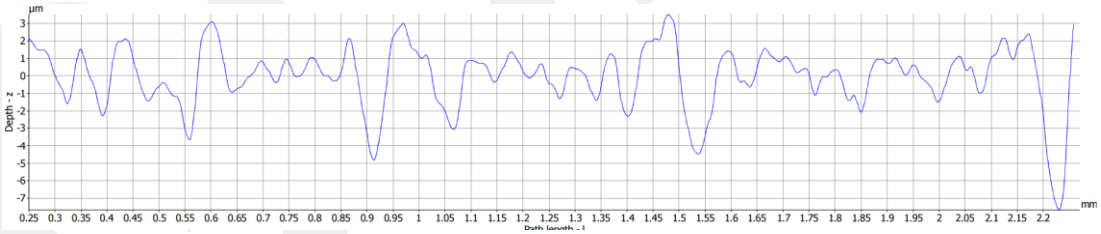

Figure 6.38 Sample 74, Region 2 Profile Graph

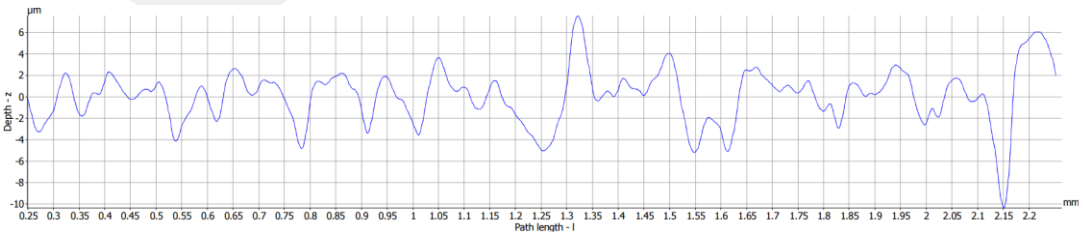

Figure 6.39 Sample 74, Region 3 Profile Graph

Table 15 Comparison of Surface Roughness Parameters Across Different Regions Sample No. 74

Name	Region 1 Value	Region 1 Unit	Region 2 Value	Region 2 Unit	Region 3 Value	Region 3 Unit
Elements	1640	-	1640	-	1640	-
Classes	112	-	106	-	180	-
Mean Value	-0.05	µm	0.03	µm	0.05	µm
Standard Deviation	1.75	µm	0.91	µm	2.54	µm
R_a	1.26	µm	0.71	µm	1.90	µm
R_q	1.75	µm	0.91	µm	2.54	µm
R_t	11.19	µm	5.30	µm	17.95	µm
R_z	7.68	µm	3.91	µm	10.70	µm
R_{max}	10.62	µm	5.30	µm	16.46	µm
R_p	3.52	µm	2.39	µm	7.57	µm
R_v	7.67	µm	2.91	µm	10.37	µm
R_{p5}	2.94	µm	1.90	µm	4.79	µm
R_{v5}	4.73	µm	2.01	µm	5.91	µm
R_c	4.72	µm	2.86	µm	7.13	µm
R_{sm}	171.67	µm	131.19	µm	191.99	µm
R_{sk}	-1.3407	-	0.092705	-	-0.335	-

6.4.3. Surface Roughness Measurements of Sample No. 134

Table 16 Comparison of Surface Roughness Parameters Across Different Regions Sample No. 134

Name	Region 1 Value	Region 1 Unit	Region 2 Value	Region 2 Unit	Region 3 Value	Region 3 Unit
Elements	1640	-	1640	-	1640	-
Classes	181	-	107	-	107	-
Mean Value	-0.01	µm	-0.02	µm	-0.02	µm
Standard Deviation	1.56	µm	1.57	µm	1.57	µm
Ra	1.20	µm	1.22	µm	1.22	µm
Rq	1.56	µm	1.57	µm	1.57	µm
Rt	9.04	µm	10.67	µm	10.67	µm
Rz	7.53	µm	7.10	µm	7.10	µm
Rmax	9.04	µm	8.00	µm	8.00	µm
Rp	3.65	µm	4.80	µm	4.80	µm
Rv	5.39	µm	5.87	µm	5.87	µm

Table 16 Comparison of Surface Roughness Parameters Across Different Regions Sample No. 134 (Cont.)

Rv5	4.09	µm	3.39	µm	3.39	µm
Rc	4.52	µm	4.81	µm	4.81	µm
Rsm	114.58	µm	112.35	µm	112.35	µm
Rsk	-0.30164	-	0.021999	-	0.021999	-

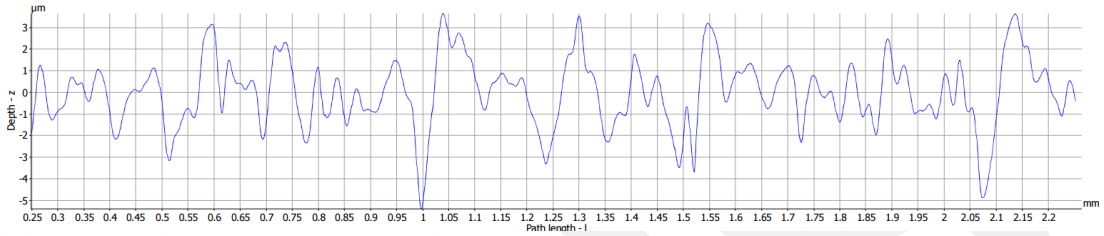

Figure 6.40 Sample 134, Region 1 Profile Graph

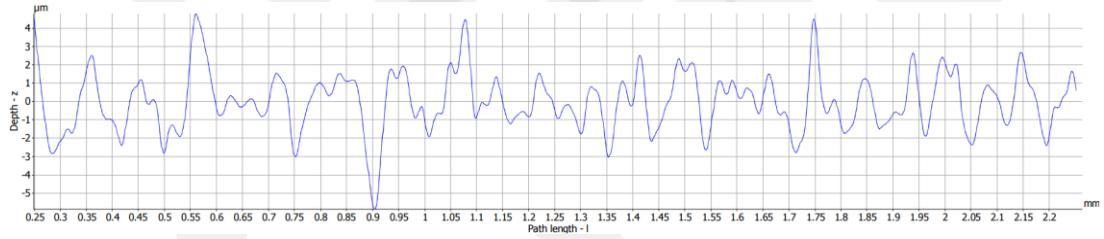

Figure 6.41 Sample 134, Region 2 Profile Graph

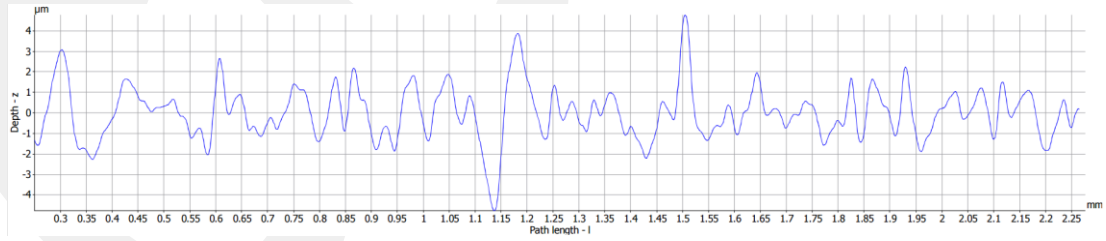

Figure 6.42 Sample 134 Region 3 Profile Graph

6.4.4. Surface Roughness Measurements of Sample No. 254

Table 17 Comparison of Surface Roughness Parameters Across Different Regions Sample No.254

Name	Region 1 Value	Region 1 Unit	Region 2 Value	Region 2 Unit	Region 3 Value	Region 3 Unit
Elements	1640	-	1640	-	1640	-
Classes	125	-	116	-	164	-
Mean Value	-0.01	µm	-0.02	µm	0.01	µm
Standard Deviation	0.86	µm	1.01	µm	1.36	µm
R_a	0.65	µm	0.79	µm	1.06	µm
R_q	0.86	µm	1.01	µm	1.36	µm
R_t	6.23	µm	5.76	µm	8.19	µm
R_z	3.87	µm	4.10	µm	6.10	µm
R_{max}	6.23	µm	5.50	µm	7.52	µm
R_p	2.45	µm	3.02	µm	3.86	µm
R_v	3.78	µm	2.74	µm	4.32	µm
R_{p5}	1.90	µm	2.03	µm	2.99	µm
R_{v5}	1.97	µm	2.07	µm	3.11	µm
R_c	2.63	µm	2.97	µm	4.34	µm
R_{sm}	136.30	µm	117.67	µm	123.60	µm
R_{sk}	0.18043	-	0.021999	-	0.25309	-

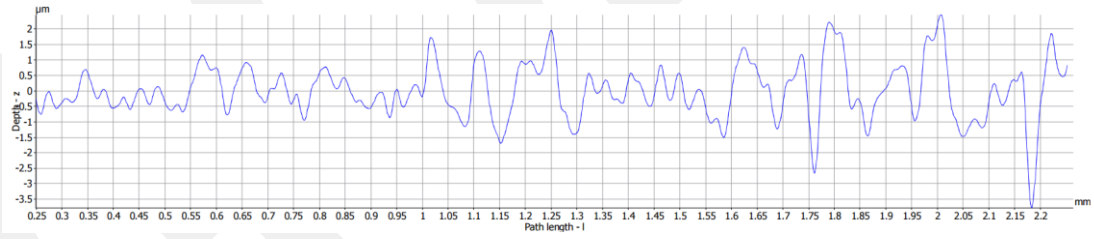

Figure 6.43 Sample 254, Region 1 Profile Graph

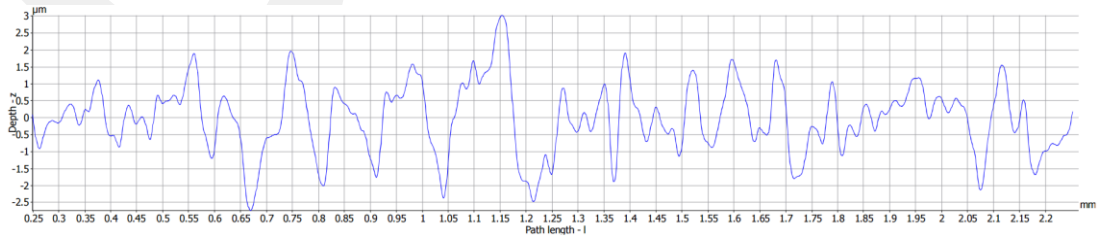

Figure 6.44 Sample 254, Region 2 Profile Graph

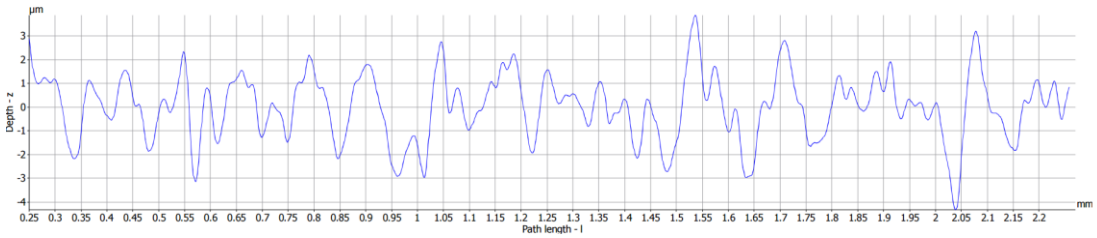

Figure 6.45 Sample 254 Region 3 Profile Graph

6.5 Microstructural Analysis of Welding Zone

In this thesis, internal structure analyses were performed using scanning electron microscopes to understand the material properties of the welded area formed because of the welds. The untreated material and the welded material were compared, the differences between them were compared and the properties of the welded area were explained.

The Zeiss Merlin is a high-resolution scanning electron microscope that is a versatile electron beam characterization tool for materials science research. It offers high-resolution secondary electron imaging thanks to the inner lens secondary electron detector. It also features a scanning transmission electron microscope (STEM) detector that enables the examination of electron-transparent thin film samples. It includes dedicated software support for the reconstruction of three-dimensional surface topography, as well as EDS for X-ray microanalysis and elemental distribution determination, and EBSD systems for crystallographic texture studies [58].



Figure 6.46 ZEISS MERLIN Scanning Electron Microscope used during the experiments [58].

Table 18 Feature Table [58]

Feature	Value
Resolution	~0.6 nm (at 30 kV with FEG filament)
Sample Chamber	330 mm diameter, 270 mm height
Analytical Working Distance	8.5 mm
Magnification Range	12x - 2,000,000x (based on Polaroid image format)
Acceleration Voltage	0.02 kV - 30 kV

Table 19 Table of Capabilities [22]

Capabilities
Morphological analysis
Internal structure analysis
Fracture surface and crack analysis
Surface element analysis
Regional chemical element mapping
EBSD analysis
Surface coating thickness and characterization

After the welding process, aluminium alloy samples were cut perpendicular to the joint surface and to examine the structural differences formed on the joint surface, their surfaces were sanded with 320-1200 mesh sandpaper and then polished with 9-3-1 μm diamond paste, respectively. Keller chemical etchant was prepared for microstructure analyses and etching was performed. SEM examinations were performed for microstructure analyses of welded joints. After the tensile test, the fractured surfaces of the samples were examined, and SEM analyses were performed. SEM images of the samples joined using parameter variables such as different friction times etc. are given in Figure 6.48a and 6.48b order. As it is clearly seen in the SEM images, it is seen that there is no gap, crack or disconnected area in the sample with the best tensile strength (No. 136). In addition, when the microstructure of the material with the lowest tensile strength (No. 356) was examined, it was seen that there was a problem in joining this material. The crack and porosity problems frequently seen in aluminium welds are clearly seen in this material.

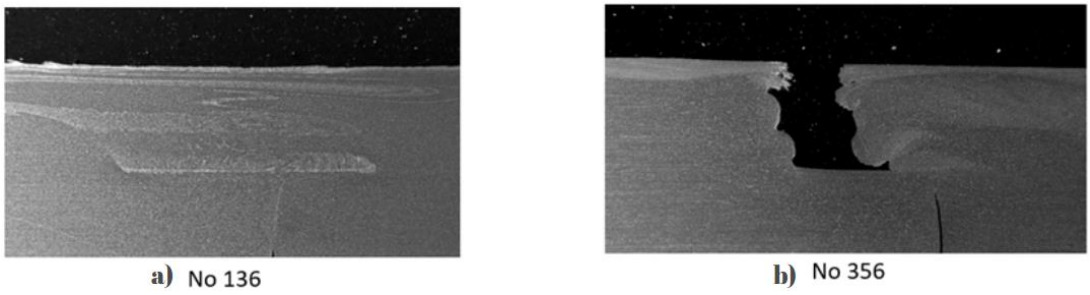

Figure 6.47 Cross-sectional microstructures of aluminium welds processed with different parameters: a) Weld No. 136 showing defect-free structure, b) Weld No. 356 exhibiting internal defects and lack of fusion

In the materials, the presence of fine grains in the joint region because of thermo-mechanical effects was observed from the SEM images, and it was also determined that there were grain orientations under axial pressure and due to centrifugal effects. It is also clearly seen from the images that there is a thin joint line in the joint cross-section.

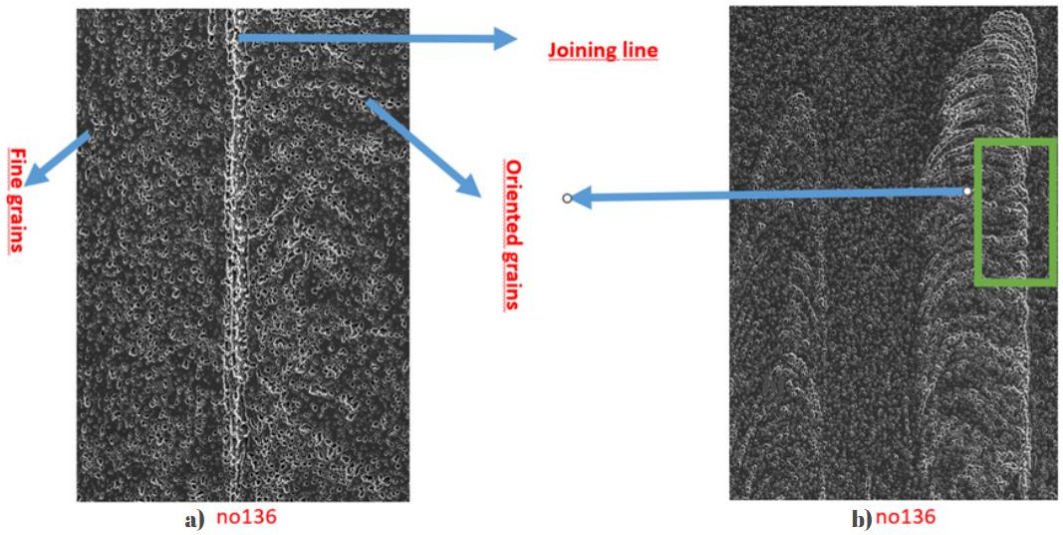

Figure 6.48 Microstructural analysis of weld No. 136: a) Fine and oriented grains along the joining line, indicating proper grain refinement; b) Detailed view of grain orientation and deformation near the weld zone, highlighting the microstructural features.

In the SEM images of the samples, fine-grained structures were formed in the partially deformed area of the weld intersection surface of sample no. 356, and these grains were oriented in the direction of rotation as a partially shrunken plate due to the heat

generated by the welding rotation speed. It is seen that there is a complete merger in the excessive deformation region and the material, which has become viscous, is directed outwards under the effect of the stacking pressure.

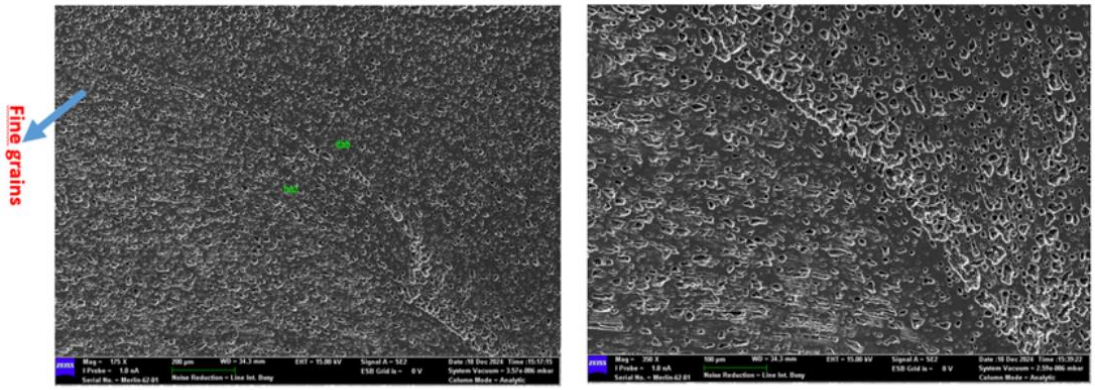

Figure 6.49 SEM images of weld No. 136: a) Fine grains observed near the weld zone, indicating effective grain refinement; b) Higher magnification showing the detailed grain structure and orientation within the weld region.

The internal structure formed in the weld zone is shown schematically. The weld zone consists of three different zones. These zones are called the dynamically recrystallizing zone (DKB), the thermomechanically affected zone (TEB) and the heat affected zone (ITAB) as in liquid state welding methods. It is defined as the dynamically recrystallizing zone (DKB) or “weld center”. The dislocation density in this zone is lower and consists of finer oriented grains. The TEB zone represents the region exposed to high deformation and temperature between the weld center and the heat affected zone. An intense forging event occurs as the grains of the base metal are extruded from the weld center to this region. The heat generated during mixing changes the microstructure and mechanical properties of this region. As a result, the grains that undergo deformation become elongated and flattened grains. The ITAB zone is the region closer to the weld metal and adjacent to the base metal that is not affected by heat.

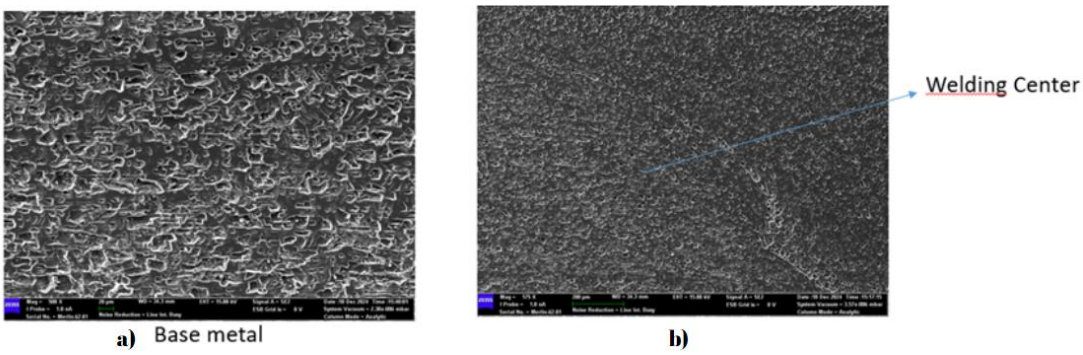

Figure 6.50 SEM images comparing the microstructure of the base metal and weld center: a) Base metal showing uniform grain structure; b) Weld center displaying refined grains and grain alignment along the welding direction.

CHAPTER 7

7. CONCLUSION

In this study, Friction Stir Welding process was performed on aluminium 5754 materials at different Rotational Speed and Traverse Speed. The force generated during welding and the roughness of the surface, mechanical properties and internal structure properties of the welded work pieces were investigated. Input parameters targeting high mechanical properties with low force output were compared. The surfaces and tensile test data of the samples made with 10 mm/min traverse speed were very low, and when the traverse speed exceeded 120 mm/min, a serious decrease was observed in the tensile test results and hardness data at each rotational speed. Therefore, data above 120 m/min will not be considered in the comparison tests. On the rotational speed side, no welding occurred under 500 rpm, and deterioration was observed on the surfaces obtained with 500 rpm. When the speed was 3500, serious decreases were observed in mechanical properties at 40 traverse speed and later. The tensile test data made with 10 mm/min traverse speed was very low. For this reason, the comparisons were made on samples between 10-120 mm/min traverse speed against rotational speed between 500 and 3500 rpm. The hardness, elongation, tensile strength and force results of the samples obtained after FSW were entered into the Pearson correlation prepared with the Python Software and the relationship between the input parameters and the output parameters were examined.

When the relationships between the mechanical properties and the input parameters were examined because of the correlation, it was observed that the Tensile strength results were not related to the Tool traverse speed, but there was an inverse proportion between them and Rotational speed.

When the Tensile strength (MPa) results were examined in the single-sided welded samples, after 83 tests, an average of 78% of the Stock material was obtained as Tensile Strength. The highest Tensile Strength was obtained with 93% in sample number 136 (1300 rpm- 80 mm/min), and the lowest Tensile Strength was obtained with 28% in sample number 356 (3500 rpm - 80)

To obtain higher mechanical properties, bidirectional friction stir welding was performed on the samples between 10 and 120 mm/min traverse speed corresponding to 700-1300 and 2500 rpm tool rotational speed. In the 700 rpm- 120 mm/min Two-Way FSW sample obtained here, 29 % higher tensile strength was obtained than the stock material.

An average of 57.36 HB was measured in aluminium 5754 stock material. The average hardness data obtained from all samples because of unidirectional friction welding is 69.72 HB. A 21% higher hardness measurement was obtained from the stock material. In the sample surfaces made at 500 rpm, sufficient stirring could not be observed, and hardness measurement could not be taken. When the test result table is examined, in return, the hardness values at 700 -900 -1100-1500 rpm have the highest values, respectively. In contrast, low hardness was measured at 3500-2500-2000 rpm. When the traverse speeds for each rotational speed were examined, it was observed that the traverse speeds did not have much effect on the hardness. Similarly, Pearson correlation examined on hardness, the effect of traverse speed on hardness was low, while rotational speed and hardness were inversely proportional.

Average roughness of profile values of stock material and 3 different samples numbered 74, 134 and 254 were examined. In each sample, 3 regions were examined as region 1, 2 and 3, which are the first contact of the tool, the middle region and the region where the tool exits, respectively. When the regions are examined, the most suitable sample approaching the 0.48 μm Ra value of the stock material is sample numbered 254 (2500 rpm) with an average of 0.83 μm, followed by sample numbered 134 (1300 rpm) with 1.21 μm and sample numbered 74 (700 rpm) with 0.29 μm, respectively. According to what is seen here, the increase in rotational speed has a positive effect on the roughness of the surface. The reason can be shown as the boiling surface becomes more sensitive as the speed increases. However, it was not included in this match due to the visible deterioration of the surface above 3000 rpm rotational speed. When the welded samples were examined by looking at their respective regions, it was observed that the best surfaces were formed in region 2 (center region).

Force measurement is one of the most important outputs for friction stir welding, the aim was to produce samples with high mechanical properties with low force. High force is harmful for the rotational speed of the milling machine Our inputs are

rotational speed (rpm) and tool movement speed (mm/min), and our measured force outputs on the tool are the maximum and average force values of F_x, F_y and F_z in 3 directions. Force measurements were taken against time on the milling machine with Dynoware. As expected, the highest forces were observed on the vertical axis, i.e. F_z direction. The highest moment of these forces is when the tool tip touches the work pieces.

When the test results and Pearson correlation are examined, F Maximum forces are observed inversely proportional to Rotational speed. In other words, lower maximum forces were observed at high rotational speeds. No effect of Tool traverse speed on maximum F_x, F_y and F_z was observed. This situation can be explained by the fact that the maximum force is now of contact between the work pieces and the tool tip, i.e. the tool advancement occurs later. On the other hand, a direct proportion was observed between Mean F_x, F_y and F_z and tool traverse speed. As the tool traverse speed increases, the average forces generated during the welding process also increases.

As a result of the study, the surface quality, hardness, internal structure, tensile strength and force outputs to be obtained because of traverse and rotational speeds were obtained. In this context, it was discussed that the input welding parameters could be selected in response to the targeted output for aluminium 5754 Friction Stir Welding.

CHAPTER 8

8. FUTURE WORK

In the future, some additional studies can be conducted to further develop these studies, thermal camera measurements will be utilized during the Friction Stir Welding (FSW) process to analyze the correlation between welding parameters and temperature. The friction generated at the interface between the workpieces and the tool tip will be a key focus of investigation. This study aims to understand how frictional interactions influence the welding process and resulting material properties.

Additionally, a thickness-adjustable fixture design is proposed to enable the FSW of materials with varying thicknesses. This innovation will expand the versatility of the process, making it suitable for more diverse applications. Future experiments will also explore the FSW of different sheet materials, including Titanium, to assess their weldability and mechanical properties under varying process conditions.

A significant objective of the ongoing studies is to address challenges related to material elongation. Although previous experiments achieved high mechanical strength in the welded joints, the elongation of the material remained relatively low. To overcome this limitation, future work will incorporate heat treatment processes after welding. The goal is to improve the ductility of the welded material while maintaining or enhancing its mechanical strength.

By integrating advanced measurement techniques, innovative fixture designs, and post-weld treatments, this research aims to optimize the FSW process for a broader range of materials and applications. The insights gained from these studies will contribute to advancing the field of FSW, enabling the production of high-quality, reliable joints for critical engineering applications. Through these efforts, it is anticipated that the process will become more versatile, efficient, and capable of meeting the stringent demands of modern manufacturing industries.

REFERENCES

[1] ISO 857-1:2019, *Welding and related processes — Vocabulary*, International Organization for Standardization, 2019.

[2] M. P. Groover, *Fundamentals of Modern Manufacturing: Materials, Processes, and Systems*, Hoboken, NJ: Wiley & Sons, 2007, pp. 623-650.

[3] J. T. Black, *DeGarmo's Materials and Processes in Manufacturing*, Hoboken, NJ: Wiley, 2008, pp. 723-727.

[4] S. W. Kallee, E. D. Nicholas, and W. M. Thomas, "Friction stir welding invention, innovations, and applications," *8th International Conference on Joints in Aluminium, TWI Ltd INALCO*, Munich, Germany, Mar. 28-30, 2001.

[5] R. S. Mishra and P. D. Kumar, *Friction Stir Welding*, New York: Springer, 2014.

[6] M. Amatullah, M. Jan, A. S. Zargar, A. Maqbool, and N. Z. Khan, "Effect of tool rotational speed on the friction stir welded aluminium alloys: A review," *Materials Today: Proceedings*, pp. 245-250, 2022.

[7] H. Kafalı and N. Ay, "Sürtünme karıştırma kaynağıyla birleştirilmiş havacılık ve uzay yapılarında kullanılan AL 6013-T6 alaşımının mikroyapı ve mekanik özelliklerinin incelenmesi," *Havacılık ve Uzay Teknolojileri Dergisi*, p. 98, Jul. 2014.

[8] A. Kurt, M. Boz, and M. Özdemir, "Sürtünme karıştırma kaynağında kaynak hızının birleşebilirliğe etkisi," *Gazi Üniversitesi Mühendislik Mimarlık Fakültesi Dergisi*, pp. 191-197, 2004.

[9] R. Özbekmez, "Sürtünme karıştırma kaynak tekniği ile CuZn30 levhalarının birleştirilmesi ve mekanik özelliklerinin incelenmesi," *Yüksek Lisans Tezi*, Sakarya Üniversitesi Fen Bilimleri Enstitüsü, Sakarya, Jun. 2006.

[10] P. Cavaliere, "Friction stir welding of Al alloys: Analysis of processing parameters affecting mechanical behaviour," *Science Direct*, pp. 139-144, 2013.

[11] S. Kumar, D. Sethi, S. Choudhury, B. S. Roy, and S. C. Saha, "An experimental investigation to the influence of traverse speed on microstructure and mechanical properties of friction stir welded AA2050-T84 Al-Cu-Li alloys," *Materials Today*, pp. 1-7, Feb. 13, 2020.

[12] V. Borigorla, K. V. Rao, and L. S. Raju, "Multiobjective optimization of friction stir weldments of AA2014-T651 by teaching-learning-based optimization," *Journal of Mechanical Engineering Science*, Aug. 30, 2019

[13] A. Banik, A. Saha, J. D. Barma, U. Acharya, and S. C. Saha, “Determination of best tool geometry for friction stir welding of AA 6061-T6 using hybrid PCA-TOPSIS optimization method,” *Measurement*, pp. 1-10, Oct. 4, 2020.

[14] H. Su, L. Xue, and C. Wu, "Optimizing the tool pin with three flats in friction stir welding of aluminium alloy," *The International Journal of Advanced Manufacturing Technology*, vol. 109, no. 3-4, pp. 1103-1117, Feb. 2020.

[15] S. Rajakumar, C. Muralidharan, and V. Balasubramanian, “Influence of friction stir welding process and tool parameters on strength properties of AA7075-T6 aluminium alloy joints,” *Materials & Design*, pp. 535-549, Dec. 2011.

[16] N. Khan, S. Rathee, and M. Srivastava, “Friction stir welding: An overview on effect of tool variables,” *Materials Today: Proceedings*, vol. 47, part 19, pp. 7196-7202, 2021.

[17] H. Jia, K. Wu, Y. Sun, F. Hu, Y. Lin, and H. Zhang, "Experimental research and process parameter optimization of high-speed friction stir welding," *The International Journal of Advanced Manufacturing Technology*, vol. 115, no. 5-6, pp. 1563-1574, 2021.

[18] C. C. Tutum, *Optimization of Thermo-mechanical Conditions in Friction Stir Welding*, Ph.D. dissertation, Department of Mechanical Engineering, University of Twente, Enschede, Netherlands, 2011.

[19] A. Thakur, V. Sharma, N. Minhas, and R. Verma, "Achieving an improved performance in bidirectional friction stir weld joints by adjusting the welding conditions during the passes of AA6061-T6 aluminium alloy," *Micron*, vol. 177, pp. 103563, Nov. 2023.

[20] J. Tang, L. Shi, C. Wu, X. Liu, and Y. Zhao, "Improving bonding strength of medium-thick Al-Cu dissimilar joint by a novel splat cooling assisted double side friction stir welding," *Materials Characterization*, vol. 211, pp. 113878, Apr. 2024.

[21] Y. Tang, W. Li, Y. Zou, W. Wang, Y. Xu, A. Vairis, and G. Çam, "Effects of tool rotation direction on microstructure and mechanical properties of 6061 aluminium alloy joints by the synergistically bidirectional friction stir welding," *Journal of Manufacturing Processes*, vol. 126, pp. 109–123, Jul. 2024.

[22] W. M. Moore, G. P. McCabe, and B. A. Craig, *Introduction to the Practice of Statistics*, 9th ed., New York, NY, USA: W. H. Freeman, 2017, pp. 151–155.

[23] P. Hendrato, P. Puspitasari, Jamasri, and Triyono, “Fatigue crack growth rate and mechanical properties of one-step double-side friction stir welded AA6061-T6,” *Results in Engineering*, vol. 21, p. 101958, Feb. 2024.

[24] O. O. Ojo and O. A. Oboro, “Stepwise bidirectional friction stir welding: An alternative for root defect mitigation in aluminium plates with lower gauge numbers,” *Turkish Journal of Engineering*, vol. 8, no. 4, pp. 611–618, Oct. 2024.

[25] A. Thakur, V. Sharma, and S. S. Bhadauria, “Improving tensile properties by varying the welding conditions of the passes of the bidirectional friction stir welding of AZ31B magnesium alloy,” *Materials Today Communications*, vol. 34, pp. 105406, Jan. 2023.

[26] M. Haghshenas, A. Abdel-Gwad, A. M. Omran, B. Gökçe, S. Sahraeinejad, and A. P. Gerlich, “Friction stir weld assisted diffusion bonding of 5754 aluminium alloy to coated high strength steels,” *Materials and Design*, vol. 55, pp. 442–449, 2014.

[27] M. I. Costa, D. Verdera, C. Leitão, and D. M. Rodrigues, “Dissimilar friction stir lap welding of AA 5754-H22/AA 6082-T6 aluminium alloys: Influence of material properties and tool geometry on weld strength,” *Materials & Design*, vol. 87, pp. 721–731, 2015.

[28] A. Ghiasvand, E. Ranjbarnodeh, and S. E. Mirsalehi, “The microstructure and mechanical properties of single-pass and double-pass lap joint of Al 5754H-11 and Mg AZ31-O alloys by friction stir welding,” *Journal of Materials Research and Technology*, vol. 23, pp. 6023-6038, 2023.

[29] D. Datta and A. Bhargava, “Investigation of friction stir welding parameters on microstructure, mechanical properties and formability of AA6061 and AA5754 aluminium alloys,” *Materials Today Communications*, vol. 42, p. 105788, 2024.

[30] F. Mindivan, H. Kaya, M. Özer, M. Uçar, and R. Samur, “Investigation of corrosion behaviour of the AA5754 aluminium alloy joined using friction stir welding method,” *CBU Journal of Science*, vol. 11, no. 3, pp. 413–422, 2024.

[31] F. Sarsılmaz, S. Özel, and İ. Candan, “Sürtünme karıştırma kaynak yöntemiyle birleştirilen farklı tipteki alüminyum bağlantıların tahribatlı ve tahribatsız muayenesi,” *Süleyman Demirel Üniversitesi Fen Bilimleri Enstitüsü Dergisi*, vol. 13, no. 1, pp. 88–95, 2009.

[32] R. Çakır and S. Çelik, “Al 5754-Cu malzeme çiftinin alın sürtünme karıştırma kaynak kabiliyeti,” *El-Cezerî Journal of Science and Engineering*, vol. 4, no. 1, pp. 82–91, 2017.

[33] F. Tolun, “EN AW-5754 ve EN AW-5083 alüminyum alaşımlarının sürtünme karıştırma kaynağı ile birleştirilmelerinde kullanılan farklı takım geometrilerinin kaynaklı birleştirmeye etkilerinin araştırılması,” *Balıkesir Üniversitesi Fen Bilimleri Enstitüsü Dergisi*, vol. 22, no. 1, pp. 334-344, 2020.

[34] Kistler Instrumente AG, *Data sheet, 3 component force sensor (type 9017B)*, 2010.

[35] Kistler Instrumente AG, *Data sheet, 3 component force link (type 9317B)*, 2004.

[36] A. Ray, D. Pendokhare, and S. Chakraborty, "A comprehensive review of multi-objective optimization of friction stir welding processes," *Welding in the World*, vol. XX, 2024, pp. 1–20.

[37] K. Panneerselvam and K. Lenin, "Parameters optimization in FSW of polypropylene based on RSM," *Multidisciplinary Modeling in Materials and Structures*, vol. 11, pp. 32–42, 2015.

[38] D. Vijayan and V. S. Rao, "A multi-response optimization of tool pin profile on the tensile behaviour of age-hardenable aluminium alloys during friction stir welding," *Research Journal of Applied Sciences, Engineering and Technology*, vol. 7, pp. 4503–4518, 2014.

[39] D. Venkateswarlu, P. N. Rao, M. M. Mahapatra, S. P. Harsha, and N. R. Mandal, "Processing and optimization of dissimilar friction stir welding of AA 2219 and AA 7039 alloys," *Journal of Materials Engineering and Performance*, vol. 24, pp. 4809–4824, 2015.

[40] M. Ghafarpour, A. Aziz, and T. H. Hejazi, "Optimization of friction stir welding parameters using multiple response surface methodology," *Proceedings of the Institution of Mechanical Engineers, Part L: Journal of Materials: Design and Applications*, vol. 231, pp. 571–583, 2017.

[41] C. Rathinasuriyan and V. S. Kumar, "Modelling and optimization of submerged friction stir welding parameters for AA6061-T6 alloy using RSM," *Kovove Mater.-Metallic Materials*, vol. 54, pp. 297–304, 2016.

[42] A. K. Lakshminarayanan, "Enhancing the properties of friction stir welded stainless steel joints via multi-criteria optimization," *Archives of Civil and Mechanical Engineering*, vol. 16, pp. 605–617, 2016.

[43] S. A. Amin, M. Y. Hanna, and A. F. Mohamed, "Modelling and optimization of bobbin friction stir welding for AA6061-T6 alloy utilizing response surface methodology," *Journal of University of Babylon for Engineering Sciences*, vol. 26, pp. 1–17, 2018.

[44] M. S. Rao and N. Ramanaiah, "Optimization of process parameters for FSW of Al-Mg-Mn-Sc-Zr alloy using CCD and RSM," *Journal of Mechanical Engineering*, vol. 68, pp. 195–224, 2018.

[45] Y. K. Periyasamy, A. V. Perumal, and B. K. Periyasamy, "Optimization of process parameters on friction stir welding of AA7075-T651 and AA6061 joint using response surface methodology," *Materials Research Express*, vol. 6, no. 096558, 2019.

[46] S. Verma, M. Gupta, and J. P. Misra, “Optimization of process parameters in friction stir welding of armor-marine grade aluminium alloy using desirability approach,” *Materials Research Express*, vol. 6, no. 026505, 2018.

[47] R. Pandiyarajan, P. Maran, N. Murugan, S. Marimuthu, and T. Sornakumar, “Friction stir welding of hybrid AA 6061-ZrO2-C composites FSW process optimization using desirability approach,” *Materials Research Express*, vol. 6, no. 066553, 2019.

[48] W. M. Moore, G. P. McCabe, and B. A. Craig, *Introduction to the Practice of Statistics*, 9th ed., New York, NY, USA: W. H. Freeman, 2017, pp. 151–155.

[49] M. J. Umar, P. K. Palaniappan, and R. Pandiyarajan, “Investigation and optimization of friction stir welding process parameters of stir cast AA6082/ZrO/BC composites,” *Materials Science-Poland*, vol. 38, pp. 715–730, 2021.

[50] S. M. Senthil, R. Parameshwaran, S. R. Nathan, B. M. Kumar, and K. Deepandurai, “A multi-objective optimization of the friction stir welding process using RSM-based-desirability function approach for joining aluminium alloy 6063–T6 pipes,” *Structural and Multidisciplinary Optimization*, vol. 62, pp. 1117–1133, 2020.

[51] M. D. Bindu, P. S. Tide, A. B. Bhasi, and K. K. Ramachandran, “Modelling and parametric optimization of friction stir welding of aluminium alloy AA7068-T6 using response surface methodology and desirability function analysis,” *Bulletin of the Polish Academy of Sciences Technical Sciences*, vol. 69, pp. 1–9, 2021.

[52] R. Kumar, V. Upadhyay, and C. Sharma, “Modelling and optimization of process parameters for friction stir welding of dissimilar aerospace alloys AA2014 and AA7075,” *Engineering Review*, vol. 42, pp. 59–78, 2022.

[53] R. Sandeep and A. Natarajan, “Application of machine learning approaches to predict joint strength of friction stir welded aluminium alloy 7475 and PPS polymer hybrid joint,” *Proceedings of the Institution of Mechanical Engineers, Part C: Journal of Mechanical Engineering Science*, vol. 236, pp. 9003–9011, 2022.

[54] K. P. Vasantha Kumar and M. Balasubramanian, “Multi-response optimization of FSW parameters for dissimilar Al-Mg alloys,” *Tehnički Vjesnik*, vol. 29, pp. 926–932, 2022.

[55] A. Kumar, S. Rathee, and S. Kumar, “A state-of-the-art literature review on friction stir welding of 7075 aluminium alloy: Tool geometry, environmental factors and mathematical modelling,” *International Journal of Interactive Design and Manufacturing*, vol. 18, 2024.

[56] Atilim University Metal Forming Center of Excellence, “Alicona InfiniteFocus,” [Online]. Available: https://www.atilim.edu.tr/tr/msmm/page/3112/alicona-infinitefocus. [Accessed: Jan. 2, 2025].

[57] The Welding Institute (TWI), “What is Friction Stir Welding?” [Online]. Available: https://www.twi-global.com/technical-knowledge/faqs/what-is-friction-stir-welding. [Accessed: Jan. 2, 2025].

[58] “Zeiss Merlin Scanning Electron Microscope,” *Atilim University*, [Online]. Available: https://www.atilim.edu.tr/tr/msmm/page/3139/zeiss-merlin-taramali-elektron-mikroskobu. [Accessed: Dec. 16, 2024].

[59] W. M. Moore, G. P. McCabe, and B. A. Craig, *Introduction to the Practice of Statistics*, 9th ed., New York, NY, USA: W. H. Freeman, 2017, pp. 151–155.

APPENDIX A

CODE OF PEARSON PRODUCT MOMENT CORRELATION COEFFICIENT

```
import pandas as pd
import numpy as np
import matplotlib.pyplot as plt
import seaborn as sns
from scipy.stats import skew
data = pd.read_csv('fsw.csv')
#Corelation analysis - 1 (%100 Direct correlation), -1 (%100 Indirect Correlation)
input_params = ['Rotation Speed (N)', 'Tool Traverse Speed (v)']
output_results = ['Hardness', 'RP 0.2', 'Rm', 'A', 'Fy']
correlations = data[input_params + output_results].corr()
plt.figure(figsize=(12, 8))
sns.heatmap(correlations, annot=True, cmap='coolwarm', fmt='.2f')
plt.title('Correlation Heatmap of FSW Experiments')
plt.show()
```

APPENDIX B

SEM IMAGES

SEM images of samples after FSW

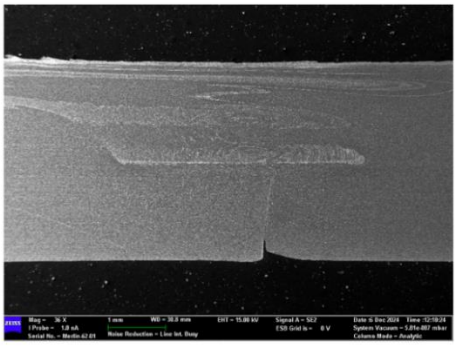

a)

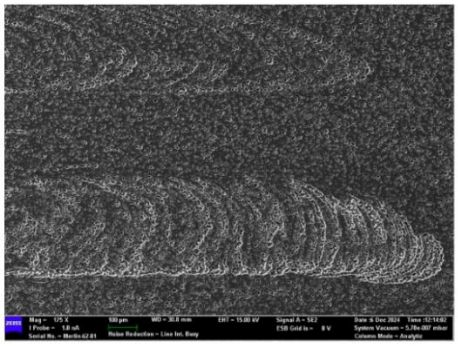

b)

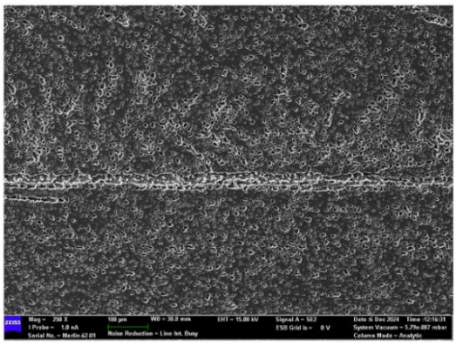

c)

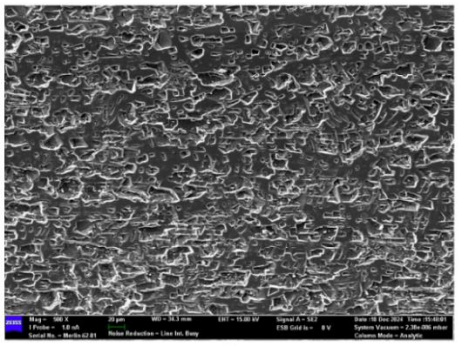

d)

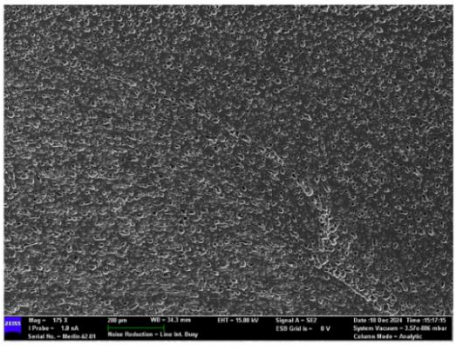

e)

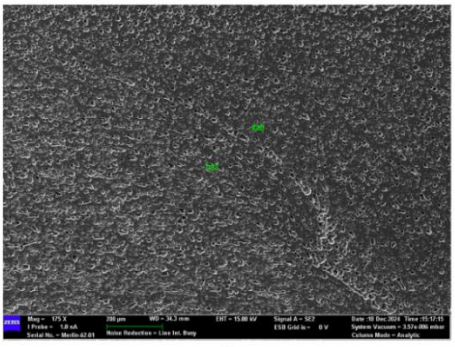

f)

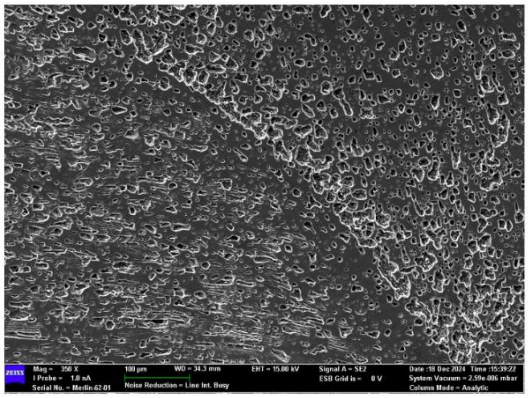

g)

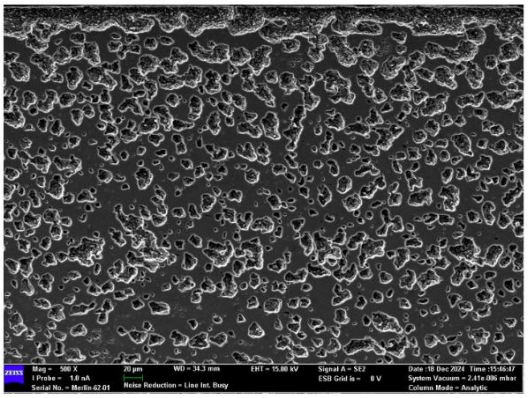

h)

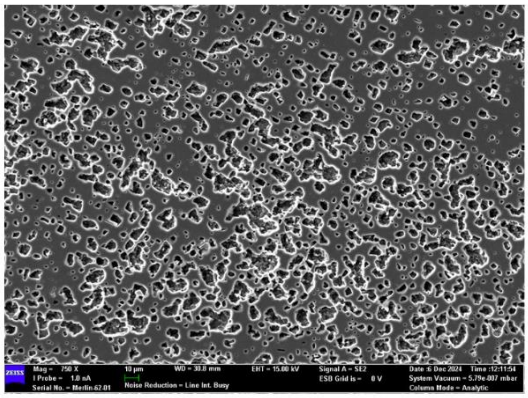

i)

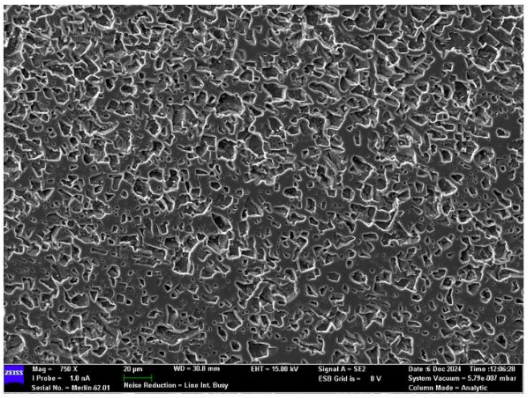

j)

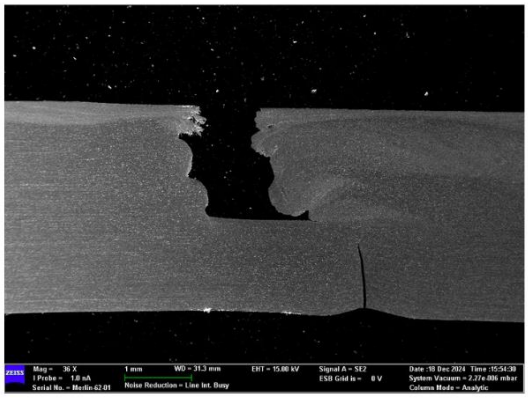

k)

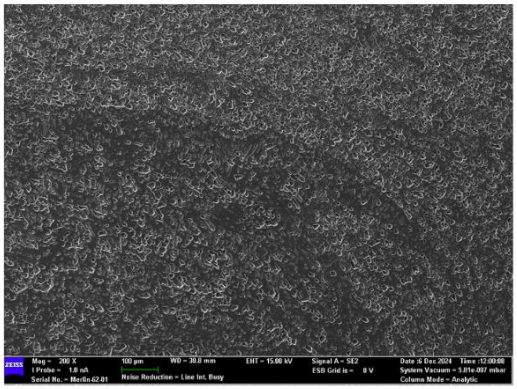

l)

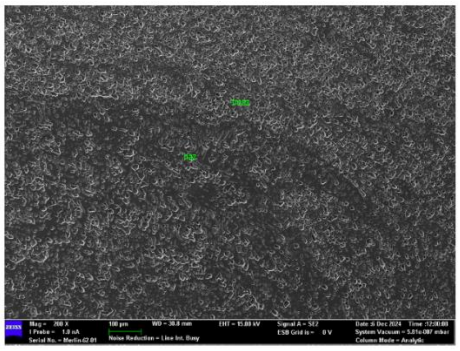

m)

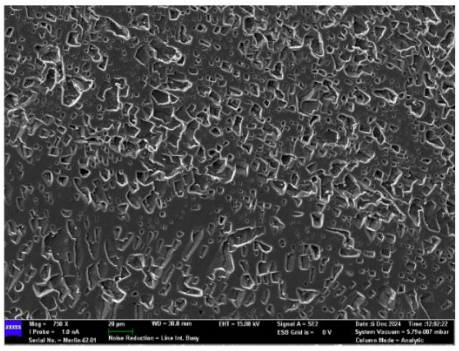

n)